Functional Dissociation of Ongoing Oscillatory Brain States Revealed by a Custom-Developed Brain Computer Interface

Dissertation

zur Erlangung des akademischen Grades
Dr. rer. nat.
an der Fakultät für Mathematik, Informatik und Naturwissenschaft
der Universität Hamburg

eingereicht beim Fachbereich Informatik von

Neda Salari

aus Teheran (Iran)

Hamburg, 2012

Abstract

The state of a neural assembly in the human brain preceding an incoming stimulus is assumed to modulate the processing of subsequently presented stimuli. The nature of this state can differ with respect to the frequency of ongoing oscillatory activity. Oscillatory activity of specific frequency range such as alpha (8-12 Hz) and gamma (30-45 Hz) band oscillations is hypothesized to play a functional role in visual object processing. However, the precise role of prestimulus alpha or gamma band oscillations for visual object processing is not completely understood. Therefore, a selective modulation of this prestimulus activity could clarify the functional role of these oscillations. We hypothesized that an increase in gamma band activity as compared to an increase in alpha band activity over the visual cortex by BCI manipulation would enhance subsequent visual object processing.

In contrast to previous studies in which oscillations of prestimulus activity were correlated with visual performance, we attempted to put the volunteers directly in control of the oscillatory brain activity. To this end, we designed and implemented a non-invasive brain computer interface (BCI) method to train volunteers to selectively increase their alpha or gamma band activity in the occipital cortex. During training, oscillatory brain activity was estimated online and fed back to the volunteers to enable a deliberate modulation of alpha or gamma band oscillations. The visual stimuli were presented during specific brain states in an individually adapted manner. During the testing phase which followed the training phase, alpha or gamma band activity was classified online and at predefined levels of activity, visual objects embedded in noise were presented in order to assess the influence of frequency modulation on subsequent visual object processing.

In the process of developing a BCI method based on gamma band oscillations, several important aspects had to be considered, including presence of artifacts, experimental design and topographical precision of BCI training. We therefore perfected our BCI method with online artifact control for artifact suppression, a special visual display design to avoid distraction yet motivate volunteers, and a source-based BCI method to limit training to a distinct neural area in the visual cortex. In a series of experiments, we first evaluated the accuracy of the BCI method and then explored the specific effect of gamma band training on visual object perception. Finally, we compared the specific effect of gamma band training to the well defined alpha band.

Our results demonstrated that volunteers learned to selectively modulate alpha or

gamma band oscillations in the visual cortex with a high level of specificity regarding frequency range and localization. During phases of increased gamma band activity, visual object processing was improved. The functional specificity of gamma band oscillations was demonstrated by a direct comparison to alpha band oscillations.

Hence, the BCI method allows a selective manipulation of gamma band activity in the visual cortex and supports a prominent role of prestimulus gamma band activity for visual object processing.

Zusammenfassung

Der Zustand eines Nervenzell-Verbandes, welcher einem eintreffenden Reiz vorangeht, kann die Verarbeitung nachfolgend dargebotener Reize beeinflussen. Der Zustand solch eines Zellverbandes kann bezüglich der Frequenz der zugrundeliegenden oszillatorischen neuronalen Aktivität voneinander abweichen. Die Hypothese besteht, dass die oszillatorische Aktivität bestimmter Frequenzbereiche, wie z.B. Alpha- (8-12 Hz) und Gamma- (30-45 Hz) Band Oszillationen, eine funktionale Rolle bei der Verarbeitung visueller Objekte besitzen. Allerdings ist die genaue Rolle der prä-Stimulus Alpha- oder Gamma- Band Oszillationen bei der visuellen Objektverarbeitung nicht vollständig geklärt. Aus diesem Grund könnte eine selektive Modulation dieser prä-Stimulus Aktivität dazu beitragen, die funktionale Rolle dieser Oszillationen zu klären. Dabei nahmen wir an, dass eine Erhöhung der Gamma-Band Aktivität im visuellen Kortex mit Hilfe der Brain-Computer-Interface (BCI)-Methode zu einer anschließenden Verbesserung der visuellen Objektverarbeitung führt.

In Abgrenzung zu früheren Studien, in denen die Korrelation zwischen der prä-Stimulus Oszillationen und der visuellen Leistung bestimmt wurde, versuchten wir, den Versuchsteilnehmern die direkte Kontrolle ihrer oszillatorischen Hirnaktivität zu ermöglichen. Zu diesem Zweck entwickelten wir eine nicht-invasive BCI-Methode. Durch diese lernt der Versuchsteilnehmer, die eigene Alpha- oder Gamma- Band Aktivität im visuellen Kortex selektiv zu erhöhen. Während des Trainings wurde die oszillatorische Hirnaktivität geschätzt und für den Versuchsteilnehmer auf dem Bildschirm visualisiert, um eine bewusste Modulation der Alpha- oder Gamma- Band Oszillationen zu ermöglichen. Danach wurden visuelle Reize während bestimmter Zustände des Gehirns präsentiert. Während der Testphase, die im Anschluss an die Trainingsphase erfolgte, wurde die Alpha- oder Gamma- Band Aktivität „online" klassifiziert. Visuelle Reize wurden während vordefinierten Stufen der Aktivität präsentiert, um den Einfluss dieser Frequenzmodulation auf die nachfolgende visuelle Objektverarbeitung zu untersuchen.

Während der Entwicklung einer BCI-Methode auf der Basis von Gamma-Band Oszillationen, mussten einige wichtige Aspekte berücksichtigt werden. Dazu gehören das Auftreten von Artefakten, das experimentelle Design und die topographische Präzision des BCI-Trainings. Aus diesem Grund wurde die BCI-Methode mit einer „online" Artefakt-Kontrolle zur Artefakt-Unterdrückung ausgestattet. Weiterhin wurde ein spezielles Display-Design entworfen, um den Versuchsteilnehmer nicht abzu-

lenken und um ihn zugleich zu motivieren. Um das Training auf eine spezielle neuronale Region zu beschränken, wurde eine quellen-basierte BCI-Methode eingeführt. In einer Reihe von Experimenten analysierten wir zunächst die Genauigkeit der BCI-Methode und untersuchten daraufhin die spezifische Wirkung des Gamma-Band-Trainings auf die visuelle Objektverarbeitung. Schließlich verglichen wir die spezifische Wirkung des Gamma-Band-Trainings auf die visuelle Objektverarbeitung mit dem eindeutig definierteren Alpha-Band.

Im Hinblick auf den Frequenzbereich und die Lokalisation lernten die Versuchsteilnehmer mit einem hohen Grad an Genauigkeit eine selektive Modulation der Alpha- und Gamma- Band Oszillationen im visuellen Kortex. In Phasen erhöhter Gamma-Band Aktivität wurde die visuelle Objektverarbeitung verbessert. Die funktionale Spezifität der Gamma-Band Oszillationen wurde durch einen direkten Vergleich zu den Alpha-Band Oszillationen nachgewiesen

Die BCI-Methode ermöglicht eine selektive Modulation der Gamma-Band Oszillationen im visuellen Kortex und belegt die funktionale Relevanz der Gamma-Band Aktivität für die visuelle Objektverarbeitung.

Acknowledgments

First of all I would like to thank Dr. Michael Rose for providing me with such an interesting topic for my thesis. I would like to thank him for his invaluable support and his knowledgeable guidance throughout the dissertation. Working with Dr. Michael Rose has been a truly rewarding experience.

I would also like to thank Prof. Stiehl for giving me the opportunity to write this thesis under his supervision. His critical and inspiring reviews of my work have been very constructive and helpful. I would also like to thank Prof. Büchel for giving me the opportunity of writing my thesis at the Department of Systems Neuroscience.

Special thanks also goes to Niklas Stein, Mathias Pietsch, Eszter Schoell, Catherine Hindi Attar and Alexandra Thanellou for discussing and proofreading some aspects of my work.

Last but not least I would like to thank my family. I am very grateful to my parents for their love and steady encouragement at each time. Without your trust in my capabilities and your support I would have not been able to finish this work. Thank you mom and dad for always believing in me. A special thanks also goes to my lovely husband Navid, who had to endure the ups and downs of my mood, in particular within the first year of marriage! I thank you for being extremely supportive and for being there for me. I would also like to thank my brothers Nima and Soroush. I thank Nima for inspiring me for natural sciences and I thank Soroush for being my personal motivation coach and for encouraging me to believe in myself.

Contents

Chapter 1

Introduction

The human brain has the remarkable ability to perceive an object in a visual scene within a fraction of a second. This object perception process right after object presentation (stimulus presentation) has been shown to increase the intrinsic fluctuations of neural activity in a specific brain region in the visual cortex. Interestingly, it is argued that the state of neural activity directly preceding an incoming stimulus could also have a prominent impact on the processing of that stimulus.

A relevant amount of the variability in human task performance can be attributed to intrinsic fluctuations of neural activity prior to actual processing. The electrical brain activity in this neural state can be characterized by the frequency of ongoing oscillations, including delta (1-4 Hz), theta (4-7 Hz) alpha (8-12 Hz), beta (13-30) and gamma band (30-100 Hz) frequencies. Prestimulus oscillations in different frequency ranges have been shown to influence visual performance (Supèr et al., 2003; Dijk et al., 2008; Linkenkaer-Hansen et al., 2004; Hanslmayr et al., 2007; Monto et al., 2008). Studies have indicated that a high amount of low frequency oscillations, i.e. the alpha band, impair perception while high gamma band frequencies have been observed to enhance visual perception (Wyart & Tallon-Baudry, 2009). These results suggest that neuronal oscillations with different frequencies within specific brain areas in the visual cortex have a strong influence on visual object processing. However, the observation of prestimulus oscillatory activity in correlation to visual object processing is not sufficient evidence to claim a causal relevance.

To establish a more causal relation between ongoing oscillatory activity and visual object processing, several methods have been used to directly modulate electrical brain activity and examine the consequences. These methods included an exogenous

activation of interneuron's using optogenetic techniques (Cardin et al., 2009; Sohal et al., 2009), direct electrical stimulation (Romei et al., 2010; Marshall et al., 2006) or attention (Tiitinen et al., 1993; Gruber et al., 1999; Fries et al., 2001; Tallon-Baudry et al., 2005) to experimentally determine the relationship of electrical brain activity and behavior (including visual performance) more directly. However, the specificity of most of these methods is limited with respect to the time-, frequency- or space- domain, i.e. most studies have not assessed whether the methods affected only a distinct frequency of oscillations at a limited brain region directly preceding the stimulus processing.

In this thesis, we propose a new non-invasive method to examine the relevance of ongoing brain activity for visual object processing by (i) training volunteers to deliberately modulate oscillatory brain activity in a specific frequency range and brain area (ii) a real-time classification of the actual oscillatory brain state and (iii) and an adaptive presentation of visual stimuli within predefined brain states.

In order to train volunteers to enhance natural fluctuations of neural activity, we designed and implemented a customized brain computer interface (BCI). With electroencephalography (EEG) based BCI, brain signals are recorded along the scalp, while relevant components are extracted and fed back to the volunteer in the form of visual information using an online feedback loop. In addition to the feedback training of ongoing brain activity, we extended our BCI method with online artifact detection and online features extraction with an adaptive presentation of visual stimuli.

Using this method we focused on the role of alpha and gamma band oscillations in the visual cortex for the subsequent processing of visual stimuli. Since previous studies indicate a different role of gamma and alpha band frequencies for perceptual and memory related information processing (Wyart & Tallon-Baudry, 2009; Romei et al., 2010), we used this method to examine common and dissociable effects of ongoing alpha and gamma band oscillations.

In section (1.1.1), we will first give an introduction to the relevant neuroscientific background related to this thesis. This includes a brief introduction to the visual cortex and neuronal oscillations. In section (1.1.2), the historical background of the BCI method is introduced followed by the state of the art in BCI research. Research questions for the present thesis are outlined based on the state of the art of research.

1.1 State of Art

1.1.1 Neuroscientific Background

This section provides a brief overview of the basic neuroscientific concepts concerning visual object processing in the human brain based on (Kandel et al., 1991; Squire, 2003). First we will introduce the brain areas of interest followed by the frequency range of oscillations which we aim to modulate with our BCI method.

1.1.1.1 The Visual Cortex

The human brain is a complex organ responsible for interpreting and managing vast amounts of continuously incoming signals. With a relatively small mass of about 1.4 kg, the brain contains approximately 100 billion neurons (Kandel et al., 1991). As the human brain receives signals from many sources, these neurons process the incoming signals in a highly organized fashion and within a short amount of time.

Anatomically, the human brain is divided into two cerebral hemispheres. The cerebral cortex is divided into four anatomically distinct parts: the frontal, parietal, temporal and occipital lobes (see Figure 1.1a) (Kandel et al., 1991). Each lobe includes specific functional areas. The occipital lobe, for example, is known as the primary visual processing centre of the human brain (Kandel et al., 1991). The temporal lobe has specific areas dedicated to auditory (Penfield & Perot, 1963), visual (Kreiman et al., 2000) and memory (Squire & Zola-Morgan, 1991) functions. The parietal lobe contains the primary somatic sensory cortex which is involved in sensation (touch, pressure) and the frontal lobe has areas that carry out functions related to the control of movement (Kandel et al., 1991).

Since the focus of this thesis is based on the principal processes within the visual domain, we will focus on the major visual brain areas.

The visual cortex encompasses the primary visual cortex (V1) and extra-striate visual cortical areas such as V2, V3, V4 and V5 (see Figure 1.1b). The primary visual cortex is located in the occipital lobe. Visual information is processed in multiple cortical areas that are fed by at least two neural pathways. These parallel pathways convey information from the retina via V1 to parietal and temporal cortical areas. In 1983, Leslie Ungerleider and Mortimer Mishkin suggested that these extra-striate visual areas are organized into two pathways: a dorsal pathway from V1 to
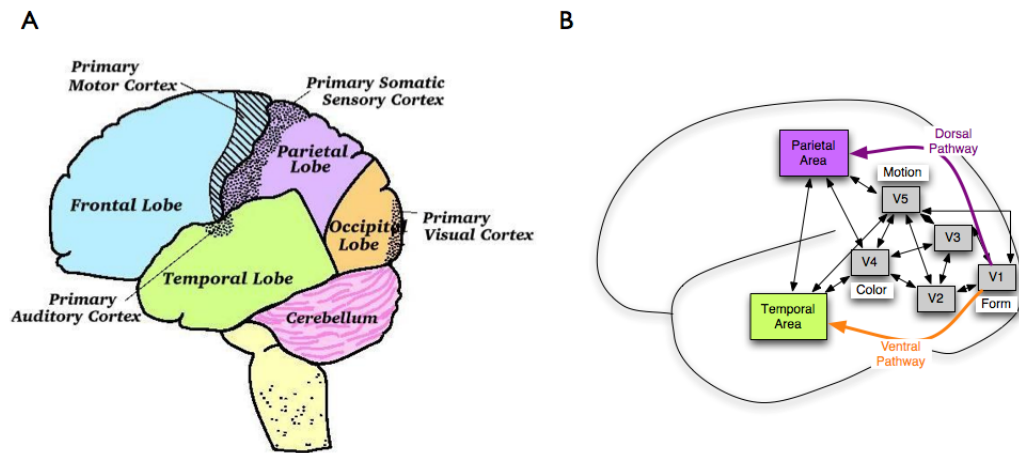
Figure 1.1: (a) Gross anatomical subdivision of the human brain. (Adapted from Palmer 1999) (b) Topography of the visual areas V1-V5 in the primary visual cortex. (Adapted from Engel, Singer, 1997)

the posterior parietal cortex, concerned with localizing 'where' objects are, and a ventral pathway extending from V1 to the inferior temporal cortex, concerned with identifying 'what' the objects are (see figure 1.1b). However, this oversimplification has been criticized and findings have shown that basic object information related to shape, size and viewpoint may be similarly represented in the ventral and dorsal visual pathways (Konen & Kastner, 2008).

Neurons in each of the visual ares V1 to V5 are, at least to some degree, selective for a characteristic subset of stimuli features. Some areas, for example, are devoted to the analysis of local orientation of stimuli (form) or to motion; others are specialized for different wavelengths (color) and others are involved in processing texture and global shape (Kandel et al., 1991). Consequently, a single visual stimulus activates neurons in several visual areas.

Thus, the question arises of where this spread of activity can be integrated to yield instantly recognizable representations of visual objects. In 1995, the process of integration leading from local feature analysis to object detection in the human visual cortex was explored in a functional magnetic resonance imaging study (Malach et al., 1995). The study reported evidence for activation related to objects in the lateral occipital lobe close to the motion-sensitive area MT/V5, in a region known as the lateral occipital cortex (LOC) (Malach et al., 1995). In this study, volunteers viewed images of objects and a wide range of texture patterns. Results clearly showed enhanced activity in the LOC during the presentation of objects, while the
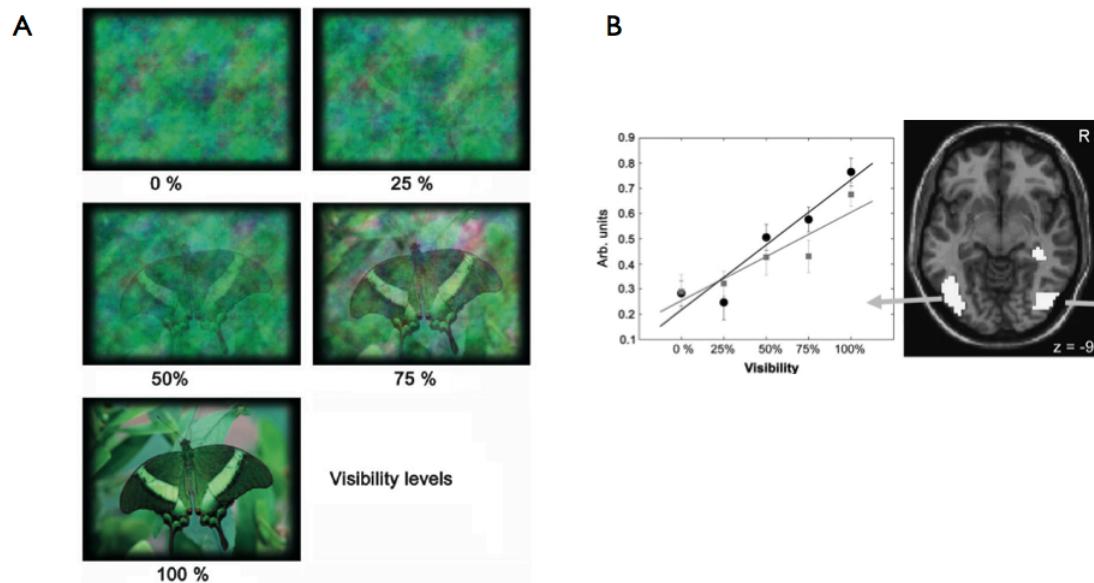
Figure 1.2: (a) Visibility levels of visual stimuli with five levels of scrambling. (b) Increased activity in the LOC with higher object visibility. (Adapted from Rose, 2005, with permission from Oxford University Press)

presentation of the textures revealed no such effects. Based on these results, a study by Rose et al. (2005) was able to show that this perceptual process can be modulated by top-down processes (Rose et al., 2005). In this experiment, the volunteers saw objects with different levels of visibility (see Figure 1.2a). Results clearly revealed increased activity in the LOC for increasing object visibility (see Figure 1.2b).

In summary, the LOC is known to be involved in the critical perceptual process of object perception (Malach et al., 1995; Kourtzi & Kanwisher, 2001; Grill-Spector et al., 1998) and this process can be modulated by top-down processes (Rose et al., 2005). Hence, the LOC is a well-studied brain area involved in visual object processing and is therefore selected as the brain region of interest for our BCI modulation.

1.1.1.2 Neuronal Oscillations involved in Visual Object Processing

Oscillations in the alpha and gamma band range are thought to play an active role in visual processing. These neuronal oscillations can be recorded from electrodes placed inside (invasive) and outside (non-invasive) the brain. Non-invasive methods allow a harmless acquisition of data without surgical interventions, whereas invasive methods require the implantation of intracranial electrodes. EEG is a common non-invasive method for monitoring brain activity recorded from electrodes placed on the

scalp. The voltage fluctuations registered by the EEG are summed activities of large populations of cortical neurons. Further non-invasive methods include magneten-cephalography (MEG), positron emission tomography (PET), functional magnetic resonance imaging (fMRI) and near-infrared spectroscopy (NIRS). However, compared to all other methods, EEG equipment is inexpensive, is well studied, provides high temporal but low spatial resolution and is therefore an efficient acquisition method for real-time BCI.

Neuronal oscillations occur at different frequency ranges in different brain areas and are associated with different functions. Historically, several types of continuous rhythmic sinusoidal EEG activity are defined (Kandel et al., 1991) (see Figure 1.3 for an overview):

- Slow cortical potentials (SCPs) are slow voltage changes (0.1 - 2 Hz) related to the overall preparatory excitation level of the cortex (Birbaumer et al., 1990). Negative SCPs are associated with increased cortical activity, while positive SCPs are associated with reduced cortical activity (Rockstroh, 1989; Birbaumer, 1997).

- Delta frequencies (up to 4 Hz) occur in deep sleep and in some abnormal processes.

- Theta frequencies (4 to 8 Hz) are associated with the early stages of sleep and the process of dreaming and play a functional role in memory processing (Guderian et al., 2009a).

- Alpha and mu waves (8-12 Hz) are characteristic for a relaxed, alert state of consciousness. Primary sensory-motor cortical areas (see Figure 1.1) often display alpha and mu activity, when they are not engaged in processing sensory input or producing motor output (Gastaut, 1952; Kozelka & Pedley, 1990). The activity is called mu rhythm when measured over somatosensory or motor cortex and visual alpha rhythm when measured over the visual cortex. Mu activity corresponds to motor preparation and imagination of movements (Pfurtscheller et al., 2006; Wolpaw & McFarland, 2004).

- Beta is the frequency range between 12-30 Hz. Beta frequencies are measured when listening and thinking during analytical problem solving, judgment and decision making (Kandel et al., 1991). Central beta activity (13-25 Hz) is recorded over the motor cortex. During actual movement and in particular during mental imagery of movement a decrease of mu and central beta activity
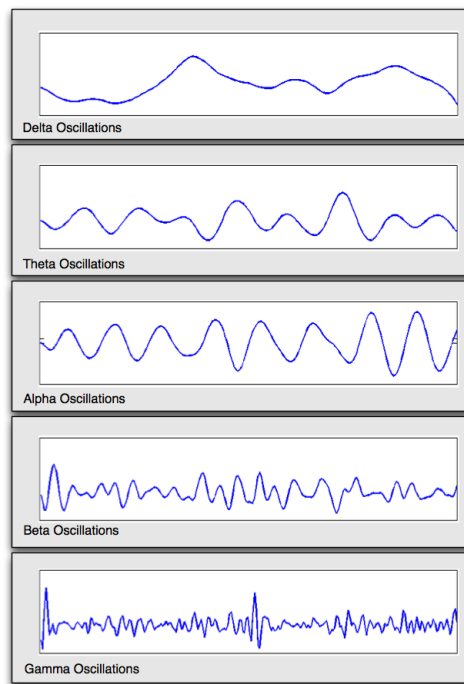
Figure 1.3: EEG oscillations in specific frequency bands.

is measured (Pfurtscheller & Silva, 1999; Neuper et al., 2005).

- Gamma band frequencies are separated into low gamma (30-45 Hz) and high gamma (45 to 100Hz). Gamma rhythms are associated with higher mental activity including perception, problem solving, fear and consciousness (Kandel et al., 1991). Oscillations in the gamma band play a functional role in visual processing (Tallon-Baudry et al., 2005).

Oscillations in the alpha band have been extensively examined in previous studies. Results have shown that alpha band oscillations have effects on different performance measures such as semantic working memory (Vernon, 2005) and mental rotation ability (Hanslmayr, Klimesch, et al., 2005; Vernon, 2005; Gruzelier et al., 2006; Zoefel et al., 2010). Several studies have used transcranial magnetic stimulation (TMS) to stimulate oscillations in the alpha band. These studies have found that parietal stimulation of the alpha frequency band enhances performance in visual mental rotation of three-dimensional cubes.

In contrast, several studies have shown that prestimulus alpha activity is differentially related to perception and memory performance. While high prestimulus alpha activity enhances memory performance (Jensen et al., 2002), studies have demon-
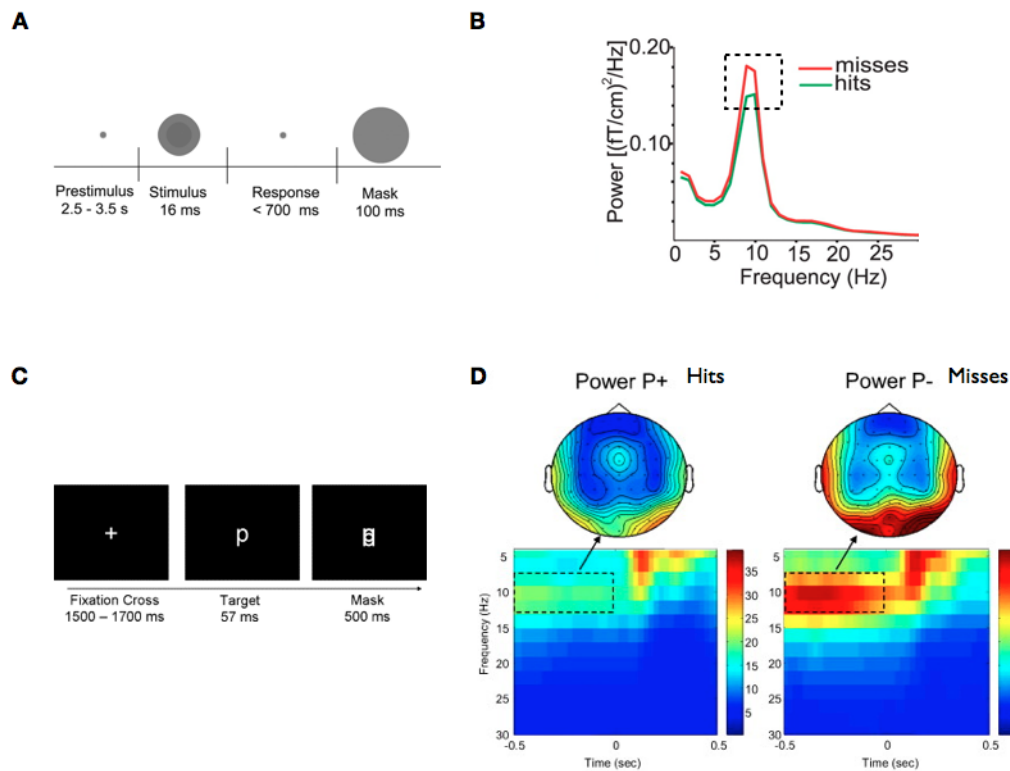
Figure 1.4: (a) Experimental task using two discs with different grey levels. Participants were instructed to press a button if a grey level difference between the two discs was detected. (b) Frequency distribution showing higher prestimulus alpha band activity (around 10 Hz (dashed box)) for undetected stimuli (misses) compared to detected stimuli (hits). (Adapted from van Dijk, 2008, with permission from the Journal of Neuroscience) (c) Experimental task with four possible letters as stimuli (p,q,b,d). Participants were instructed to detect the correct letter. (d) Time frequency plot showing increased prestimulus alpha band activity (around 10 Hz dashed box) for undetected letters (misses) and decreased prestimulus alpha activity for detected letters (hits). (Adapted from Hanslmayr, 2007, with permission from Elsevier)

strated an opposite effect on perception, as high prestimulus alpha activity impairs perception (Ergenoglu et al., 2004; Hanslmayr, Klimesch, et al., 2005; Dijk et al., 2008). In the study by van Dijk, i.e., volunteers were instructed to detect a difference in the grey levels between two discs (see Figure 1.4a). Results of the experiment showed that visual discrimination ability was decreased with increase in prestimulus alpha power changes. Participants detected the different grey values (hits) more often during decreased prestimulus alpha band (around 10 Hz) activity (see Figure 1.4b). In a further study by Hanslmayr (2007), volunteers were instructed to detect a target consisting of one of four letters (p, q, b, d), which was presented for 57 ms (see Figure 1.4c). The volunteer was then instructed to press one of four key
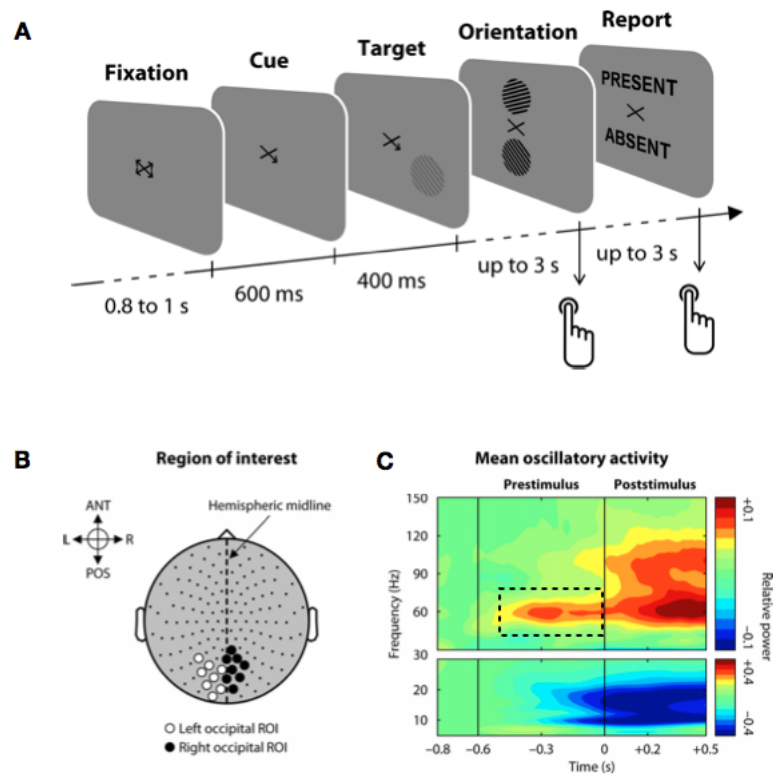
Figure 1.5: (a) Experimental design. (b) Region of interest in the LOC. (c) Time-frequency anlaysis of pre- and poststimulus activity. Results showing increased gamma band activity around 60 Hz in the prestimulus period (dashed box). (Adapted from Wyart, 2009, with permission from the Journal of Neuroscience)

buttons for the letter seen. Again, results revealed an increase of prestimulus alpha band activity for stimuli that were not detected (miss) compared to a decrease of prestimulus alpha activity for detected stimuli (hits) (see Figure 1.4d). In a recent study, occipital and parietal TMS at alpha frequency has been found to impair target detection in the visual field contralateral to the stimulated hemisphere (Romei et al., 2010). Hence, oscillations in the alpha band are discussed to play an inhibitory role on visual object perception (Dijk et al., 2008; Hanslmayr et al., 2007; Ergenoglu et al., 2004). Nevertheless, several studies also indicate an active functional relevance of alpha band oscillations for visual object processing (Babiloni et al., 2006; Klimesch et al., 2003; Hanslmayr, Sauseng, et al., 2005).

A further frequency band that is hypothesized to be of functional relevance to visual object perception is the gamma band. In particular, fluctuations in the gamma band before stimulus onset are assumed to influence the conscious detection of upcoming stimuli. A high level of gamma band activity in the visual cortex has been shown

to enhance visual processing (Wyart & Tallon-Baudry, 2009). In this experiment volunteers were cued to attend either to their left or right lower visual field (see Figure 1.5a). A low-contrast grating was then presented either at the cued or uncued location. Participants were instructed to first select the orientation of the grating and were then told to address whether a grating was presented during the trial. Results of the experiment revealed an increase of prestimulus gamma band activity in the visual cortex for detected as compared to undetected stimuli (see Figure 1.5b). In addition, the results were not due to attentional effects as attended stimuli as compared to unattended stimuli revealed no prestimulus gamma band effects.

Therefore, fluctuations in the gamma band before stimulus presentation appear to be important for the establishment of neural activity patterns that encode new input. This is in agreement with observations linking gamma band activity in general with perception (Tallon-Baudry & Bertrand, 1999), learning (Miltner et al., 1999) and memory (Sirota et al., 2008).

In summary, results of previous and present studies suggest that prestimulus alpha band activity has an inhibitory function on perception. However, in apparent conflict with these studies alpha band oscillations have also been suggested to enhance perception. Prestimulus gamma band activity is assumed to have an enhanced function on perception. Thus, in order to disentangle the functional relations of the different oscillations, a direct manipulation of ongoing alpha or gamma band oscillations using BCI would be of high interest. In the following section, we introduce the BCI method.

1.1.2   Brain Computer Interface

1.1.2.1   History of BCI - From Human Computer Interaction to BCI

Human computer interaction (HCI) describes an interdisciplinary field focusing on the interaction between humans and computer applications (Ebrahimi et al., 2003). The research field combines different disciplines including computer science, psychology, software engineering and ergonomic design. The interaction between humans and computer applications is based on input and output devices, which connect the human and the machine. Today's most common devices for interacting with computer applications include the mouse, keyboard, CRT or LCD screens. Apart from the traditional devices, several attempts have been made to exploit human senses

(e.g. vision, hearing, smelling, taste and touch) as a tool for HCI. These senses are detected or measured by different devices such as cameras (vision), microphones (hearing), olfactory (smell) or haptic sensors (touch). Extensive research has been done on HCI based on natural human actions such as e.g. vision based facial expression analysis (Fasel & Luettin, 2003; Yang et al., 2002), motion analysis (Hu et al., 2004; Sibert & Jacob, 2000), audio-visual automatic speech recognition (Potamianos et al., 2004) or haptic based analysis (Benali-Khoudja et al., 2004).

An emerging field of scientific interest seeks to take advantage of the development of unimodal techniques (in speech, audio processing, etc.) and combine them for human computer interaction (Jaimes & Sebe, 2007). During multimodal human-human communication, several modalities such as speech, gesture and voice are combined, which highly ease the understanding of communication. In multimodal HCI, the input modalities are usually a combination of human senses and computer input devices, which allow a variety of HCI interfaces. The most commonly combined modalities are speech with vision based technologies, such as speech-lip movement analysis systems (Chibelushi et al., 2002; Zhang et al., 2002; Potamianos et al., 2003). Other possibilities are combining head tilt and gesture with audio feedback to control a mobile device (Brewster et al., 2003) or using eye tracking with video, head tracking and hand motion (Yu & Ballard, 2004).

People with disabilities can also benefit from multimodal HCI research. Several research groups have worked on smart wheel chairs with voice recognition to execute commands (Simpson & Levine, 1997; Katevas et al., 1997) or facial gesture interpretation for wheel chair navigation (Duchowski, 2002). Others have developed multimodal systems with audio-haptic tools enabling visually impaired people to explore digital images using hearing and feeling modalities (Roth & Pun, 2003) or to explore tactile maps with verbal assistance (Habel et al., 2010).

The field of Brain Computer Interface (BCI) focuses on human brain and computer system interactions. A BCI method captures neurophysiological signals of the human brain and transforms these to simple input commands for communication and control of i.e. external devices. A direct interaction between the human brain and computer systems is of high interest in various research areas including HCI (Ebrahimi et al., 2003). In particular, BCI methods for patients with severe disabilities such as amyotrophic lateral sclerosis (ALS), brainstem stroke patients or muscular dystrophies, which disrupt the communication channel between neural pathways and muscles, receive high attention. Patients suffering from the for men-

tioned disorders usually lose the ability to move their legs, arms or body. A far more severely affected group of patients may additionally lose eye and respiration control, referred to as being in a complete paralyzed locked-in state (Borasio et al., 1998). Thus, these patients would benefit from advanced technologies that do not depend on healthy motor output pathways in order to communicate with their environment or to control external devices (Wolpaw et al., 2002).

A BCI method can provide a powerful tool for HCI systems, as it can be used and combined with other input modalities. The combination of BCI with other input modalities has been defined as Hybrid BCI by Pfurtscheller (2010) and is a new area of research.

1.1.2.2   Types of BCI

BCI approaches can be categorized into two different areas of application. The first area is focused on training volunteers to deliberately modulate brain activity. This approach is termed active BCI or neurofeedback (Zander & Kothe, 2011). Volunteers are continuously informed about a specific brain signal of interest presented as visual or auditory feedback information. Before training, volunteers are instructed either to increase or decrease the activity of interest. Through continuous neurofeedback training volunteers can learn to modulate and control brain electrical activity.

The second area is mainly based on the detection and recognition of relevant brain signals, which are evoked by external stimulation. Participants in experiments are i.e. exposed to visual stimuli that generate a desired signal (such as an evoked potential), which is detected by the BCI method (Kelly et al., 2005; Middendorf et al., 2000; Donchin et al., 2000). This BCI approach is defined as a reactive BCI and is based on advanced decoding algorithms in order to classify and interpret specific brain states (Zander & Kothe, 2011).

1.1.2.3   BCI Research

Several different neurophysiological signals with different specific features have been used in BCI research. In the following, we will outline existing studies in the research area of reactive BCI, active BCI and studies in which both forms are combined.

1.1.2.4 Research in Reactive BCI

Visual evoked potentials (VEPs) are small amplitude changes recorded in the brain signal evoked by sensory stimulation of a volunteer's visual field. Several studies have used VEPs to control the BCI method including the works of Vidal, Sutter and Middendorf (Vidal, 1973; Sutter, 1992; Middendorf et al., 2000). Vidal used VEP recorded over the visual cortex to determine the direction of eye gaze in order to move a cursor to the desired direction. Sutter used a brain response interface in which volunteers faced a video screen displaying letters. The BCI method used VEPs to detect the letters that the volunteer was gazing at.

The *P300* is a positive deflection in the EEG, which is evoked by auditory, visual or somatosensory stimuli about 300 ms after the stimulus is received. The P300 is typically evoked when volunteers attend to rare target stimuli presented within a stream of frequent standard stimuli. BCIs based on P300 evoked potentials uncover the volunteers choices by distinguishing between parietal cortex responses to the preferred versus non-preferred stimuli (Donchin et al., 2000; Piccione et al., 2006; Sellers & Donchin, 2006).

1.1.2.5 Research in Active BCI

In 1968 Kamiya reported the first neurofeedback training of EEG alpha waves. In a typical neurofeedback study, the volunteer sits in a room in front of a monitor and is instructed to deliberately modulate a specific frequency range represented i.e. as a bar on the screen. A successful modulation of the trained frequency range would result in an upward movement of the bar and a rather unsuccessful self-regulation in a downward movement of the bar.

The self-regulation in a neurofeedback approach has been shown to be of considerable value for clinical applications (Vernon et al., 2003). Neurofeedback has been applied for the treatment of attention deficit hyperactivity disorder (ADHD) (Lubar & Shouse, 1976; Fox et al., 2005), epilepsy (M. B. Sterman & Egner, 2006), anxiety disorders (Hammond, 2005), post traumatic stress disorder (Peniston et al., 1993), sleep disorder (M. Sterman, 1977) and schizophrenia (Gruzelier et al., 2006). ADHD is the most common psychiatric disorder in children and adolescents (prevalence: ranging from 2 to 29 percent; (Barkley, 2006)) characterized by inattention, impulsiveness and hyperactivity (American Psychiatric Association, 1994). Children

with ADHD typically show specific electrophysiological patterns such as increased theta and decreased alpha and beta band activity (Monastra et al., 2005, 2005). Therefore, in training protocols in neurofeedback therapy of children with ADHD the children are trained to decrease activity in the theta band and to increase activity in the beta band (Gevensleben et al., 2009). The treatment of ADHD with neurofeedback has found increased acceptance (Drechsler, 2011). A recent study examined the effect of neurofeedback treatment for children with ADHD with a large sample of participants and showed that 51% of the children showed a reduction of ADHD symptoms due to neurofeedback training (Gevensleben et al., 2009).

Nearly 50 million people currently suffer from epilepsy, according to the World Health Organization. The treatment of epilepsy with neurofeedback is based on increasing 12-15 Hz activity at the motor cortex (sensorimotor rhythm SMR) (M. B. Sterman & Egner, 2006; Lubar & Shouse, 1976). In a review paper summarizing epilepsy research, Sterman (2000) found that 82% of 174 patients had shown significantly improved seizure control, due to SMR neurofeedback training.

Neurofeedback in combination with a source-based low-resolution electromagnetic tomography (LORETA) method has been used to train brain oscillations in a selective brain region in the human brain. Initially, LORETA based neurofeedback was used in a study, in which volunteers were trained to enhance low beta (16-20 Hz) and to suppress low alpha (8-10 Hz) in the anterior cingulate cortex (ACC) (Congedo et al., 2004). Based on this study, a further study explored the effect of training in the ACC on anterior regions (Cannon et al., 2007).

1.1.2.6   Research in combined Active and Reactive BCI

Several studies have used a neurofeedback approach to train volunteers to regulate SCPs, mu and beta frequencies in order to control a BCI method (Pham et al., 2005; Nijboer et al., 2008). Recent studies have shown that people can learn to modulate mu and beta frequencies evoked by motor imagery of simple movements (hand or foot) to control output devices (Blankertz et al., 2010; Cincotti et al., 2008). The Wadsworth BCI group trained people with or without motor disabilities to learn to control mu or beta rhythm amplitude to move a cursor in one, two or even three dimensions (McFarland et al., 2010) on a computer screen.

Other studies have demonstrated that volunteers can learn to modulate SCPs in order to control a BCI (Kubler et al., 1999; Birbaumer et al., 2000). In addition,

SCPs have been exploited as a source of control to train patients with severe motor disabilities, such as ALS, to control a spelling device in order to communicate (Birbaumer et al., 1999, 2000).

1.1.3   Summary and Motivation

Gamma band oscillations in the LOC play a functional role in visual object processing. While prestimulus gamma band oscillations are hypothesized to improve perception, alpha band oscillations have been shown to impair perception. However, several studies also assume an active role of alpha band oscillation for visual object processing. Therefore, an experimental manipulation of alpha and gamma band oscillations could clarify the functional role of these fluctuations for visual object processing. We hypothesize that only increased prestimulus gamma band activity enhances the perceptual processing of subsequent visual stimuli, while increased prestimulus alpha band activity should not affect or even impair visual object processing.

The BCI is introduced as a method that can be used to train volunteers to modulate oscillations in various frequency bands. BCI applications can be divided into active and reactive BCI. Active neurofeedback systems can be used to train volunteers to modulate oscillations in different frequency ranges and reactive BCI can be used to trigger specific commands as specific frequencies are classified.

In this thesis, we developed a new non-invasive BCI method to modulate ongoing brain activity in the alpha and gamma band range in order to investigate their influence on visual performance. To this effect, we designed and implemented a combined active and reactive BCI method, with an integration of neurofeedback in BCI. The active BCI includes a neurofeedback method to train volunteers to deliberately modulate brain activity in different frequency bands and topographic areas. The reactive BCI includes signal preprocessing and feature extraction with an adaptive presentation of visual stimuli (i.e. stimuli in Figure 1.2a) within specified brain states. Thus, with this combined BCI method we aimed to manipulate brain activity in the alpha and gamma band in real-time in order to test for visual performance consequences during frequency manipulation.

In the next section, we outline the research questions, which we aimed to answer with our custom-designed BCI.

1.2   Research Questions

The main neuroscientific research question and hypothesis in this thesis is:

- **Increased gamma band activity in the visual cortex improves visual object processing**

If our first hypothesis is true we aim to test for the following hypothesis:

- **Improvement of visual object processing is specific to gamma band oscillations**

Since volunteers were trained to modulate brain activity in the alpha and in particular the gamma band range, several important aspects had to be considered during the development of the BCI method. Hence, the BCI method had to account for the following aspects:

- Artifacts: Oscillations in the gamma band are extremely susceptible to artifacts, such as eye or muscle movement, which occur in a common frequency range. In particular, microsaccadic eye movements can affect gamma band activity (Yuval-Greenberg et al., 2008). Thus, one has to make sure that the modulated gamma band activity is not affected or influenced by artifacts and represents pure neural activity.

- Design: Another consideration conserns the visual display of the neural feedback signal. The display should include all relevant information in a compact form to avoid distraction, allow a rapid extraction of the information and at the same time motivate volunteers to learn to increase gamma band activity.

- Trainability: The volunteers should be able to deliberately modulate oscillations in the gamma band throughout the neurofeedback training (Zoefel et al., 2010). A spectral effect should be found in the trained gamma band range.

In a series of experiments, the custom developed BCI method was applied to reveal the functional role of alpha and gamma band oscillations in the visual cortex. Within Experiments I to IV, the BCI method included

- neurofeedback training of a specified frequency range

- online estimation of the predefined oscillatory activity

- immediate presentation of stimuli triggered by the results of ongoing estimation

- customized experimental design

- offline detection of artifacts

- offline evaluation of trainability and accuracy of BCI training

In Experiment V, the BCI method was enhanced with

- online detection of artifacts

- incorporation of a source-based BCI method with LORETA. This combination allows the modulation of oscillatory activity in a selective brain region in the human brain leading to a more precise training. This source-based approach increases the accuracy of BCI training, as will be shown.

In the following, we will briefly introduce the experiments and the scientific questions they addressed.

1.2.1 Experiment I

The first experiment was designed to train volunteers in order to increase oscillations in the gamma band range (30 to 45 Hz) in the visual cortex.

Experiment I was designed to answer the following research questions:

- Can we apply a BCI method to modulate oscillations in the gamma band?

- Can volunteers learn to deliberately modulate oscillations in a predefined frequency range and in a selected area?

1.2.2 Experiment II

In Experiment II, the induced increase of gamma band activity was used to examine the impact on visual object processing as volunteers had to perceive an object presented in a noisy environment (i.e. stimuli in Figure 1.2a). The object perception task was performed during ongoing gamma band BCI training as images were shown either during phases of successfully increased gamma band activity or during phases of lower gamma band activity. If ongoing gamma band activity over the visual cortex is causal for an enhanced processing of visual stimuli, we expected that a high level of prestimulus gamma band activity should improve the perception of objects

in a noisy environment.

Experiment II was designed to answer the following research questions:

- Does the manipulation of gamma band activity lead to an improvement of visual performance?

- Do volunteers perceive and recall more images during high gamma band power as compared to low gamma band power?

1.2.3   Experiment III

In a third experiment, two different frequency ranges were trained. Using a different feedback display, the volunteers were now instructed to increase gamma band (30-45 Hz) as well as alpha band (8-12 Hz) oscillations. The aim was to examine a possible transfer from volunteers that had already learned a deliberate influence on the gamma band power to a more complex and new task. Trained volunteers from the previous experiments took part in this experiment that was designed to imitate a simple computer game in which a ball should be moved along a track.

Experiment III was designed to answer the following research questions:

- Can volunteers learn to switch between modulating different frequencies?

- Does the new display design have a positive motivation effect on the volunteers?

1.2.4   Experiment IV

Experiment IV was designed to test for the specificity of the feedback effect with a control group that was situated in an identical setting but without any influence on the displayed signal, thus without real feedback. The results from Experiment II showed an influence of the induced gamma band increase on visual processing during feedback. In Experiment IV, we tested for possible longer lasting improvements of visual skills induced by the feedback training as both groups conducted behavioral experiments before and after training.

Experiment IV was designed to answer the following research questions:

- Is the effect of gamma band increase specific to the BCI training or are equal effects found in a control group without BCI training?

- Is there an improvement of visual skills even after BCI training was stopped?

1.2.5 Experiment V

In this experiment, a source-based BCI method was applied to train volunteers to deliberately switch between modulating alpha (8-12Hz) and gamma band oscillations (40Hz) in a selective brain region in the visual cortex. As in Experiment II, noisy images were presented during BCI sessions of the alpha and the gamma band.

Experiment V was designed to answer the following research questions:

- Does an online feedback of eye and muscle artifacts improve BCI training?

- Can we use source information to train alpha and gamma band frequencies in a defined region?

- Which areas are affected topographically by alpha and gamma band training and are they restricted to the selected trained area?

- Do volunteers detect more images shown during gamma band or alpha band BCI training?

In summary, with our custom-developed BCI method, we aimed to manipulate oscillations in the alpha and gamma band frequencies in order to explore the effect of this frequency modulation on visual object processing.

Chapter 2

The Developed Brain Computer Interface

In this chapter we introduce the BCI method, which was designed and implemented in order to train volunteers to modulate alpha or gamma band activity in the visual cortex. First the experimental setup of the BCI is introduced, including a description of the utilized hardware (section 2.1) followed by a detailed description of the BCI setup (section 2.2). In section 2.3, we will outline how data was processed in Experiments I to V together with a detailed description of the signal processing and feature extraction methods. For the realization of our BCI method, several novel signal processing modules were developed and implemented in $C\#$, which are introduced in the following. In the last section (2.4) of this chapter, we will outline the importance of timing for a real-time BCI.

2.1 Hardware

2.1.1 Electrodes

Electroencephalography, as introduced in the last chapter, is applied to measure electrical activity from the scalp. The brain activity is measured with electrodes attached on an elastic brain cap placed on the volunteers head. These electrodes are usually made of gold and silver and are covered with a chloride layer. A centered circular in the electrodes allows the conductor of the experiment to fill in electrolyte
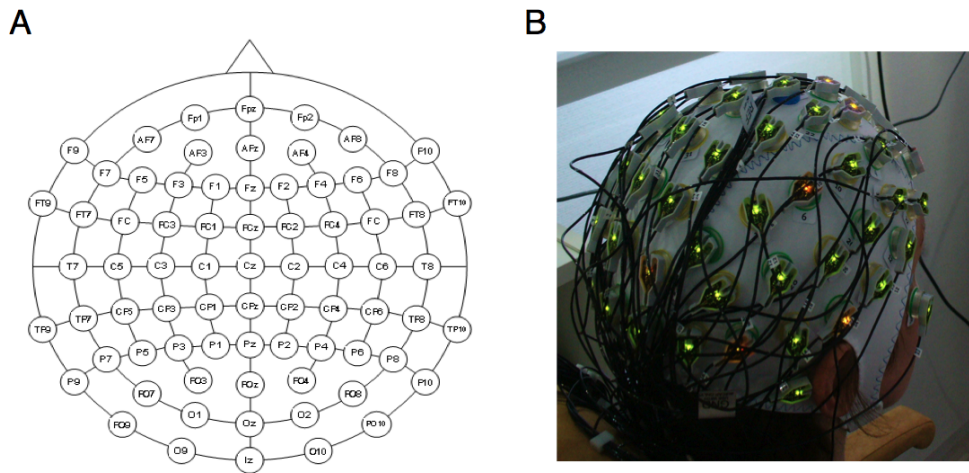
Figure 2.1: (a) Positions of electrodes and nomenclature of the corresponding EEG channels according to the international 10-20 system of electrode positions. (b) ActiCAP brain cap.

gel in order to attain an incessantly conducting connection between the volunteers head and the electrode plate.

Within the last years active electrodes have been introduced (ActiCAP, BrainProducts). ActiCAP combines active electrodes based on Ag/AgCL sensors with integrated noise subtraction circuits. The electrodes are attached on the brain cap according to a international standard 10-20 system montage (see Figure 2.1a). The standard montage handles up to 32 electrode positions and can be extended with additional electrodes by placing them in between the standard system. The brain caps can handle up to 128 electrodes and depending on requirements of an experiment referring to spatial resolution less electrodes can be used. The electrode positions and naming are referred to anatomical structures such as occipital (O), parietal (P), frontal (F), temporal (T) or the central (C) sulcus and numbering denote sagittal (anterior-posterior) lines.

EEG activity is derived bipolar, i.e. either the activation is measured between two electrodes or all electrodes are referred to a common reference electrode. Bipolar electrode arrangements function to suppress signals common to both electrodes in order to reveal the electric potential difference. The reference electrode is mostly placed on the nose or measured bipolar at the left and right mastoids. Further electrooculographic (EOG) electrodes are attached vertically (VEOG) and horizontally (HEOG) from below the left eye (supraorbital VEOGS and infraorbital VEOGI)

and from the outer canthi of the eyes (left HEOGL, right HEOGR), for detecting eye movements. In addition, electromyography (EMG) can be used as a technique for evaluating electrical activity generated by muscle activity. EMG is typically derived bipolar with two electrodes attached along the muscle. In our experiments two electrodes N1 and N2 were attached along the trapezius muscle in order to derive neck muscle activity.

2.1.2   Amplifier and PCs

As the electrodes are attached to the brain cap, the electrode wires are then connected to the corresponding amplifiers (BrainVision BrainAmp from Brain Products GmbH, Munich, Germany). The amplifier can be used to record EEG, EOG, EMG signals as well as evoked potentials with a sampling rate of 5 kHz per channel with a frequency up to 1 kHz. At this point the analogous voltage change of the channels is A/D converted and the acquired EEG data is transmitted to the recorder PC (see Figure 2.2). The recorder PC is a common Intel Pentium D machine with 3.4 GHz and 3 GB of RAM running Microsoft Windows XP. The feedback PC is a common Intel Pentium D machine with 3 GHz and 1 GB of RAM running Microsoft Windows XP.

2.2   BCI Setup

In a typical BCI setup the volunteer sits in a separate room and looks at a display monitor with a viewing distance of 1m as illustrated in Figure 2.2. A brain cap with mounted electrodes is then placed on the volunteers head and connected to the BrainProducts BrainVision amplifier. The electrical brain activity is measured and the analogous voltage change of all channels is transferred to the amplifier. The amplifiers perform an A/D conversion and the acquired EEG data at a sampling rate of 5 kHz is transmitted to the recorder PC. The BrainVision recorder software stores the data in raw format in a database. In addition, the recorder software acts as a Remote Data Access (RDA) server, which allows EEG data to be passed via TCP/IP to other computers in a network. In this process the recorder PC acts as the server and a second computer, the feedback PC, runs the corresponding client with the BrainVision RecView (Recording Viewer) software. The feedback PC (with the running RecView software) receives the data via TCP/IP and allows for the
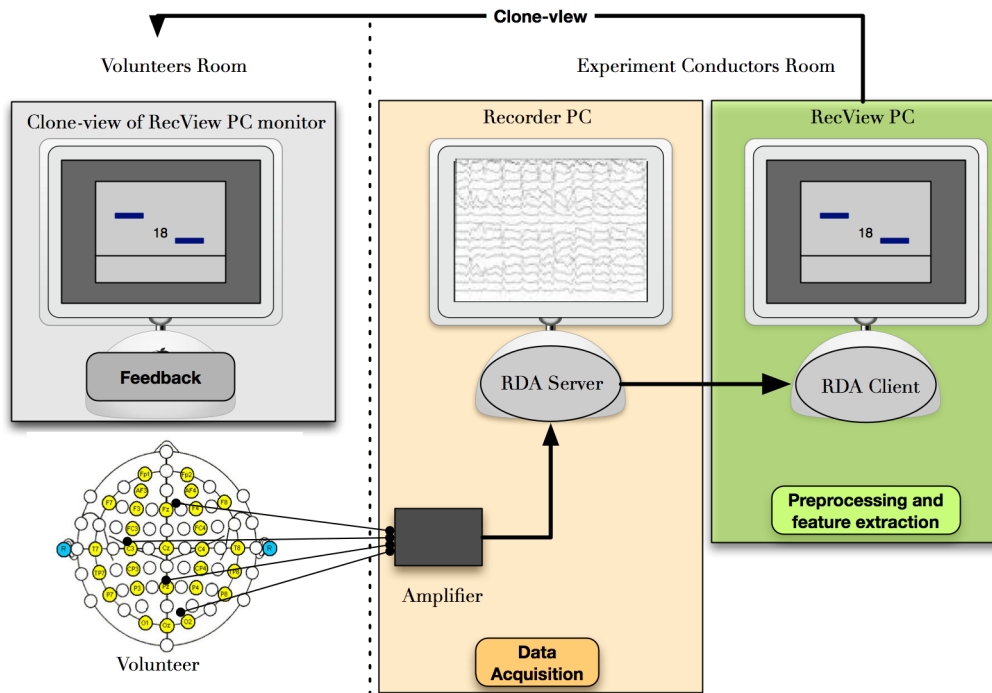
Figure 2.2: Abstract overview of the experimental setup. The volunteer is situated in a soundproof room facing the feedback monitor and wears the brain cap with the mounted electrodes, which is connected to the amplifier. The recorded EEG signals are first transferred to the recorder PC, where the data is stored for later offline analyses. The recorder PC acts as the server and transmits the data to the client feedback PC over the network.

incorporation of additional novel modules for data preprocessing, data classification and visual data presentation. As the incoming data is analyzed and classified the volunteer is visually informed about a successful manipulation of the desired signal of interest on the feedback monitor. A clone view is established for the experiment conductor in order to monitor the volunteer's performance.

2.3   Data Processing

2.3.1   Data Acquisition

A BCI method consists of three main components, namely data acquisition, data preprocessing with feature extraction and the visual feedback for the volunteer as illustrated in Figure 2.2. For the real-time processing of EEG data, an access to the continuously incoming data has to be established first. The recorder software
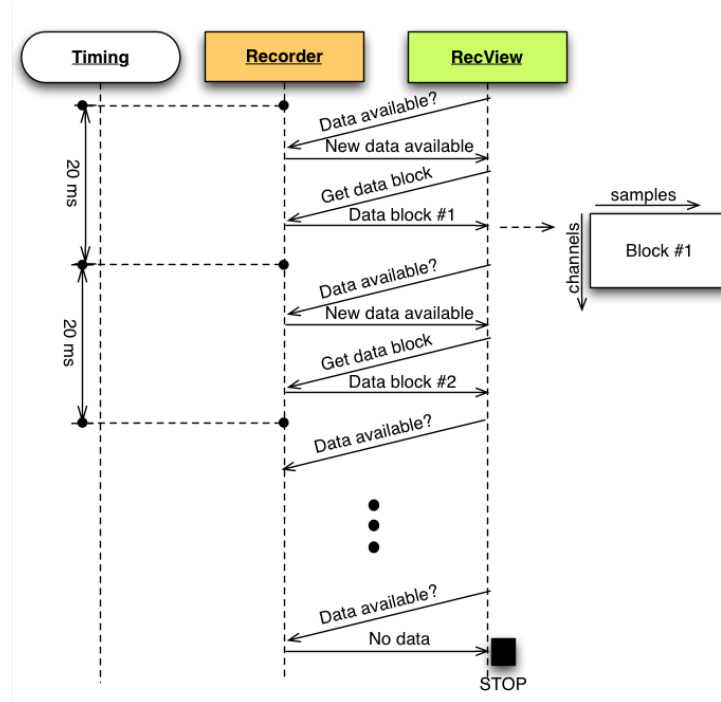
Figure 2.3: Timeline diagram of the TCP/IP protocol between the Recorder and the RecView software.

provides the specification of a TCP/IP protocol under which data is transferred to the RecView software as visualized in Figure 2.3. After a TCP/IP connection is established the RecView client is set up to receive data. If data is available, then the Recorder transmits one block of data at a time. A block of data contains a data matrix of dimensions channels-by-samples. The number of channels depends on the number of utilized electrodes for measuring EEG activity and the number of samples in a block depends on the subsampling rate set in the Recorder software. In Experiments I and II, i.e., we measured EEG with 28 electrodes with a subsampling rate of 250 Hz. With these settings the Recorder transmits a data matrix of 28 channels -by- 5 samples ($\frac{1000ms}{250} \times 5$) every 20 ms. Once the RecView software receives a block of data, the data matrix can be processed using signal preprocessing and feature extraction algorithms.

In this thesis, the RecView software was mainly used for data acquisition. The modular structure of RecView allowed for extending the software by incorporating additional algorithms. For the realization of our BCI method based on gamma band oscillations several novel algorithms were necessary. These algorithms can be integrated in the RecView software with the implementation of a collection of

Table 2.1: RecView interfaces.

Interfaces	Description
IDataIn	This interface is mandatory. It receives the data, setup information and status information from the previous module.
IDataOut	This interface is optional. If the results of the module are to be passed to RecView so that they can be viewed or distributed to further modules, this interface has to be implemented. It establishes the connection between the module and another IDataIn interface supplied by RecView.
IFilterParameters	This interface is optional. This interface allows to enter parameters, It displays a user dialog box on request.
ISimpleView	This interface is optional and can be used for the visualization of data.

RecView interfaces within a class (see Table 2.1 for an overview). These classes were developed using Microsoft Visual Express 2008 in the C# programming language. In RecView a module is defined to consist of a single class or several classes.

In the following sections we will introduce our custom-written modules (highlighted in red in Figures 2.4 and 2.8) and the interfaces which were implemented. Furthermore, we will outline how the data was preprocessed in order to conduct our experiments. The data processing steps in Experiments I to IV are similar and therefore summarized in section 2.3.2. In Experiment V, however, the processing of data differed to all other experiments (see Figure 2.8) and is therefore explained in detail after the description of signal processing in Experiments I to IV given in section 2.3.3.

2.3.2 Data Processing in Experiments I to IV

2.3.2.1 Fast Frequency Transformation

In Experiments I to IV we aimed to train volunteers to deliberately increase oscillations in the gamma frequency range (30-45 Hz). In order to analyze the incoming data for their gamma frequency content, the data had to be converted from the time domain into the frequency domain. The method applied is known as the Fourier Transform. The Fourier transform is based on decomposing signals into sinusoids. Jean Baptiste Joseph de Fourier (1768-1830) claimed that any continuous periodic signal could be represented as a sum of properly chosen sinusoidal waves. The discrete Fourier Transform (DFT) is the numeric form of Fourier Transform for signals
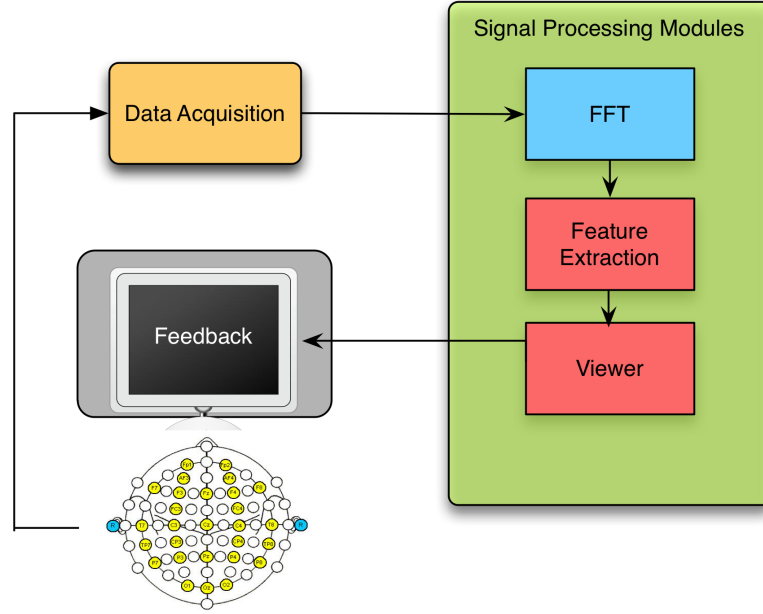
Figure 2.4: Experiment I to IV: Overview of signal processing modules. The modules in red represent novel custom-written modules, while blue colored modules represent software's modules.

defined at discrete time points and assumed to repeat in a periodic fashion. The discrete Fourier Transform is defined as:

$$F(u) = \sum_{x=0}^{N-1} f(x)e^{-j\frac{2\pi x}{N}u}, \quad u = 0, 1, \ldots, N-1 \tag{2.1}$$

where $f(x), x = 0, 1, \ldots, N-1$ is a discrete time signal in a finite interval represented by N samples.

The equations for calculating the real and imaginary part of the frequency domain are given by

$$\Re\{F(u)\} = \sum_{x=0}^{N-1} f(x)\cos\frac{2\pi ux}{N} \quad \text{and} \tag{2.2}$$

$$\Im\{F(u)\} = -\sum_{x=0}^{N-1} f(x)\sin\frac{2\pi ux}{N}, \tag{2.3}$$

respectively.

The Fast Fourier Transform (FFT) is a rapid and more efficient version of the DFT. In most cases and especially in real-time applications the computational impletation of the DFT is accomplished using the FFT algorithm (Cooley & Tukey, 1965). As the FFT module is present in the RecView software, the incoming data are first transmitted to the software's FFT module for the evaluation of the frequency spectra for Experiments I to IV (see Figure 2.4). As the algorithm is present in the RecView library, we will not enter into further algorithmic details. In short, Cooley and Tukey discovered that when the DFT of length N is a non-prime number, a divide-and-conquer method would allow for faster computation of the DFT. The FFT algorithm requires the number of samples in the signal to be a power of 2. The algorithm computes a DFT significantly faster with a maximum of $O(NlogN)$ operations where, by definition, the DFT would require $O(N^2)$ operations.

As the EEG data was subsampled with 250 Hz in the recorder software and the FFT algorithm requires a sampling number of a power of two for faster processing (such as 256 samples), the FFT module of RecView uses a process called zero-padding. The zero-padding simply fills the remaining spaces with zero-valued samples at the tail of the sequence. In our case it would zero-pad the 250 sample signal with 6 zeroes. The sharp boundary is softened by the windowing function of the FFT. The zero-padding with the windowing does not add new information, but rather increases spectral resolution (Park, 2010). The resulting spectra of the zero-padded version is an interpolated version of the original with 3 more frequency bins ($\frac{250}{2} = 125$ bins, $\frac{256}{2} = 128$ bins). Every second the FFT module returns a vector with as many complex valued Fourier coefficients as there are values in the input signal. Thus, applying an FFT on 2 selected channels the resulting vector consists of a real and imaginary component for each channel in each frequency resulting in a vector length of 512 (128 frequency bins × 2 channels × 2 real and imaginary components = 512).

As demonstrated in Figure 2.5, the data is saved in the vector in a multiplexed order, which has to be considered for further processing of data. The time-diagram in Figure 2.5 visualizes when the FFT module is called by the RecView software. Since 5 data samples are transmitted per data block, the FFT module caches 50 data blocks (50 × 5 = 250) and then computes the FFT algorithm. The resulting data vector is then transmitted back to RecView and can be processed by further modules.
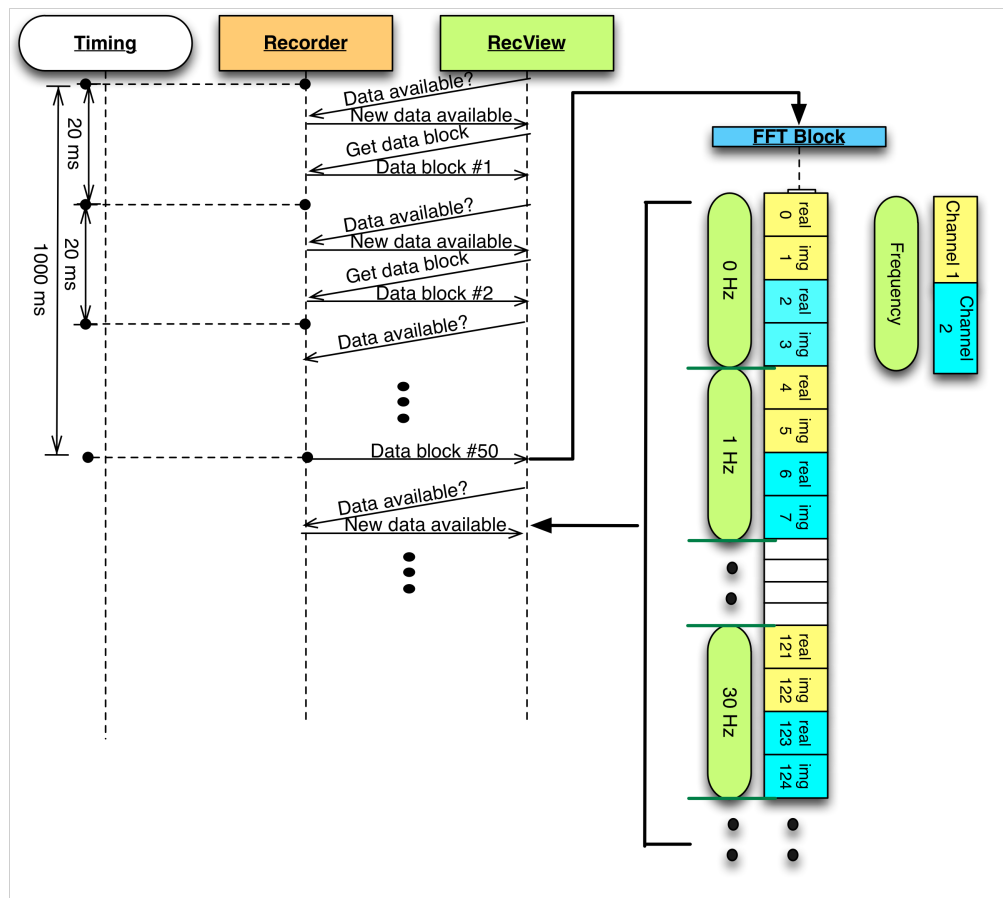
Figure 2.5: Resulting data vector after the FFT is applied. Example is drawn for 2 channels, as each channel consists of a real and imaginary component for each frequency.

2.3.2.2 Feature Extraction Module

The resulting data vector of the FFT module contains frequency information of frequencies from 1 to 128 Hz. In the first experiment we aimed to extract frequencies in the gamma band range from 30 to 45 Hz and to feed the gamma band content back to the volunteer. Therefore, a novel module `FeatureExtraction` was implemented to extract the relevant frequencies.

In Experiments I to IV, the proportion of gamma band activity in the total spectrum of the EEG in the channels PO7 (= channel1) and PO8 (= channel2) was extracted (in Experiment III, alpha band activity was extracted in addition to the gamma band activity). Channels PO7 and PO8 were selected as feedback electrodes, as these are spatially closest to the lateral occipital lobe which we aimed to modulate

(see section 1.1.1.1). Therefore, the relevant real and imaginary components of the gamma band from 30 to 45 Hz were selected from the resulting FFT vector. The real and imaginary pairs of a channel are converted to the amplitude by:

$$\|F(u)\| = \sqrt{\Re\left\{F(u)\right\}^2 + \Im\left\{F(u)\right\}^2} \tag{2.4}$$

where $\Re$ the real and $\Im$ is the imaginary component. The power is calculated as the square of the amplitude $\|F(u)\|^2$. Thus, for the extraction of frequencies $f_i = 30, 3, \ldots, 45$ Hz the power value in channels $c_j = $ PO7, PO8 for the relevant frequencies was calculated and added up:

$$\textsc{sumPower} = \sum_{i=1}^{15}\sum_{j=1}^{2}\|F(u)\|_{f_i,c_j}^2 \tag{2.5}$$

In all experiments, change in alpha or gamma band activity was calculated as the percentage change in band power during a certain interval compared to a reference measure. The reference measure was calculated during a passive period. A passive period was usually set for 10 seconds. In each second the sumPower for alpha or gamma band activity was calculated and a mean sumPower baseline value (meanPowerPassive) was derived at the end of the passive period. During feedback periods (10s), every second the percent change of power activity to the passive baseline (powerContent) was calculated.

Throughout the experiments the arrangement of passive and feedback periods changed (for an overview see Figure 2.7). Within the first two experiments a passive period (length 10s) was measured before each feedback period. A session consisted of 11 passive-feedback paired periods. In the third experiment a session consisted of two passive periods at the beginning followed by a single feedback period with variable length depending on the volunteer's performance. The fourth and fifth experiment started off with two passive periods followed by eight feedback periods. In all experiments except for Experiment III, a success display was presented after each feedback period. The success period was added to inform volunteers about their overall performance in modulating band power after each feedback period and in addition served as a short break. The success display in Experiment III was however, presented within the feedback period, not serving as a break, rather than to motivate volunteers to improve performance.
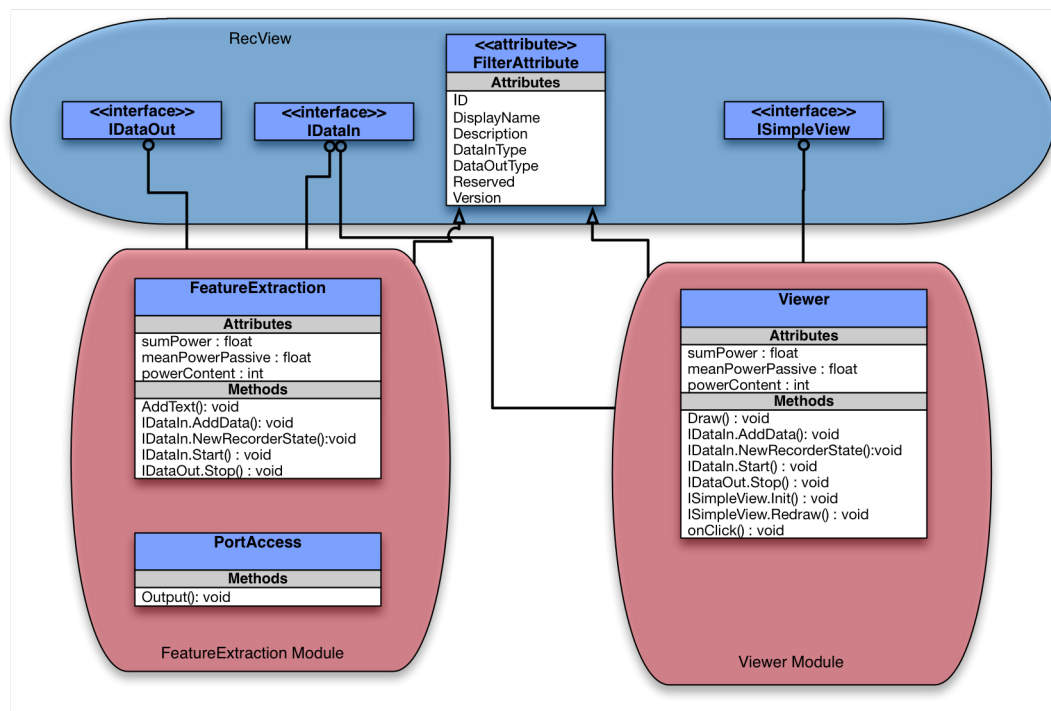
Figure 2.6: UML diagram of Experiment I to IV.

Interface

Our `FeatureExtraction` module implements a filter attribute in order to be identified as a module in RecView (see Figure 2.6). The `FilterAttribute` defines 7 elements. The first element defines the 128-bit globally unique identifier (GUID) of the module. The second and third element consist of the display name and a short description of the module. The following four elements define the input and output data types. In our module, we expect the input data from the FFT module in the frequency domain `DataTypes.FrequencyDomainComplex` and output data in the frequency domain `DataTypes.FrequencyDomain`. The last two parameters are reserved and set to 0.

Furthermore, the interfaces `IDataIn` and `IDataOut` were implemented in the `FeatureExtraction` class in order to access the data and to forward data to subsequent modules, respectively (see Table 2.1). The `IDataIn.Start()` method, i.e., can be applied for a modulation of channel names or channel information. The most relevant method was the `IDataIn` interface method `IDataIn.AddData()` which received the incoming data, i.e., the FFT vector. Within this method we implemented equations 2.4 and 2.5 in order to determine the POWERCONTENT.

The `PortAccess` class allows to send event markers via parallel port to the recording EEG PC. Hence, during important events, such as the presentation of an image an event marker can be sent and marked in the EEG recordings in order to ease later offline analyses.

In the following section, we will describe how the POWERCONTENT was visually fed back to the volunteer.
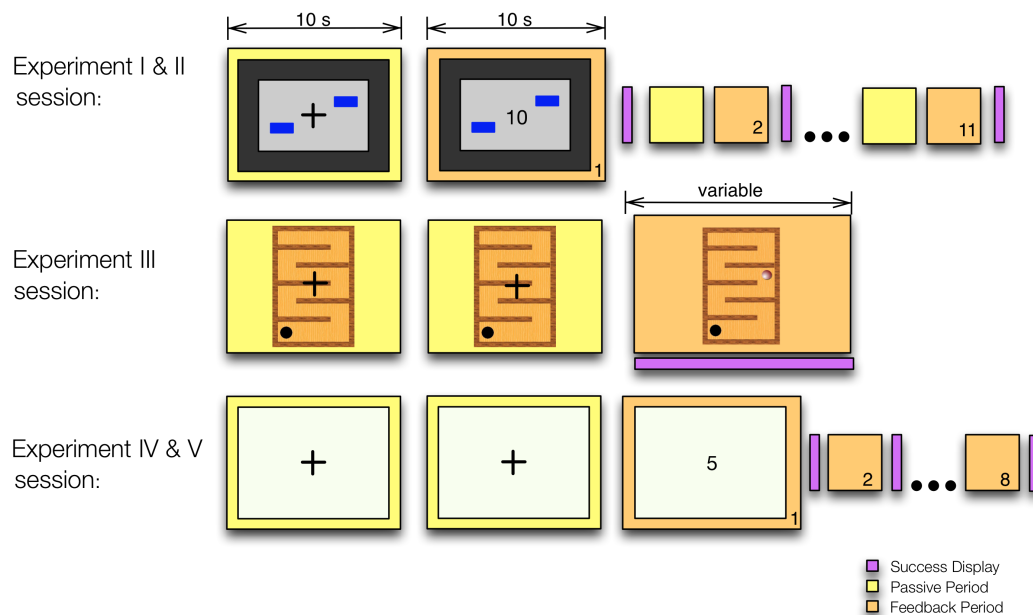
2.3.2.3   Viewer Module

Figure 2.7: Overview of passive and feedback period arrangement in a session of each experiment. The numbering of each feedback period represents the number of feedback periods in each session of the experiments.

For each experiment, we designed and implemented individual `Viewer` modules for the visual feedback of power activity (see Figure 2.7 for an overview). In Experiment I, i.e., the POWERCONTENT was visualized by a value at fixation during the feedback period. However, in Experiment III the POWERCONTENT was visualized by a ball in a labyrinth, which moved when increased power activity was measured. The visual feedback changed along the experiments as we aimed to include all relevant information in a compact form to avoid distraction and at the same time motivate volunteers to learn to increase alpha or gamma band activity. A detailed description

of the experimental procedure and volunteer's task for all experiments is outlined in the next chapter.

Interface

In the `Viewer` module we implemented the interfaces `IDataIn` and `ISimpleView`. The interface `ISimpleView` allows to visually present the incoming data. The method `Draw()` draws the visual feedback display and the method `onClick()` detects mouse key buttons. This was necessary during tasks in which volunteers were told to press a mouse button if an object was detected in an image. When and how these images were presented is outlined in the next chapter.

In summary, the change of alpha or gamma band activity is calculated in the `FeatureExtraction` module and visually presented by the `Viewer` module.

2.3.3   Data Processing in Experiment V

In Experiment V, a source-based BCI method is realized to train volunteers to deliberately switch between modulating alpha and gamma band oscillations in a selective brain region in the visual cortex. During BCI training we aimed to detect and inform volunteers about occurring online artifacts. In order to realize a source-based BCI method with artifact detection new custom-written modules had to be implemented and added to the RecView software. In Figure 2.8 an overview of the signal processing modules in Experiment V is presented. The `FrequencyFilter` and the `LORETA` module are present modules in the RecView software (colored blue) while the `Preprocessing`, `ArtifactDetection`, `FrequencyExtraction` and `Viewer` modules were specifically developed for this experiment (colored red). In the following, each module is introduced in the order in which the signal is actually processed and explained in detail.

2.3.3.1   Preprocessing Module

The `Preprocessing` module was implemented in order to preprocess selective channels for the `ArtifactDetection` module. This included the bipolar calculation of EOG channels for blink detection, the Neck channel for muscle artifact detection and the removal of amplitude drifts in EOG channels.
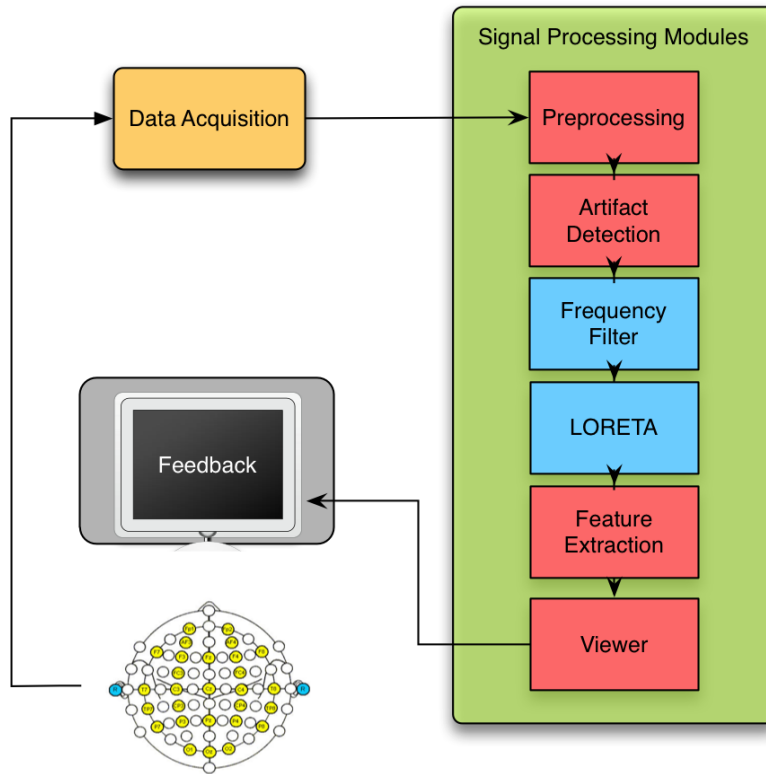
Figure 2.8: Experiment V: Overview of signal processing modules.

Bipolar Calculation

The module included the bipolar calculation of the new channels vertical EOG (VEOG), horizontal EOG (HEOG) and Neck channels (see section 2.1.1) which are derived as follows:

$$VEOG = VEOGS - VEOGI \tag{2.6}$$

$$HEOG = HEOGR - VEOGL \tag{2.7}$$

$$Neck = N1 - N2 \tag{2.8}$$

DC-Drift Removal

Before the data is processed to the `ArtifactDetection` module, we had to consider slow amplitude drifts in the recording of the EEG, known as **Direct Current** drifts

Figure 2.9: (a) Signal without DC drift. (b) Same signal with a DC drift starting at time 1000.

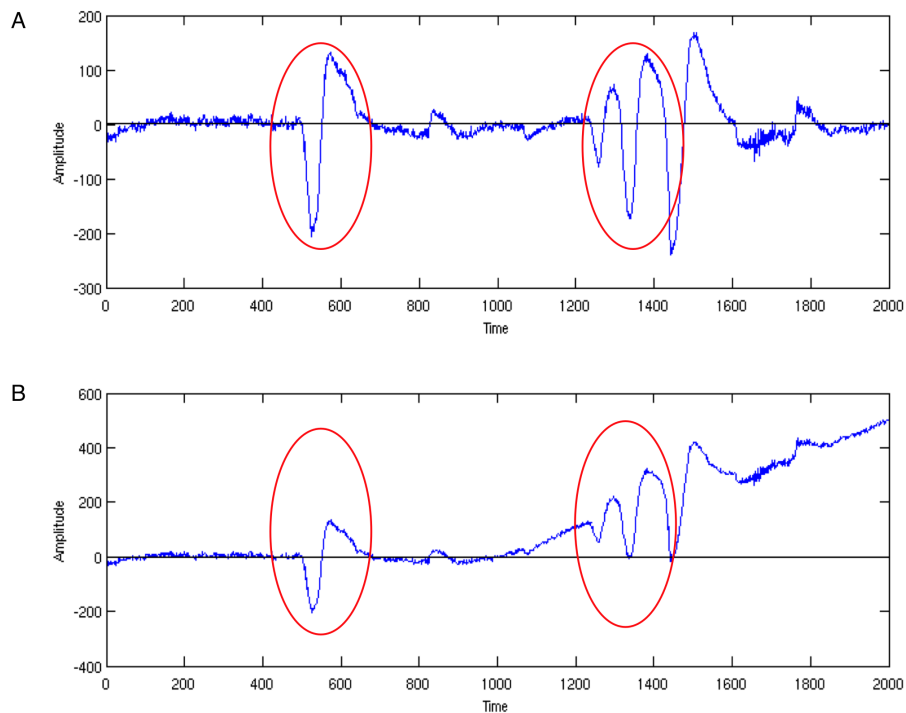(DC-drifts) (see Figure 2.9b for an example). The DC value is defined as the average value of the EEG signal around which the signal oscillates. A DC-drift is the change of the DC value over time. These drifts are influenced by electrode polarization as well as from thermal and electrochemical changes in the skin and in the electrolytes. Since the artifact detection algorithm in the following module is based on amplitude threshold levels in the VEOG, HEOG and Neck signals, the removal of DC-drifts is highly important. This issue is illustrated in Figure 2.9b. The red circled areas show typical blink artifacts. If a signal threshold of 50 μV is defined for blink detection the first blink in both signals would be correctly detected. However, due to the DC-drift the algorithm would incorrectly classify every following value in Figure 2.9b above 50 μV as a blink.

DC drifts are very slow oscillations in a low frequency range, usually smaller than 0.5 Hz. In order to remove DC drifts we implemented and designed a digital high-pass filter that allows frequencies higher than 0.5 Hz to pass and blocks lower frequencies.

Design of a High-Pass Filter

This section provides a brief overview of the theory behind the design of a high-pass filter and is based on (Milivojevic, 2009; Parks & Burrus, 1987; Rabiner & Gold, 1975; Mirta & Kaiser, 1993; Smith et al., 1997).

In an ideal high-pass filter with a cut-off frequency of $\omega_c = 0.5$ Hz, the passband frequencies $\omega \geq \omega_c$ would remain unchanged, while the stopband frequencies $\omega < \omega_c$ would be completely attenuated. The amplitude response (or magnitude frequency response) is defined as a function giving the gain of a filter at every frequency. The amplitude response of an ideal high-pass filter is visualized in Figure 2.10a. The ideal high-pass filter would have a sharp roll-off gain $= 0$ at the cut-off frequency and a flat amplitude response in the passband and the stopband. However, such ideal filters are impossible to realize in practice without having signals of infinite extent in time. Therefore, in practice a real-time high-pass filter has to be realized as an approximation of the the ideal high-pass filter.

The four major approximation methods encompass the Butterworth, Chebyshev, inverse Chebyshev, and Elliptic approximations. In comparison to all other methods, Butterworth filters are characterized by a maximally flat magnitude (no ripples) in the passband and stopband (see Figure 2.10a). The filter design usually begins with the definition of a normalized low-pass filter (cut-off frequency $\omega = 1$), which is then modified into a high-pass filter. The Butterworth approximation's magnitude response (gain) for a low-pass filter is defined as:

$$|H(j\omega)|^2 = \frac{1}{\sqrt{1 + \omega^{2N}}} \tag{2.9}$$

where N represents the filter order. As $N \to \infty$ we get the ideal low-pass response. Due to the magnitude flatness the Butterworth filter achieves a wide transition region from stopband to passband (slow roll-off), which can be improved by choosing a higher filter order (see Figure 2.10b). The higher the filter order, the steeper the filter gain falls. As maximally flat pass- and stopbands are important and less restrictions on roll-off characteristics are allowed, we apply the Butterworth filter.

Once the Butterworth filter is designed for the continuous-time case (analog filter), it is then converted into a digital filter. The advantage of using digital signals is due to the efficient and cost effective transmission of information. In order to design a digital high-pass filter the type of filter is selected first. Digital filters can
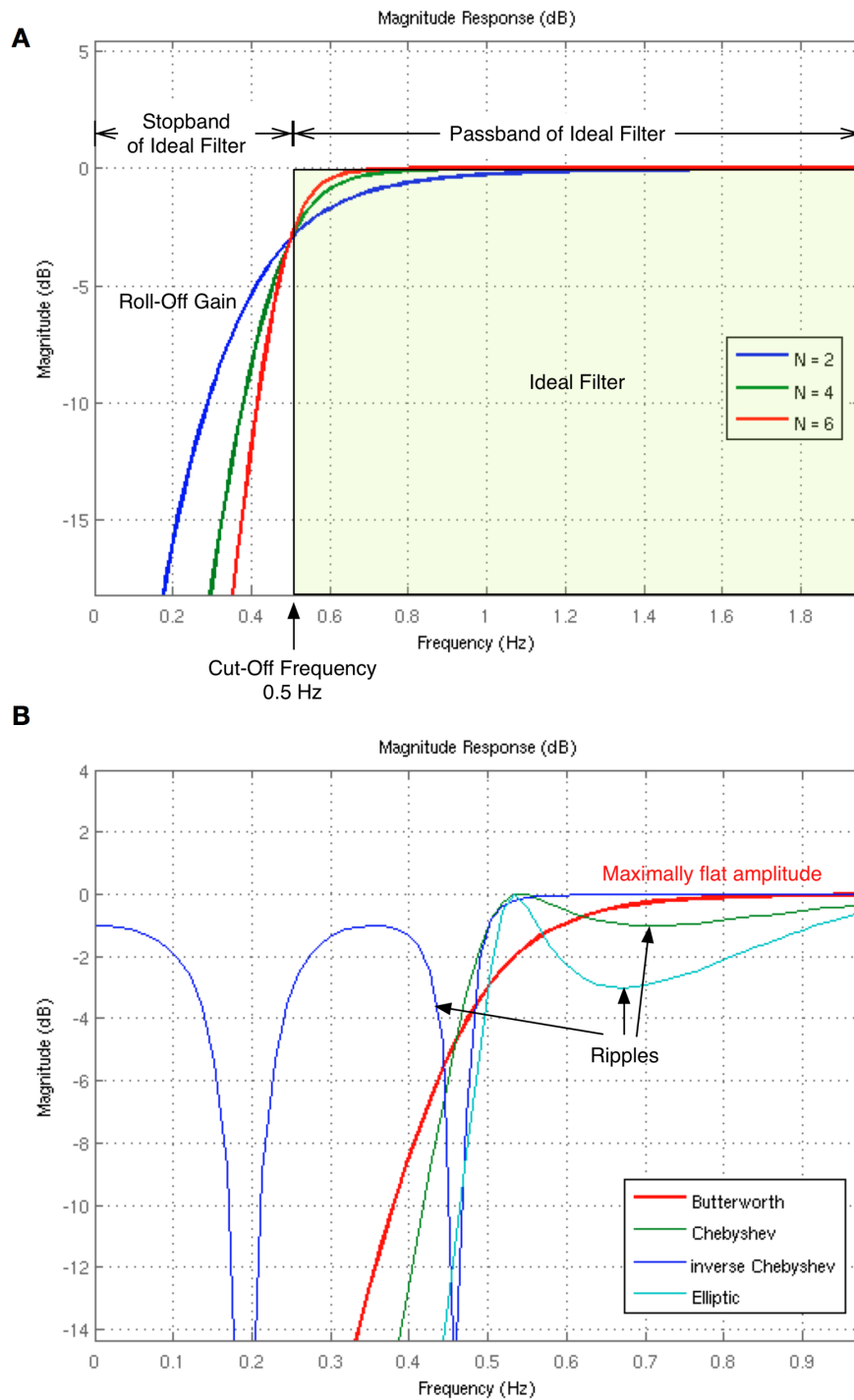
Figure 2.10: (a) The magnitude response of an ideal high-pass filter and the 2nd, 4th and 6th order Butterworth approximation for a cut-off frequency of 0.5 Hz. An interesting property of the Butterworth filter is given in the case of $\omega = \omega_c$, then the amplitude response is equal to -3dB, regardless of the filter order. (b) The magnitude response of the Butterworth, Chebyshev, inverse Chebyshev, and Elliptic approximations in comparison for a 4th (we selected the 4th order for visualization as the ripples can be nicely seen) order filter with a cut-off frequency of 0.5Hz.

be subcategorized into finite impulse response (FIR) and infinite impulse response (IIR) filters (Smith et al., 1997). An impulse is defined as a signal x with

$$x = \begin{Bmatrix} 1, & t = 0 \\ 0, & else \end{Bmatrix} \tag{2.10}$$

If the impulse is set as the input to a FIR filter, the resulting output impulse response of the filter has compact support, i.e., is non-zero for a finite period of time. However, for an IIR filter, the impulse response is non-zero over an infinite length of time. This is due to the definition of the IIR filter also known as a recursive digital filter, in which the output is the weighted sum of the current past samples of input. The IIR filter is defined as:

$$y(n) = \sum_{k=0}^{M} x(n-k)b_k - \sum_{k=1}^{N} y(n-k)a_k, \tag{2.11}$$

with M as the feedforward filter order with the current and past input samples, the feedforward coefficients b_k, the feedback filter order N with the past output samples, the feedback coefficients a_k, the input signal $x(n)$ and the output signal $y(n)$. In contrast to the definition of the IIR filter, the FIR filter does not include previous output values. The decision which filter to use is based on the characteristics of the filters. IIR filters are usually applied when the frequency response is of importance rather than the linear phase information. Compared to FIR filters, IIR filters require less memory and calculation to execute similar filtering operations (Smith et al., 1997). Hence, we implemented an IIR digital filter.

The b_k and a_k coefficients in equation 2.11 are determined based on the selected analog filter type and calculated within the design process of the IIR Butterworth filter which is described in the following and based on (Milivojevic, 2009; Parks & Burrus, 1987). In a first step a reference analog prototype filter, usually a low-pass filter, is designed. The resulting reference analog prototype transfer function $H_a(s)$ is then transformed to the appropriate type of analog filter, i.e., high-pass, band-pass or band-stop with predetermined passband and cut-off frequencies, resulting in $H(s)$. In the last step the analog filter is then transformed into a digital filter using a bilinear transformation (transformation of the continuous-time system to a discrete-time system), resulting in $H(z)$ which includes the coefficients b_k and a_k (Milivojevic, 2009). Based on the order of transformation the IIR filter design

process can be split into several steps as outlined in the following and described in (Milivojevic, 2009)

1. Setting of filter specifications:

- Type of filter: High-pass filter

- Sampling frequency $f_s = 250$ Hz

- Filter order $N = 2$. A second order filter response rolls off at -12 dB per octave (-6dB per order).

- Passband cutoff frequency $f_c = 0.5$ Hz.

- Selected analog filter type: Butterworth filter

2. Transformation of analog filter system from the time domain into the frequency domain: by using the transfer function $H_a(s)$ with $s = j\omega$ representing the complex frequency (from Laplace transform). Substituting $s = j\omega$ in equation 2.9 we get:

$$H_a(s)H_a(-s) = \frac{1}{1 + \left(\frac{s}{j}\right)^{2N}} \tag{2.12}$$

3. Determination of poles and zeros of the transfer function: For an easier explanation, the transfer function can be written in the form $H(s) = \frac{N(s)}{D(s)}$. The systems zeros are the s-values that cause the numerator $N(s)$ to become zero. The systems poles are the s-values for which the denominator becomes zero $D(s) = 0$.

The Butterworth reference filter has no zeros, $(N(s) = 1)$. The denominator $1 + \frac{s_k}{j}$ is equal to zero in the case of $(\frac{s}{j})^{2N} = -1$. With $e^{j\pi(2k-1)} = -1$ and $j = e^{j\pi/2}$ we obtain:

$$s^{2N} = e^{j\pi(2k-1+N)} \tag{2.13}$$

Solving the equation for s_k we obtain the poles of $H_a(s)H_a(-s)$ which can be presented in the complex unit circle at:

$$s_k = e^{\frac{j\pi}{2N}(2k+N-1)}, \quad k = 0, 1, \ldots, 2N \tag{2.14}$$

Since we restrict $H_a(s)$ to correspond to a stable, causal filter, its poles must all be

in the left half plane of the unity circle, i.e.

$$s_k = e^{\frac{j\pi}{2N}(2k+n-1)} \tag{2.15}$$

$$s_k = \cos\frac{\pi}{2N}(2k+N-1) + j\sin\frac{\pi}{2N}(2k+N-1), \quad k = 1, 2, 3, \ldots, 2N \tag{2.16}$$

The reference analog prototype filter transfer function is, regardless of its type (Butterworth, Chebyshev,..) given by (Milivojevic, 2009):

$$H_a(s) = H_0 \frac{\prod\limits_{k=1}^{M}(s - z_k)}{\prod\limits_{k=1}^{N}(s - s_k)} \tag{2.17}$$

where H_0 is a constant, z_k the zeros of the transfer function, s_k the poles of the transfer function, M the number of zeros of the transfer function and N number of poles. The transfer function of the Butterworth reference analog prototype filter has no zeros and is therefore defined as:

$$H_a(s) = \frac{1}{\prod\limits_{k=0}^{N-1}(s - s_k)} \tag{2.18}$$

4. Transformation of the Butterworth reference analog filter into a high-pass analog filter with the specified cut-off frequency ω_c. By performing the following transformation

$$s \rightarrow \frac{\omega_c}{s} \tag{2.19}$$

the Butterworth reference analog filter 2.18 is transformed into a high-pass analog filter with:

$$H(s) = \frac{1}{\prod\limits_{k=1}^{N}(-s_k)} \frac{s^N}{\prod\limits_{k=1}^{N}\left(s - \frac{\omega_c}{s_k}\right)} \tag{2.20}$$

and the analog prototype filter cut-off frequency ω_c is determined as:

$$\omega_c = \tan\left(\pi \frac{f_c}{f_s}\right) \tag{2.21}$$

5. Bilinear transformation of the analog filter to a digital filter:

$$s = \frac{1 - z^{-1}}{1 + z^{-1}} \tag{2.22}$$

Substituting the complex variable s in 2.20 we obtain:

$$H(z) = H_0(-1)^{N-M} \frac{\prod\limits_{k=1}^{M}(1 - z_k)}{\prod\limits_{k=1}^{N}(1 - s_k)} \left(1 + z^{-1}\right)^{N-M} \frac{\prod\limits_{k=1}^{M}\left(1 - \frac{1+z_k}{1-z_k}z^{-1}\right)}{\prod\limits_{k=1}^{N}\left(1 - \frac{1+p_k}{1-p_k}z^{-1}\right)} \tag{2.23}$$

With a more condensed form of the previous expression with the coefficients a_k and b_k we obtain:

$$H(z) = \frac{\sum\limits_{k=0}^{M} b_k z^{-k}}{1 + \sum\limits_{k=1}^{N} a_k z^{-k}} \tag{2.24}$$

The coefficients were precalculated and fed to equation 2.11 for the benefit of saving computational cost. For the outlined steps in the calculation of a 2nd order Butterworth IIR filter with a cut-off frequency of 0.5 Hz, see Appendix.

Interface

In the `Preprocessing` module we implemented the interfaces `IDataIn`, in order to get the data samples for preprocessing and `IDataOut`, in order to pass the preprocessed data to the next module. We derived three new channels VEOG, HEOG and Neck which are passed to RecView for further processing. An overview of the UML diagram of Experiment V is given in Figure 2.11.

In summary, in our custom-written `Preprocessing` module we prepared the relevant electrodes VEOG, HEOG an Neck in order to apply artifact detection algorithms on these channels in the following module. Therefore, we derived the bipolar measured VEOG, HEOG and Neck channnels. In addition we implemented an IIR Butterworth filter in order to remove DC-drifts in electrodes VEOG, HEOG and Neck.

2.3.3.2 Artifact Detection Module

During BCI training it is important to address non-cerebral sources of artifacts. Undesired artifacts can establish significant changes in the EEG and, thus, can change or manipulate brain signals (Ebrahimi et al., 2003; Fatourechi et al., 2007). Two groups of artifacts characterize a serious problem for neurofeedback applications: electrical activity generated by muscle contraction in jaw, neck or shoulders (EMG artifacts) and activity generated by eye blinks, eye movements (EOG artifacts) or microsaccades. In the custom-written `Artifact Detection` module we implemented three artifact detection algorithms that constantly monitored EOG, microsaccadic and EMG activity during the neurofeedback sessions. An overview of all detected artifact types is given in Table 2.2.

EOG
For the detection of eye blinks, the bipolar derived channel VEOG from the `Preprocessing` module was used. Thresholds for blink detection and eye movement detection were established in a pilot study with twenty volunteers. The average value of detected blinks over all volunteers was 140 μV with a standard deviation of 104 μV. Thus, the threshold was set at 50 μV to assure the detection of smaller blinks. Furthermore, blink artifacts are large amplitude distortions followed by negative voltage deflections. The negative deflections usually appear within a range of 300 ms around the positive peak. This a priori knowledge was used to improve the detection of blinks and extensive vertical eye movements. Thus, if the VEOG signal exceeds the threshold value and the difference between the maximum and minimum values exceeds 60 μV, a blink is detected.
For the detection of eye movement, the bipolar derived HEOG channel was utilized. While eye blinks produce spikes, vertical, horizontal and circular eye movements produce rather square shaped EOG (Krishnaveni et al., 2006). Therefore, we specified that if a value exceeds the threshold value (average amplitude = 64 μV, sd = 34 μV, threshold = 20 μV), all data within the following 40 ms has to be greater than the threshold value.

Microsaccades
A general concern has aroused towards the neural origin of gamma band activity in non-invasive recordings. A recent study has proposed that scalp recorded gamma-

band oscillations in parietal electrodes in EEG-data are influenced by microsaccades instead of neuronal processes (Yuval-Greenberg et al., 2008). In order to assure the neural origin of the measured gamma band increase and to estimate the influence of saccadic activity, we applied a recently proposed saccadic spike potential (SP) detection method (Keren et al., 2009), which allows an accurate detection of microsaccades directly in EEG traces without acquiring fast eye-tracking. Ocular artifacts such as the SP are most prominent in the peri-orbital electrodes when referenced to occipital or parietal electrodes (Boylan & Doig, 1989). Thus, for the offline detection of SPs, a further 'radial' electrooculogram channel (REOG) was derived as recommended (Keren et al., 2009). The REOG channel is defined as the average of all EOG channels referenced to the electrode Pz (see Figure 2.1 for Pz location):

$$REOG = \frac{VEOGS + VEOGI + HEOGL + HEOGR}{4} - Pz \qquad (2.25)$$

As suggested by Keren et al. (2009), the REOG channel was filtered with a Butterworth IIR filter of an order of 6, with a pass-band of 30-100 Hz for the detection of microsaccades.

The detection threshold was set to 2 standard deviations above the mean of the filtered signal. As the filtered signal was computed online we applied an online continuous standard deviation to avoid memory access (Welford, 1962; Knuth, 1998). Here, the standard deviation is refreshed with incoming online data from the passive and feedback periods. The success display period was not encountered for the calculation of the standard deviation as the period served as a break. After a short initialization phase within the passive period the standard deviation converges to a stable value. We exploited the saccade detection algorithm to determine the amount and mean amplitude of detected SPs in both passive and feedback periods to test for saccadic changes between the periods and across training. The REOG trace yields reasonable accuracy for saccades above 0.2°, which should be sufficient to detect saccadic activity in visual paradigms (Keren et al., 2009). During the success display volunteers were informed about their average SPs per second and SP amplitude in the two passive periods and in the passed feedback period. Thus, volunteers were informed if they exceeded the average SP amount or amplitude in the passed feedback period.

Table 2.2: Overview of detected artifact types for the custom-written `Artifact Detection` module.

Artifacts	Type	Detection	Channels
Eye Artifacts	Eye blinks	signal threshold	VEOG
	horizontal eye movement	signal threshold	HEOG
	vertical eye movement	signal threshold	VEOG
	Microsaccades	signal threshold	REOG
Gamma band specific artifacts	neural source of gamma activity	Variable threshold = gamma band activity in ROI channels	VEOG HEOG
Muscle artifacts	Neck muscle activity	Threshold = mean 70-80 Hz activity during passive baseline	Neck
	Jaw clenching	Threshold = mean 70-80 Hz activity during passive baseline	T7 T8

EMG

Most common sources of EMG are muscles, when closing, opening or clenching the jaw. These muscle contractions generate high gamma frequencies, which are measurable close to the temporal locations (T7, T8). Moreover, muscle contraction in the neck can generate high frequencies as well. To control for possible EMG contamination, channels T7, T8, and the bipolar derived Neck channel were subjected to sixth order Butterworth filtering in the band-pass 70-80 Hz. During the passive periods the average activity in the channels T7,T8 and the neck was calculated and set as a baseline for the following feedback periods.

All EMG, EOG and microsaccade algorithms were tested online and offline with identical results.

Interface

In the `ArtifactDetection` module we implemented the interfaces `IDataIn` and `IDataOut`. The attributes `blinkCounter`, `eyeMovCounter` and `saccadeCounter` returned a value of 1 if eye blinks, eye movements or saccadic eye movements were detected, respectively, and a value of 0 if no artifacts were detected. The band-pass
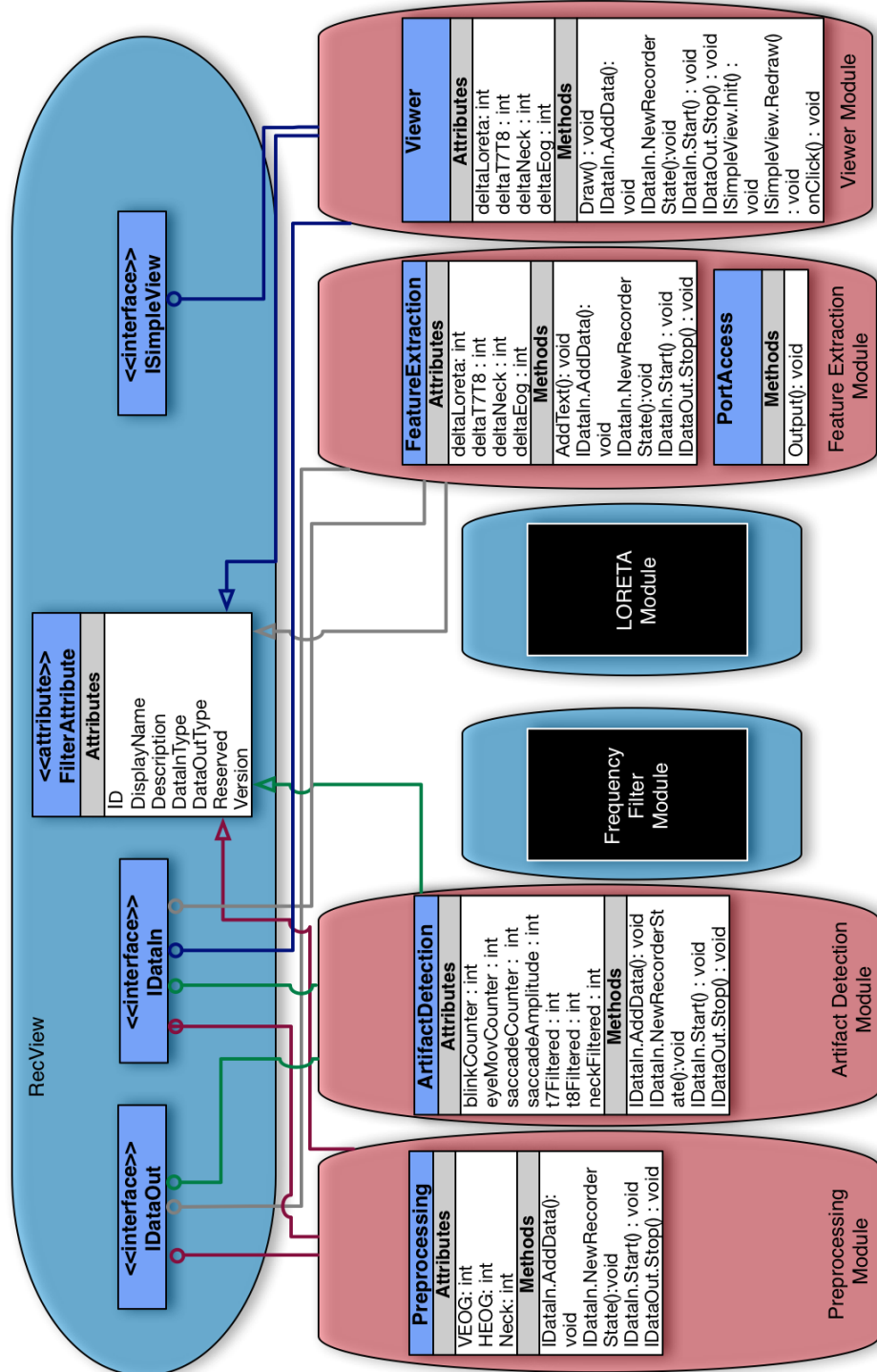
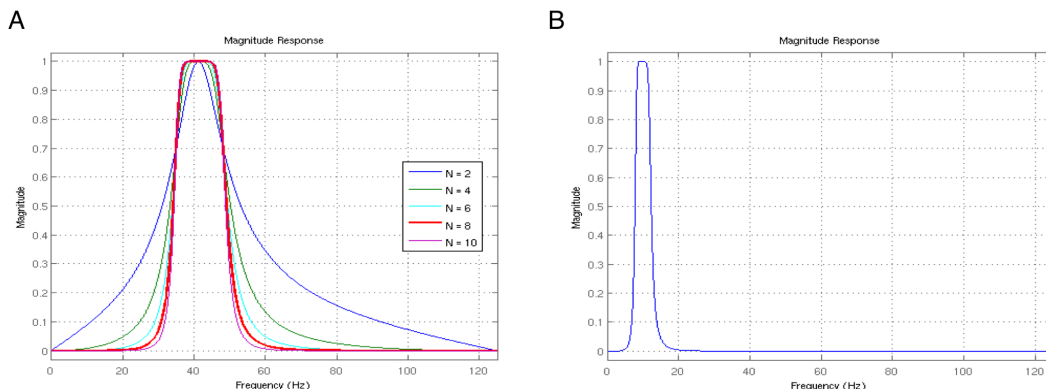Figure 2.11: UML diagram of Experiment V.

A

B

Figure 2.12: Frequency range settings in the FrequencyFilter module. (a) Magnitude response for the gamma band frequency range with orders 2, 4, 6, 8, and 10. (b) Magnitude response for the alpha band frequency range.

filtered channels T7, T8 and Neck were passed to RecView and were processed in the `FeatureExtraction` module (see Figure 2.11).

In summary, the `Artifact Detection` module was implemented in order to detect muscle and eye artifacts during online BCI training.

2.3.3.3   Frequency Filter Module

After preprocessing of the incoming data and artifact detection the `Frequency Filter` module of the RecView software is utilized. As we aim to selectively modulate oscillations in the alpha and gamma band range, we use the `Frequency Filter` module to extract the amount of alpha or gamma band activity in the recorded EEG. The `Frequency Filter` module implements an IIR Butterworth filter and allows for the selection of a specific frequency range of interest and the filter order (see section 2.3.3.1 for details on the Butterworth IIR filter). Hence, for the gamma band sessions the filter was set around 40 Hz (48 dB per octave, order 8) with a notch filter of 50 Hz (to remove 50 Hz power line interference). A filter order of 8 was selected in order to sufficiently limit the band-pass region within the gamma band frequency range (30-45 Hz) and to suppress other frequencies. Figure 2.12a illustrates the magnitude response for order levels of 2, 4, 6, 8 and 10 for the gamma band range. Higher orders would improve the frequency limitation, however the difference between the magnitude response of order 8 and order 10 is very small. Therefore, we selected a filter order of 8 in order to additionally save computational

cost, as higher filter orders are more cost intensive with $O(N)$ operations. For the alpha sessions the filter was set around 10 Hz (48 dB per octave, order 8) before transmitting the data to the `LORETA` module (see Figure 2.12).

2.3.3.4   `LORETA` module

Using electrical brain activity acquired from electrodes placed on the scalp, the low-resolution electromagnetic tomography (LORETA) method estimates the distribution of electrical neural activity in three-dimensional space (Pascual-Marqui et al., 1994). The LORETA localization method has been evaluated independently in several laboratories (Yao & He, 2001; Phillips et al., 2002a, 2002b; Fuchs et al., 1999) and has been extensively used in electrophysiological research (Pizzagalli et al., 2002; Mulert et al., 2002).

In Experiment V, we aimed to combine LORETA with the BCI technique in order to train gamma band and alpha band oscillations in the lateral occipital cortex (LOC). As explained in the previous chapter (see section 1.1.1.1), gamma band oscillations are important for visual object processing and the LOC is a functionally well defined neural area for this process (Malach et al., 1995; Rose & Buchel, 2005). It has been demonstrated that by combining LORETA with the BCI technique more spatially specific information can be derived (Congedo et al., 2004). Hence, instead of training the amount of alpha or gamma band activity in the electrodes PO7/PO8 as in Experiment I to IV, we aimed to train volunteers to directly modulate alpha or gamma band activity directly localized in the LOC, for a more precise training. The selected regions of interest (ROIs) were selected in the left LOC ([x,y,z] = [34, -73, -8]) and right LOC ([x,y,z] = [-34, -73, -8]) with a sphere of 12mm, encompassing a total of 7.2 cm^3 in each ROI (Figure 2.13). The choice of the ROI was determined by previous EEG studies (Rose & Buchel, 2005).

In the following subsections the mathematical background of the LORETA method (Pascual-Marqui et al., 1994) is outlined.

Inverse Problem
The LORETA method (Pascual-Marqui et al., 1994) is a mathematical approach dealing with the EEG inverse problem. The inverse problem is stated as: given N electrode scalp measurements (Microvolts) at time t estimate the source current density (Microamperes) within a three-dimensional solution space generating them. Since the number of electrodes N is typically much smaller than the number of M
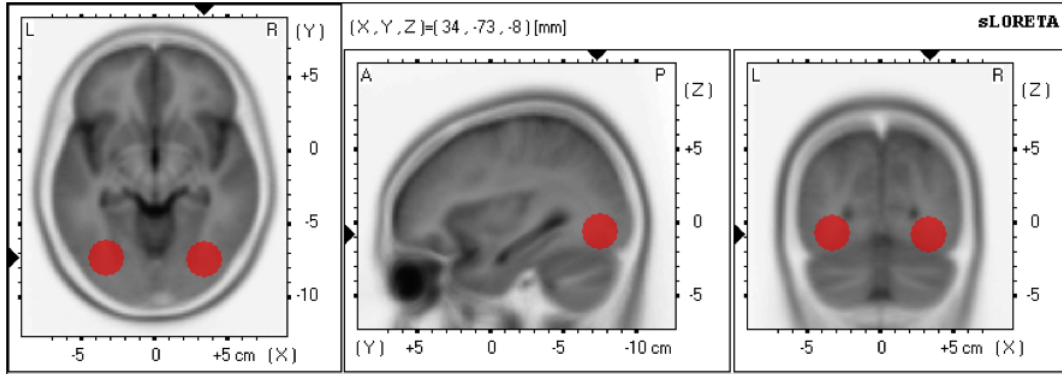
Figure 2.13: Selected ROIs in the right and left LOC for BCI training.

sources ($N \ll M$) the measurements do not contain enough information about the generators. Hence, there is an infinite number of different sources that can explain the measured electrical potential on the scalp (Pascual-Marqui et al., 1994). The inverse solution is therefore non-unique (Koles et al., 2001).

Forward Solution

If on the other way around however, the source within a 3D solution is known, the electrical potentials on the scalp can be determined with a unique solution, which is defined as the forward solution (Pascual-Marqui et al., 1994):

$$\Phi = KJ + c1 \tag{2.26}$$

where Φ is a vector with scalp potential differences measured by N electrodes with respect to a reference electrode; J is a $3M$-vector comprising the current densities at M sources. Here the factor 3 takes into account that current density is estimated in three components (dipole moments) x, y, and z, defining a three-dimensional space; M is the number of predefined points (voxels) in the brain volume, equally spaced and forming a cubic grid. **1** is a vector of ones. Constant c is a scalar reflecting the physical fact that potentials are determined up to an arbitrary additive constant (this is related to the choice of the reference electrode). K is the $N \times 3M$ lead field matrix (Burger & Van Milaan, 1948). and contains information about the geometry and conductivity of the head model (Weinstein et al., 2000).

Head Model and the Lead Field Matrix

The lead field matrix defines the contribution of each active source (voxel) at discrete locations to potential measurements on the scalp. Hence, the matrix entry value K_{ij}

at the voxel location j with the electrode i contains the estimated contribution of voxel j for the observed potential value at electrode i (see Figure 2.14).
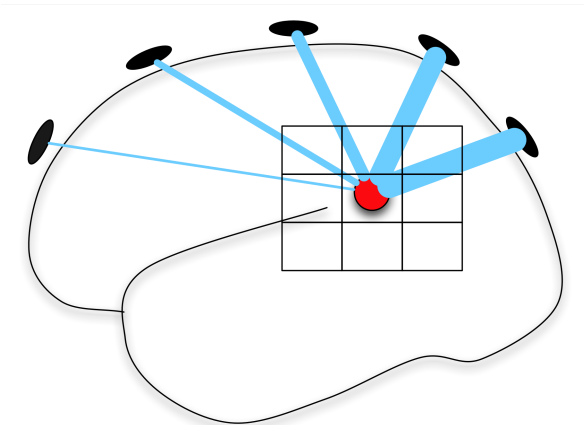

Figure 2.14: A schematic representation of the lead filed matrix with a source (red circle) in a voxel inside the brain. The thickness of the blue lines illustrate the contribution of voxel j on, i.e., five electrodes placed on the scalp (black ovals). Thicker lines illustrate a higher contribution than narrowed lines.

In order to solve the above equation, a realistic head model has to be applied in order to calculate the distribution of electric potentials for given source locations. The head model in the LORETA method uses a three-shell spherical head model representing the scalp, the skull and the brain, respectively. Using sphere shaped head models is computationally efficient. However, it lacks of modelling a realistic head shape. Therefore, the LORETA method incorporates the realistic geometry of the head and the brain with the registration of the three-shell head model to the Talaraich human brain atlas, available as a digital MR Image from the Brain Imaging Centre, Montreal Neurological Institute (Pascual-Marqui et al., 1994). The solution space was limited to cortical gray matter and hippocampus, as defined by the digitized Probability Atlas (Brain Imaging Centre, Montreal Neurological Institute). Given the neuroanatomical constraints, this yields a total of 2394 voxels at 7mm spatial resolution (distance between electrodes on the spatial surface).

Average Reference
In order to obtain source localization independent of the reference electrode, the potential measurements and the lead field are transformed:

$$\Phi \rightarrow H_N\Phi, \tag{2.27}$$

$$K \rightarrow H_N K, \tag{2.28}$$

where

$$H_N = I_N - \frac{1}{N} 1_N 1_N^T, \tag{2.29}$$

is called the average reference operator (Pascual-Marqui, 1999, 2002, 2007).

The scalp potential differences Φ are known, and the average lead field matrix corresponding to a three-shell head model is used (Ary et al., 1981). We seek to solve equation 2.26 for the unknown current density J. The inverse problem is stated as

$$\hat{J} = T\Phi \tag{2.30}$$

where T (termed as resolution matrix) is a 3MxN generalized inverse of the lead field matrix K. $\hat{J}$ denotes the estimated current densities. As described above the inverse problem is known to have infinite solutions that may satisfy equation 2.26.

Inverse Solution

In order to find a unique solution to the inverse problem, so-called regularization methods are applied in order to find the 'optimal' solution. The regularization methods include physiological or structural assumptions which add specific constraints, in order to approximate a solution to the inverse problem. The LORETA method uses regularization methods including the minimum norm solution (Hämäläinen & Ilmoniemi, 1994), the weighted minimum norm solution and maximal smoothness (Pascual-Marqui et al., 1994), which are explained as follows.

The Minimum Norm (MN) - The MN solution is based on the pseudo-inverse of the Moore-Penrose algorithm (Penrose, 1955; Barnett, 1990; Pascual-Marqui et al., 1994). This method solves the inverse problem by determining the solutions that minimize the Euclidean norm (the squared deviation of the data from a given model is minimized using a least-squares method). Hence, the MN approach selects the sources with the minimum overall current density within the brain (Koles, 1998) which best fit the actual data. The minimum norm solution to equation 2.26 is given by (Pascual-Marqui et al., 1994):

$$\hat{J} = T\Phi \text{ with: } T = K^T \{KK^T\}^+ \tag{2.31}$$

where $\left(KK^T\right)^+$ is the Moore-Penrose pseudo-inverse.

Weighted Minimum Norm (WMN) - Studies have shown that the MN solution favors superficial sources, which describes the fact that weak sources close to the electrodes have equal strength in activity as sources in deep locations (Pascual-Marqui et al., 1994). To compensate for the undesired bias, weighted minimum norm source localization has been suggested. To this effect, the columns of the lead field matrix are normalized to compensate for the lower representation of deeper sources (Jeffs et al., 1987).

$$\hat{J} = T\Phi \text{ with: } T = (W)^{-1} K^T \{KW^{-1}K^T\}^+ \tag{2.32}$$

Equation 2.31 is extended with the weighting matrix W (see Pascual-Marqui (1994) for more technical details). The minimum norm solution in 2.31 corresponds to equation 2.32 for W = I.

LORETA - Both the MN and WMN approach are based on mathematical operations, rather than physiological assumptions. The LORETA method is defined as a Laplacian-weighted minimum norm solution that is based on the physiological idea of neuronal synchronization (Gray et al., 1989). The measurement of EEG is only possible due to the fact that neighboring pyramidal neurons fire in synchrony (Hämäläinen et al., 1993). Using this physiological assumption in mathematical terms, the LORETA method forces spatial smoothness (Pascual-Marqui et al., 1999). Hence, the current density at one voxel is compared with that of its closest neighbors and set equal to the average current density of the neighbors. As a consequence of smoothing, the solution produces a blurred-localized image of a point source. Hence, the LORETA method localizes sources with a high temporal resolution and a low spatial resolution. Formally, the LORETA method corresponds to (Pascual-Marqui et al., 1994):

$$\hat{J} = T\Phi \text{ with: } T = \left(WB^TBW\right)^{-1} K^T \{K \left(WB^TBW\right)^{-1} K^T\}^+ \tag{2.33}$$

Equation 2.33 is extended with the discrete Laplacian operator B (see Pascual-Marqui (1994) for more technical details).

sLORETA - In 2002, Pascual-Marqui introduced an improvement of the LORETA method, called Standardized Low-Resolution Electromagnetic Tomography (sLORETA). Unlike LORETA, sLORETA is not based on Laplacian spatial smoothness to solve the inverse problem and does not compute current density but rather statistical scores (Pascual-Marqui, 2002). The method is based on the standardization of the minimum norm inverse solution (see Pascual-Marqui (2002) for more technical

details). Independent studies have shown that the sLORETA method has higher localization accuracy than LORETA or MN solution.

In the current study the LORETA method was used for the online calculation of the current source density in the LOC. Up to date, the online implementation of sLORETA neurofeedback has not been realized. However, we were able to calculate a few offline analyses with a free academic software that implements the sLORETA method.

Output of the `LORETA` *Module*
In the `LORETA` module of the RecView software the region of interest is selected in the LOC. Once the region of interest is set the resolution matrix T is calculated as given in 2.33. During BCI training the incoming data samples Φ are then calculated with the matrix T. The `LORETA` module estimates the average current density amplitude in the defined ROIs and presents the two ROIs as EEG signals over the time domain. Thus, a virtual channel is calculated for each defined ROI, in our case a virtual channel for the left LOC (LLOC) and right LOC (RLOC). The two new derived LORETA channels and all previous channels are then transmitted to the `Viewer` module.

In summary, the `LORETA` module estimates the average current density amplitude of alpha or gamma band frequency in the left and right LOC. The estimated values are then transmitted to the next module as data samples in the time domain in channels LLOC and RLOC.

2.3.3.5   Feature Extraction Module

In the custom-written `FeatureExtraction` module our objection was to feedback both the estimated activity in the LOC and the detected artifacts from the `ArtifactDetection` module. However, before we describe how this information was visually fed back (see following 'Viewer Module' section) we will first explain how the visual information was extracted.

As described previously, the `FeatureExtraction` module receives a data matrix of 5 samples x (58 channels (more channels in Experiment V) + LLOC channel + RLOC channel) from the `LORETA` module (see section 2.3.1). First, we summed up the values of the incoming data samples up to 250 data samples, which we will refer to as a segment in the following. The data was summed up, in order to feedback volunteers

performance with a time delay of a second. Hence, the volunteer's monitor was refreshed every second.

For each of the selected channels c (LLOC, RLOC, HEOG, VEOG, Neck, T7 and T8) the power value (not related to equation 2.5 in section 2.3.2.2) was calculated as the square of each incoming data sample x and summed up to N = 250 data samples:

$$y_c = \sum_{i=1}^{N} x_i^2 \tag{2.34}$$

Then, a mean power value was derived for $y_{loreta} = \frac{y_{LLOC}+y_{RLOC}}{2}$, $y_{eog} = \frac{y_{VEOG}+y_{HEOG}}{2}$, and $y_{t7t8} = \frac{y_{T7}+y_{T8}}{2}$. As the mean power values y_{loreta}, y_{eog}, y_{t7t8} and the power value y_{neck} in each segment are derived they are processed as visualized in Figure 2.15.

As in Experiment I to IV, the change in alpha or gamma band activity was calculated as the percentage change in band power during a certain interval compared to a reference measure. The reference measure was calculated during the passive period.

Passive Period-
During the passive period, the mean gamma (during gamma sessions) or alpha (during alpha sessions) power in the $\overline{y}_{loreta}$ and $\overline{y}_{eog}$ is computed and used as a reference measure for the following feedback periods. The $\overline{y}_{neck}$ and $\overline{y}_{t7t8}$ average power activity in the frequency range of (70-80) Hz is calculated as well in the passive period and set as measure reference for the following feedback period. However, anytime a blink or eye movement occurs during the passive period (as acquired from the Artifact Detection module), the corresponding segment (1 second) is removed to assure an artifact free baseline measurement. In addition, the session was stopped if more than 20% of the passive period contained artifacts.

Feedback Period-
During the feedback period the percent change $\Delta_c = \frac{100 \times y_c}{\overline{y}_c} - 100$ of the actual y_{loreta}, y_{eog}, y_{neck}, y_{t7t8} activity to the respective baseline is calculated (Δ_{loreta}, Δ_{eog}, Δ_{neck}, Δ_{t7t8}). The percent change in the LORETA channel Δ_{loreta} is visualized as a number on the feedback display (see Figure 2.7 Experiment V) for the volunteer if the following conditions are fulfilled:

1. The artifact module does not report any eye blinks or eye movement within the current segment.
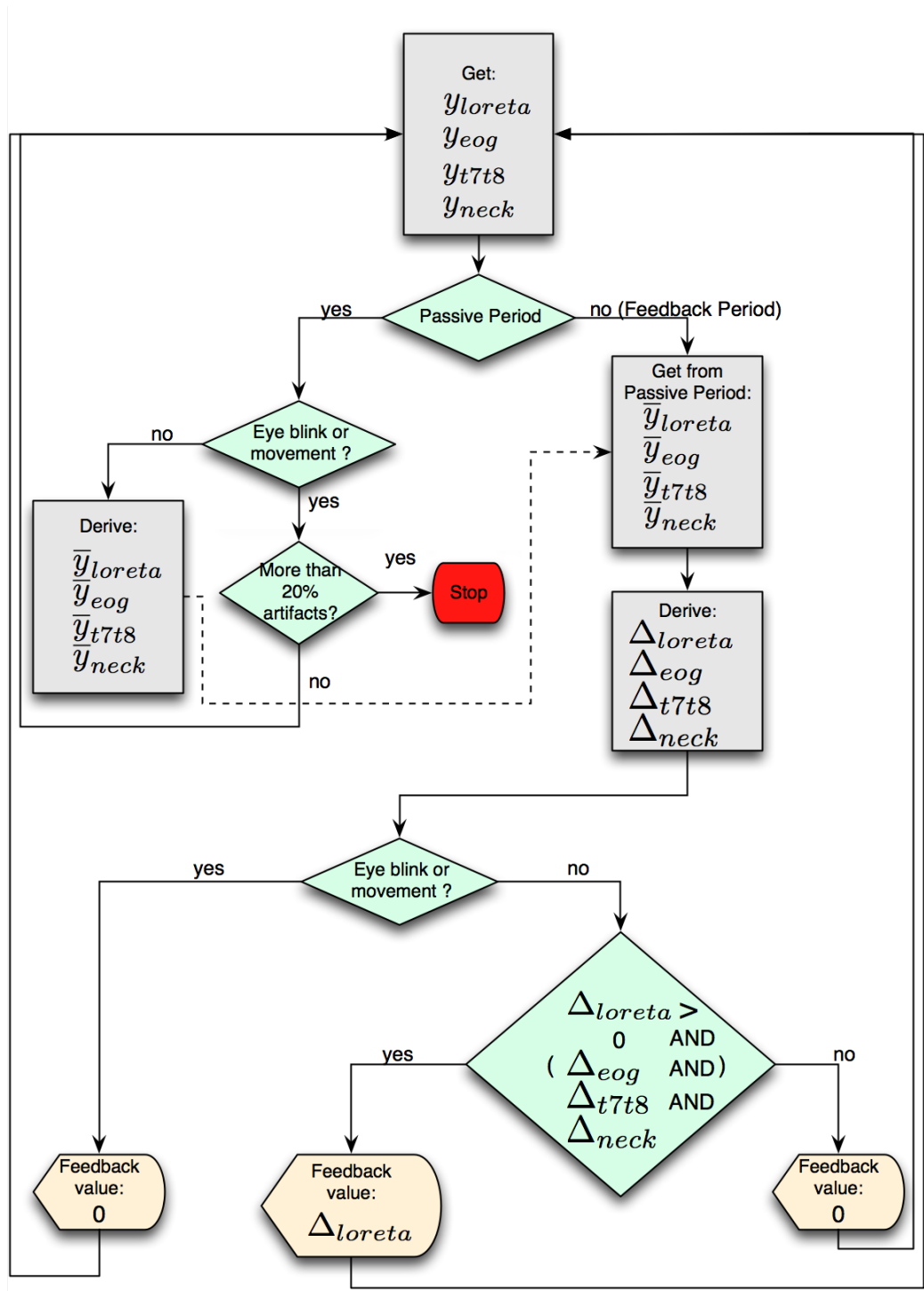
Figure 2.15: Visualization of data processing in Experiment V.

2. $\Delta_{loreta} > 0$

3. $\Delta_{loreta} > \Delta_{eog}$ - Only for gamma sessions, as gamma band activity in the EOG channels can effect gamma band activity in the LORETA channels.

4. $\Delta_{loreta} > \Delta_{neck}$

5. $\Delta_{loreta} > \Delta_{t7t8}$

If not all of the upper conditions are fulfilled, then the value 0 is presented as feedback.

Interface

In the `FeatureExtraction` module we implemented the interfaces `IDataIn` and `IDataOut`. The attributes `deltaLoreta`, `deltaT7T8`, `deltaEog` and `deltaNeck` represent the variables Δ_{loreta}, Δ_{t7t8}, Δ_{eog} and Δ_{neck}, respectively. (see Figure 2.11)
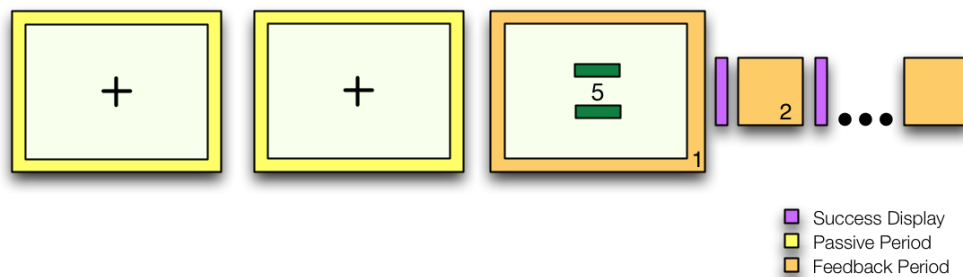
2.3.3.6 Viewer Module

Figure 2.16: Overview of passive and feedback period arrangement in a session of Experiment V.

In Experiment V, Δ_{loreta} was visualized by a value at fixation during the feedback period. In addition, two bars were added above and below the feedback value (see Figure 2.16). The bar above the feedback value represents EOG artifacts and the bar below the value represent the EMG artifacts. If no artifacts are detected within the current segment, both bars are green as visualized in the example in Figure 2.16. Hence, if all conditions are true as explained above, then Δ_{loreta} is visualized on the volunteers monitor. However, if EOG artifacts occur, the upper bar turns red and the value 0 is presented. Also, if EMG artifacts occur then the below bar turns
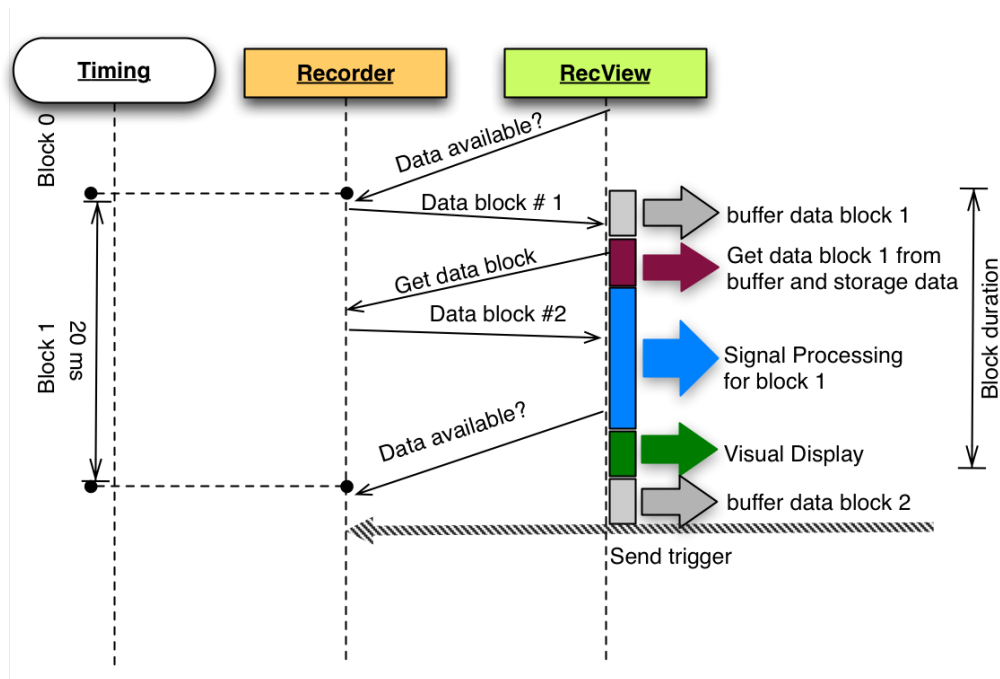
Figure 2.17: Timeline diagram for a real-time BCI (Adapted form (Wilson et al., 2010)).

red and the value 0 is presented. A more detailed description of the experimental procedure is outlined in the next chapter.

Interface

The Viewer module implemented the interfaces `IDataIn` and `ISimpleView` for the visual display of the experiment (see Figure 2.11).

2.4   Timing

Timing plays an important role for the development of a BCI method. A BCI method should process neural signals, extract specific features and provide visual feedback in real-time. However, the term real-time used in BCI studies is rather vague, as a minimal delay between signal processing and visual display is inevitable.

A BCI method is defined as a near-real-time process, if a block of data is processed before the next data block is ready (Wilson et al., 2010). This is visualized in Figure 2.17. As soon as RecView has buffered data block 1 (gray timeline) with the channels -by- 5 data samples (see section 2.3.1) the data is saved to the computer's memory (red timeline) and the signal processing and feature extraction for data samples

Table 2.3: Timing: Block jitter.

Modules	Block jitter (ms)
None	12.77
LORETA	14.57
Preprocessing	13.4
Preprocessing and Artifact Detection	12.96
Preprocessing, Artifact Detection, Frequency Filter	14.04
Preprocessing, Artifact Detection, Frequency Filter, LORETA	13.52
Preprocessing, Artifact Detection, Frequency Filter, LORETA, Viewer	12.7

in block 1 begins, as indicated by the blue area. When the feature of interest is extracted it is visualized on the volunteers monitor within the green timeline. After the visual display is presented, RecView immediately starts to wait for the next data block (block 3), while the data samples for block 2 are buffered (gray timeline).

Hence, in all experiments we assured that data processing was completed during the blue timeline before the next data block was ready. This was tested with two methods:

First, the RecView software provides a block indicator, which constantly informs whether the data blocks sent to RecView by the recorder PC have been completely processed or whether blocks have been lost during transfer. Data may get lost during transfer if RecView is unable to receive the data in time due to high loads or unfinished data processing.

Secondly, we measured the block duration by sending a trigger (time marker) to the Recorder via parallel port cable at the end of each block duration (see Figure 2.17). As the time markers were saved by the Recorder software, we were able to calculate the distance between the markers. In an ideal case, the block duration should last as long as the length of a data block (here, i.e., exactly 20ms). However, the time period between data blocks can be different than the actual block length due to inconsistencies in operating system timing, defined as 'timing jitter' (Wilson et al., 2010). The block jitter is calculated as the standard deviation across all block durations measured during a specific time period.

As several new custom-written modules were implemented in Experiment V we calculated the block jitter, in order to assure that signal processing was completed within the blue timeline. In all experiments the visual display of the volunteers was refreshed every second. Therefore, after each feedback block duration = 50 block durations (50 blocks ≈ 1000 ms) a trigger is sent to the recorder PC. First, we calculated the feedback block jitter without any modules, hence without any calculations regarding signal processing or feature extraction. Results showed a jitter value of 12.77ms with a mean feedback block duration of 1000ms, which we set as a reference measure (see Table 2.3). Successively, we added each of the modules in Experiment V and calculated the feedback block jitter for each additional module. Our results revealed similar jitter results for the added modules as compared to the reference jitter result or just the `LORETA` module demonstrating that our algorithms process data within the blue timeline and can therefore assure that no data blocks were lost. An overview of block jitter for selected modules is given in 2.3.

Chapter 3

Experimental Studies

In this chapter, the results of the 5 experiments will be presented. We conducted the experiments in order to answer the scientific questions as introduced in Chapter 1 section 1.2 and in order to test the custom-developed BCI method tailored to gamma band manipulation (for an overview see Figure 3.1). Experiment I, II and V have been published (Salari et al., 2012).

3.1 Experiment I: BCI Training of the Gamma Band Activity

In Experiment I, the volunteers were trained to intentionally increase the gamma band activity (30-45 Hz) over the occipital electrodes PO7 and PO8.

3.1.1 Volunteers and Procedure

Volunteers

Twenty healthy, right-handed volunteers with normal or corrected to normal vision participated in the BCI experiment (mean age 32 years, range 20-40, 10 females). All volunteers had no prior BCI experience. The experiment was approved by the ethics committee and volunteers gave written informed consent prior to the experiment.

Experiment	Trained Fre-quency Band	Measured Channels	Artifact Detection	Object Detection	Experiment Characteristics
Experiment I	Gamma	28	Offline	—	Gamma band BCI training
Experiment II	Gamma	28	Offline	During BCI	Object detection during BCI.
Experiment III	Alpha Gamma	2	Offline	—	New Game layout. BCI with two frequencies.
Experiment IV	Gamma	2	Offline	Before and after BCI	Integration of new game layout of Exp III. Control group to test specificity of feedback. Presentation of images before and after BCI training.
Experiment V	Alpha Gamma	58	Online	During BCI	Source based BCI (LORETA). Online detection of artifacts. Training of two frequency bands. Object detection during alpha and gamma band modulation.

Table 3.1: Overview of Experiments.

Data Collection

EEG was measured from 28 channels at standard locations (PO7, PO8, F3, F4, C3, C4, P3, P4, O1, O2, F7, F8, T7, T8, P7, P8, Fz, Cz, Pz, Fp1, Fp2, CP1, CP2, FC5, FC6, CP5, CP6, CPz) and the signals from channels PO7 and PO8 were used for the calculation of the feedback signal. The EEG of the other channels was used for later offline analyses. All 28 channels were referenced to linked mastoids. EOG and EMG channels were derived as described in section 2.1.1.

BCI Task Procedure

In Experiment I, a task period consisted of a passive period (10s) followed by a feedback period (10s) (see Figure 3.1). During both periods the volunteers screen displayed two bars (4x1.5 cm) situated 1.15° bilateral to a central fixation cross. The left bar represented a frequency range of 30 to 38 Hz and the right bar represented a frequency range of 39 to 45 Hz. The division within these two sub-bands was implemented to test for possible differences in the accessibility of the two sub-bands (no differences were found during subsequent analyses). A Fast Fourier Transform (FFT) was performed every second in channels PO7/ PO8 and the summed gamma power SUMPOWER (see section 2.3.2.2 equation 2.5) for the frequency ranges 30-38 Hz, 39-45 Hz and 30-45 Hz was computed online.

Passive Period - During the passive period, volunteers fixated on the central cross and were inactive, while the bars randomly moved upwards and downwards. This period was used to assess an actual baseline value of gamma band power (MEAN-POWERPASSIVE, see section 2.3.2.2).

Feedback Period - In the feedback period, the percentage change to the passive baseline was computed (POWERCONTENT (see section 2.3.2.2)) and fed back to the volunteer by the bars moving either above baseline for higher gamma band activity or below baseline for lower gamma band activity. In order to avoid eye movements due to the moving bars, the mean percentage change value of gamma band activity for both frequency ranges (the full gamma range 30-45 Hz) was displayed at the fixation point with a latency of 1s. In the following the gamma power change at fixation is termed 'gamma value'.

Volunteers were instructed to fixate the centre in both periods.

Success Display - The success of the feedback effort was presented after the feedback period as a bar graph indicating success (green) or failure (red) to increase the mean gamma band activity in the feedback period. The width of the bar represented the
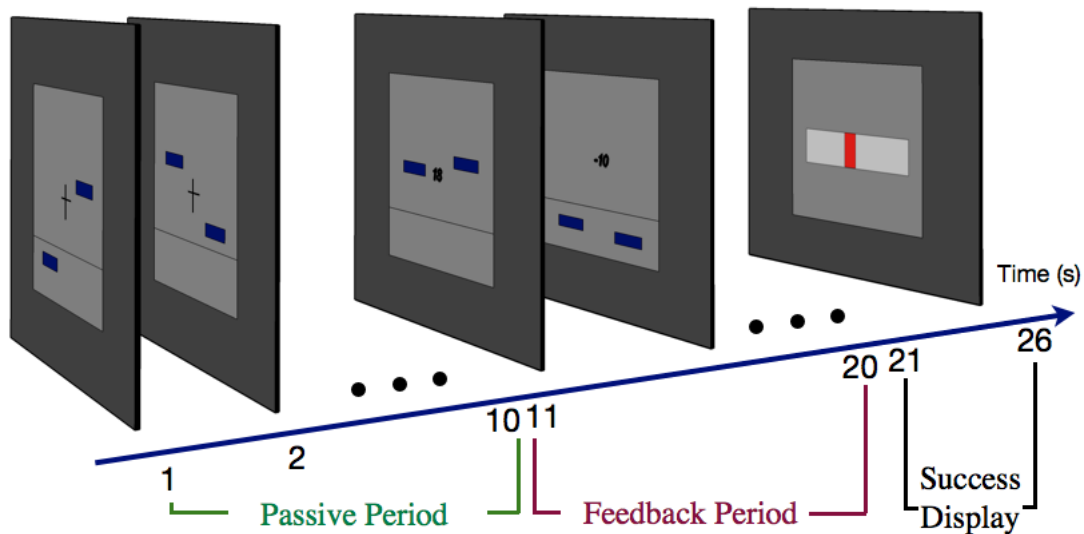
Figure 3.1: The BCI design in Experiment I. During the passive period (10 seconds) volunteers fixated the central cross and were inactive, while the bars randomly moved upwards and downwards. This period was used to assess an actual baseline value of gamma band power. In the feedback period (second 11-20) the volunteers tried to control the bars in order to increase the presented value at fixation. The line under the cross represents the mean gamma value in the passive period. Thus, volunteers tried to keep or move the bars above baseline, which is represented by feedback values above zero. The success of the feedback effort was presented after the feedback period as a bar graph indicating success (green) or failure (red) to increase the mean gamma power in the feedback period.

mean gamma value. Additionally, the success display served as a short break for the volunteers between each task period (duration 6 seconds). Four sessions with 11 task periods each were presented with short breaks between the sessions resulting in a duration of about an hour for the whole experiment. Each volunteer performed the feedback training once a week over a period of 3 weeks.

Data Analysis
For the calculation of the statistics we applied Student's t-test and analysis of variance (ANOVA). A detailed description of each of the applied statistical methods is outlined in the Appendix.

To evaluate the success of the gamma band training in each volunteer, the last training day was analyzed. In order to be included in further analysis, the volunteer had to increase the gamma value in the majority of feedback segments (more than 60% of segments (one segment = one second of feedback period) above the level of

the passive period). Furthermore, an increase across training was assumed to reflect successful training.

For the EEG offline analysis, data from all channels were segmented for each 10s passive and feedback period. To avoid effects evoked by the stimulus onset, the beginning of the period was set 1000 ms after the actual start. Each passive and feedback period was then divided into equally sized segments of one second. EEGs were corrected for blinks and eye-movement artifacts by subtracting both EOG channels weighted by their transmission coefficient (Gratton et al., 1983). For each feedback segment and the appropriate passive segment a FFT (Hanning window) was calculated.

To assess the influence of BCI gamma band training on the frequency spectrum, the change of power in each frequency from 0 to 124 Hz (divided in bins of 4 Hz) for the feedback periods compared to the passive baseline within the last training session at the channels PO7/PO8 was calculated. The significance of power change for each frequency bin to passive baseline was calculated by a t-test and corrected for multiple comparisons (Bonferroni, Figure 3.2c). The Bonferroni correction is used in this case, as several dependent tests are calculated (31 t-tests for every frequency bin). The significance level (alpha) for an individual test is calculated by dividing the error rate (= 0.05) by the number of frequency bins. Thus, with 31 frequency bins, the alpha level for an individual test would be $0.05/31 = 0.0016$. Hence, only individual tests with p<0.0016 are considered significant.

We exploited the saccade detection method algorithm offline (as described in Chapter 2, section 2.3.3.2) to derive the REOG channel (see equation 2.25) with a passband of 30-100 Hz. The detection threshold was set at 2 standard deviations of the mean filtered signal. We determined the amount and mean amplitude of detected SPs in both passive and feedback periods to test for saccadic changes between the periods and across training. Thus, we examined both parameters in all relevant analyses and estimated the saccadic effect on the feedback induced gamma band activity.

To assure that an increase of absolute gamma power in the feedback period was not due to the influence of eye movements or neck muscle activity, the gamma band change in electrodes EOG and muscle was calculated and the maximum change was subtracted from the mean gamma power change in electrodes PO7/PO8 before any statistical test. Thus, a possible transfer of gamma band activity from EOG or

muscle was eliminated.

3.1.2   Results

BCI Training of Gamma Band Oscillations

After three training sessions, 12 trained volunteers showed a clear increase in their ability to intentionally increase activity in the gamma band (more than 60% of feedback segments above baseline). The amount of feedback periods with a mean gamma power higher than in the passive period increased with practice (ANOVA, factor days, $F_{(2,22)}=3.74$, $p<0.05$). The offline analysis confirmed that volunteers were able to produce a reliably higher level of gamma band activity in the last training session as compared to the passive period ($t_{(11)}= 3.09$, $p<0.005$). In addition, the absolute power of gamma band activity clearly increased during the feedback periods of the last training session as compared to the first training session ($t_{(11)}=2$, $p<0.05$). The training success was further reflected in a reliable increase in the difference to the passive period (ANOVA, factor days, $F_{(2,22)}=12.22$, $p<0.001$, see Figure 3.2a).

The results of the training sessions clearly demonstrate that volunteers learned to intentionally increase neural activity in the gamma band over the visual cortex.

The recording of the additional EEG channels over the whole scalp allowed the calculation of the topographic specificity of the feedback effect. This analysis revealed that the increase in gamma band activity was limited to occipital electrodes and was not accompanied by a general increase of gamma band activity over the whole scalp (Figure 3.2b). This topographic specificity was accompanied by a frequency distribution that shows that the gamma band training mainly influenced higher frequencies, most prominent in the trained frequency range 30-40Hz ($p<0.001$). This effect extends to other high frequencies ($p<0.05$), but no differences were observed in lower frequencies (Figure 3.2c) (see Data Analysis section).

To assess the influence of saccadic activity on the increase of gamma band activity in the feedback period we applied a saccadic spike potential (SP) detection method to determine saccadic activity (including microsaccades) in both feedback and passive periods (see section 2.3.3.2). Within the EEG trace of this channel, the amount and mean amplitude of saccades was estimated in the baseline and feedback period to test for changes between the periods and across learning. Within the last training session no changes were found between both periods regarding the SP amount ($t_{(11)}=0.6$,
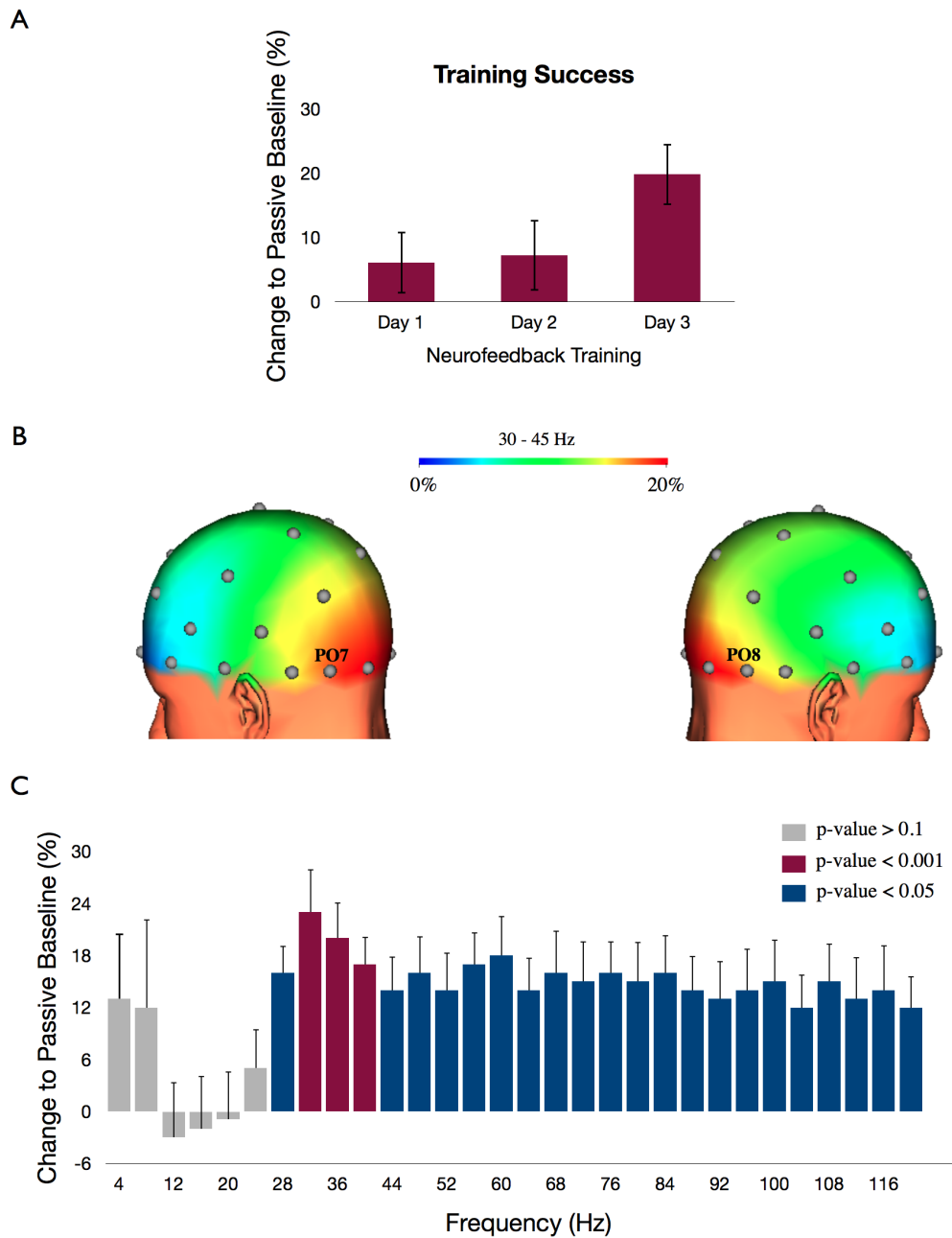
Figure 3.2: Topography and spectral specificity of gamma band feedback training. (a) Training success: Representation of the average change of gamma band activity (30-45Hz) in electrodes PO7/PO8 during the training period compared to the passive period across training days. (b) Topographic representation of the average change of the gamma band activity (30-45Hz) during the feedback period compared to the passive period within the last training session. The maximum change is localized at the electrodes over the occipital lobes that were used to calculate the feedback signal. (c) The percent change of power across frequencies from 0 to 124 Hz for the feedback periods compared to the passive periods within the last training session at the channels PO7/PO8. The different colors of the bars represent the significance of change to the passive baseline (gray bars: p-value >0.1, red bars: p-value < 0.001 (Bonferroni corrected), blue bars: p-value < 0.05). The frequency distribution shows that the training effects were most prominent in the frequency range from 30-40 Hz (p<0.001) and extended to higher frequencies but no effects were found for lower frequencies. (Salari et al., 2012)

n.s.) or SP mean amplitude (t(11)=1.18, n.s.). Furthermore, no changes were found across training during the feedback period (ANOVA, factor days, SP amount: F(2, 22)=0.31, n.s., SP amplitude: F(2, 22)=0.21, n.s.), demonstrating that the increased gamma band activity is not attributable too an increase of microsaccades but is due to neural activity.

3.1.3   Conclusion

Within the first experiment we aimed to examine whether a BCI method can be used to selectively modulate oscillations in the gamma frequency band. Results of BCI training clearly demonstrated that volunteers were able to intentionally increase neural activity in the gamma band over the visual cortex across training sessions. Although individual strategies differed, most volunteers reported using a visual imagery strategy (visualizing a concrete figure, object or number at fixation). As a next step, we examined whether increased gamma band activity has an influence on visual object processing.

3.2   Experiment II: Adaptive Stimulation during Different States of Induced Ongoing Gamma Band Activity

In Experiment II, the BCI induced variance of gamma band activity in the visual cortex was used to examine the effect of prestimulus gamma band activity on a task in which volunteers had to perceive visual objects embedded in noise. While the amount of gamma band activity was estimated online, images were presented in states of high or low levels of ongoing gamma band oscillations. The quality of object processing during increased gamma band activity was further assessed behaviorally by a surprise recognition task after the object detection task.

3.2.1   Volunteers and Procedure

Volunteers
Ten successfully trained volunteers from Experiment I participated in the object detection task of Experiment II (mean age 32 years, range 20-40, 4 females).
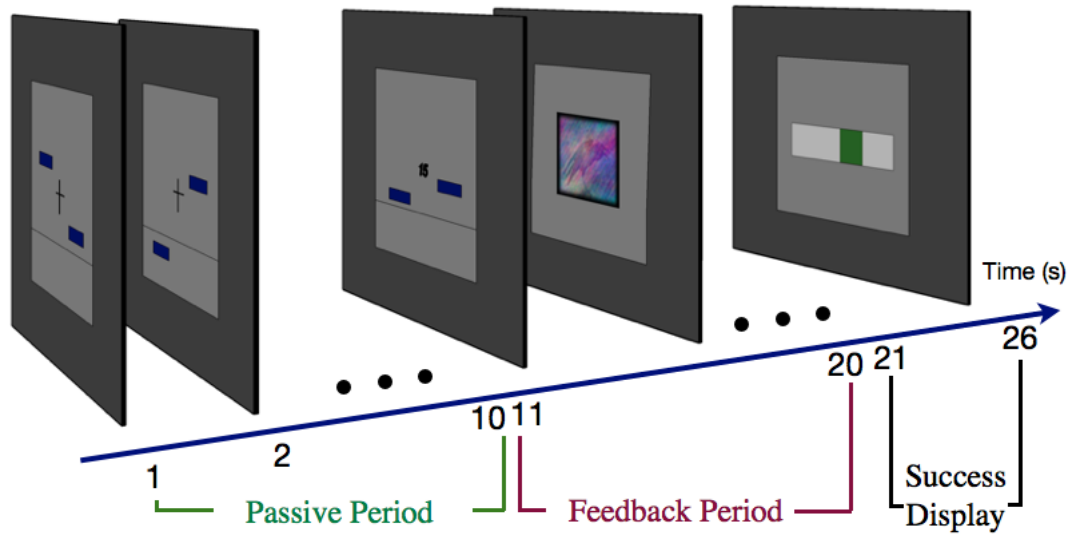
Figure 3.3: Object detection during BCI: within periods of high or low ongoing gamma band
activity instead of a feedback signal sometimes a noisy version of an image was presented
and the volunteer had to perceive the object in the image.

Data Collection

All technical details regarding data collection were the same as in Experiment I.

BCI Task Procedure

The experimental layout of the object detection task was identical to the BCI train-
ing task procedure. The only difference was that noisy images of 33% visibility were
sometimes shown during the feedback period instead of the feedback value (see Fig-
ure 3.3). The appearance of an image was dependent on the volunteer's performance
in the ability to control the gamma band. In each volunteer, individual low and high
gamma band activity levels were estimated. The individual ability of control over
the gamma band for each person was assessed by sorting the feedback values of the
last training session (percent change to passive period) and calculating the maxi-
mum of the lower third and the minimum of the upper third as indicators for low
or high gamma levels. The value during the feedback period fluctuated depending
on the volunteer's actual success in increasing the presented gamma value, which
resulted either in high (successful) and low (less successful) gamma band activity.
Thus, the value was compared online against the determined high and low gamma
levels. When the value was higher than the upper gamma level or lower than the
lower gamma level a noisy image (size: 10x7.5 cm, 33% visibility) was shown for 2

seconds instead of the feedback display. Thus, the volunteer was not informed about the actual success in this segment, which was important to avoid a strategic bias on the image processing. The volunteer was instructed to detect objects within the noisy version of the image by judging them as 'living' or 'non-living' by a button press. Participants were advised not to press a button if the object in the image was not detected. With the button press, we were able to confirm that the object in the image was perceived by the volunteer and that object detection was successful. (object detected = button pressed = object in image perceived)

Image Selection

For the object detection task, 120 different images (size 336 x 252 pixels; 24-bit color depth) were selected from a database of natural scenes and a database of objects. Visibility of images was modulated by scrambling them according to a method described previously (Rose & Buchel, 2005). In short, each image was transformed into the amplitude and phase component by a Fourier transform for each RGB color channel and a fraction (here 33%) of the image phase was manipulated before transforming the amplitude and phase components back into image space. Four sessions with 11 task periods each, were presented to assure the presentation of a maximum of 30 images for high gamma and 30 for low gamma. Overall, 60 images were shown during the object detection task and 60 additional images were used for the recognition memory task afterwards.

Recognition Memory Task

After the object detection task, a surprise recognition task was presented, which entailed the presentation of the 60 previously seen images with 60 new images. The images were randomized and presented in a pseudo randomized order while the volunteers had to judge images as 'previously seen' or 'new'.

Data Analysis

In Experiment II, the time-frequency analysis was calculated (using the open source Fieldtrip toolbox) for the trained channels PO7/PO8 based on a starting period of 1200 ms before and 1000 ms after image presentation for images shown during high and low gamma states.

3.2.2   Results

High Gamma Band Activity Improves Subsequent Visual Object Detection

In Experiment II we directly tested for the consequences of deliberately increased
gamma band activity on subsequent visual object processing. We exploited the
variability in evoking gamma band activity to test for an influence of prestimulus
gamma band activity on visual object processing. In each volunteer, individual high
and low gamma levels were estimated while volunteers tried to increase the gamma
band activity during BCI training. As volunteers achieved higher gamma values
than the high gamma level (high gamma state) or lower gamma values than the
low gamma level (low gamma state), noisy images were presented and volunteers
were instructed to press a button if they were able to detect the object in the im-
age. In accord with our assumptions, the increased gamma band activity resulted
in a significant enhancement of visual object processing. During high gamma band
activity states, more images were detected than during low gamma states (Images
detected during low gamma band state: 77.7% ± 5.6 (s.e.m) versus high: 85.23% ±
3.8 (standard error mean (s.e.m)); t(9)=2.79, p =0.02) (Figure 3.4b). The analysis
of the response times of detected images during high or low gamma states revealed
no differences.

The success of object processing was further examined in a subsequent surprise
recognition task 10 minutes after the experiment. The recognition task included
the presentation of all 60 previously seen and 60 new images, regardless of whether
they were detected in the object detection task. However, for the analysis of the
recognition task we encountered images that were detected in the object detection
task and were correctly judged as 'previously seen'. The results revealed significantly
higher recognition rates for images that were detected during high gamma states than
during low gamma states (percent correct low: 59.7 ± 4.23 (s.e.m) versus correct
high: 66.7 ± 3.94 (s.e.m); t(9)=2.69, p=0.024) (Figure 3.4c). For comparison the
false positive rate (FPR) was assessed by calculating the percentage of 'new' images
that were rated as 'previously seen'. The FPR of 17% compared to 60% correctly
remembered in the low gamma state and 67% in the high gamma state indicates
reliable formation of memory for both states.

The offline EEG analysis confirmed that the gamma band activity was reliably dif-
ferent between the high and low gamma states (high gamma against low gamma,
t(9)=4.69, p<0.001). Thus, during the time period of 1 second before image pre-
sentation, reliably more gamma band activity was evoked in the high gamma state
compared to the low gamma state. A time-frequency analysis revealed that the
increase of gamma band activity during the high gamma state was limited to the
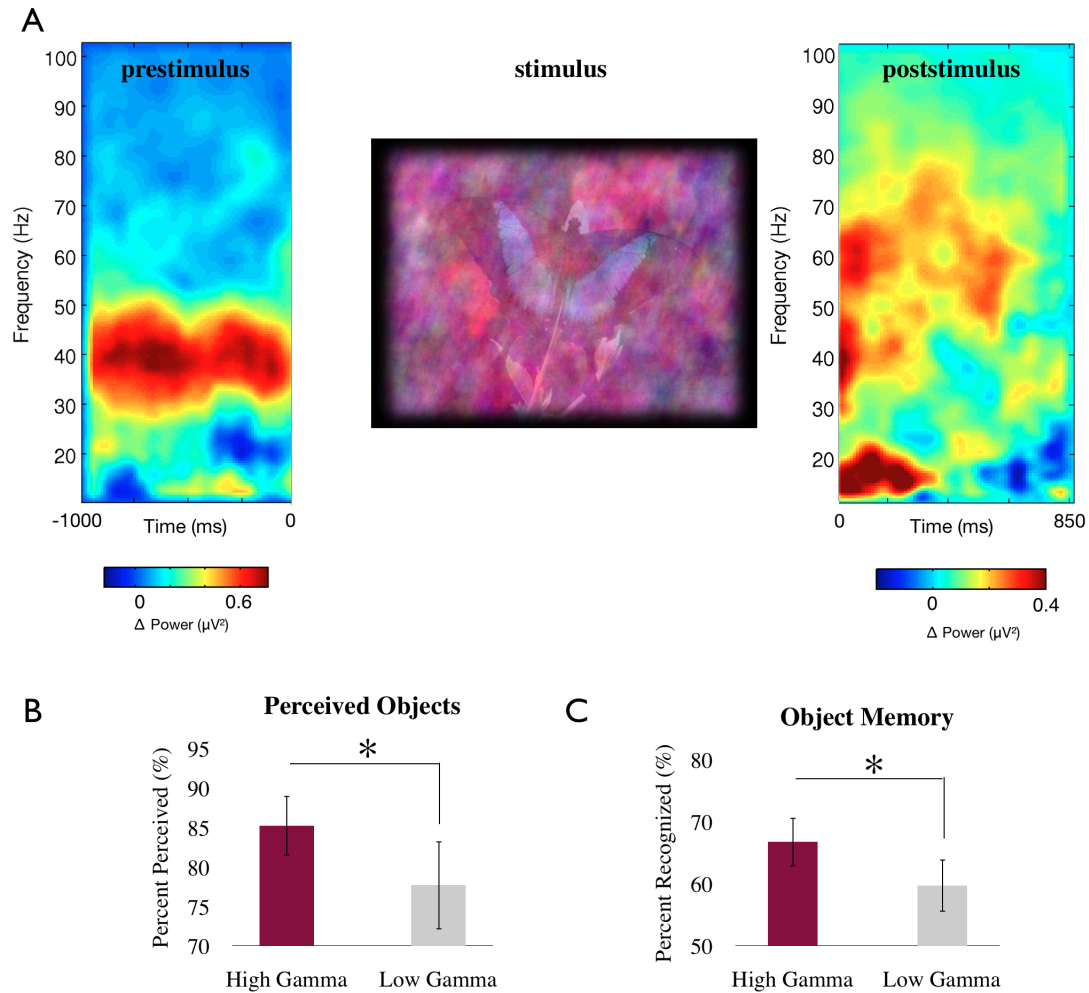
Figure 3.4: Time-frequency analysis of pre- and poststimulus periods. (a) Time-frequency analysis of the total power difference between high gamma band and low gamma band states for channels PO7/PO8 before and after stimulus onset (grand mean over all volunteers). Significantly more gamma band activity in the exact trained frequency range (30-45Hz) can be observed in the high gamma band state in the prestimulus period which resulted in significantly more gamma band activity also after stimulus onset. (b) Significantly more images were perceived during high gamma states as during low gamma states. (c) The surprise memory task afterwards revealed significantly higher recognition rates for images detected during high gamma than low gamma states. (Salari et al., 2012)
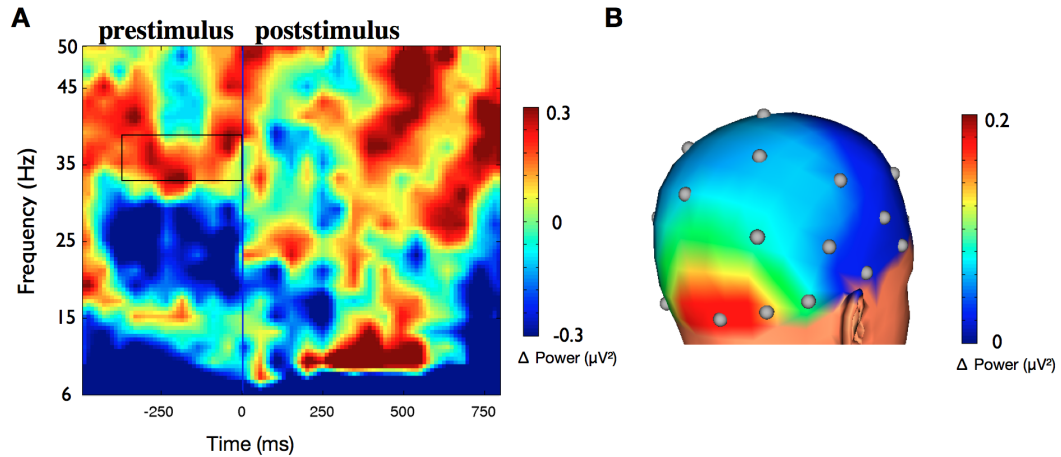
Figure 3.5: (a) Time frequency analysis of the difference between states of detected images (hits) compared to states of undetected images (misses) in electrodes PO7/PO8. The prestimulus region marked by a rectangle reveals a significant difference between both states (t(9)=2.51, p=0.03) in the gamma band. No significant changes were found in the beta band (20-30 Hz). (b) Topographic representation of the prestimulus gamma band differences of detected images compared to undetected images. The maximum difference is localized in the occipital region. (Salari et al., 2012)

trained frequency range from 30-45 Hz and was not accompanied by increases in other higher or lower frequencies (Figure 3.4a). Furthermore, this intentionally induced gamma band increase during the high gamma band state resulted in a higher level of gamma band activity during the first 500ms of subsequent image presentation (t(9)=2.09, p<0.05). A further time-frequency analysis of the state of detected images (hits) minus undetected images (misses) showed a reliable power difference within the trained gamma band range 34-40 Hz in a prestimulus period of -400 ms to stimulus presentation (t(9)=2.51, p=0.03, Figure 3.5a). Thus, the prestimulus difference is restricted to the trained frequency range and the different performance cannot be explained by additional prestimulus oscillatory activity of other frequencies. In addition, we performed a topography analysis of all electrodes for the prestimulus state of detected images compared to prestimulus states of undetected images. The analysis demonstrates that the difference between hit and miss states for the gamma band is topographically specific with a maximum difference in the occipital region (Figure 3.5b). Thus, the prestimulus difference is restricted to the trained frequency range and brain region.

Importantly, results of the SP detection method revealed no changes between the amount of and amplitude of detected SPs in the high and low states one second before and after image presentation (n.s.). Thus, results of the BCI training as

well as the object detection task demonstrated no influence of microsaccades for the deliberately evoked gamma band activity. Interestingly, the comparison of the number and amplitude of saccades in the phases before and after stimulus presentation revealed a significant increase in the amount of SPs ($F(1, 9)=9.39$, $p<0.05$) and SP amplitude ($F(1, 9)=21.92$, $p<0.001$) during stimulus presentation, as has been reported previously (Yuval-Greenberg et al., 2008).

3.2.3 Conclusion

With the object detection task of the second experiment, we directly tested the hypothesis that a high level of gamma band activity induced by the BCI manipulation can improve subsequent visual object processing and memory compared to trials with a low level of gamma band activity. In accord with our assumptions, results clearly confirmed that the increase of the gamma band activity over the visual cortex by BCI manipulation enhanced the processing and subsequent detection of the objects.

In the next experiment a new feedback display is designed in order to motivate volunteers to modulate two different frequency bands.

3.3   Experiment III: Modulation of the Alpha and Gamma Band in a Game Layout

In Experiment III, volunteers were trained to modulate two different frequency bands, the alpha band (8-12 Hz) and the gamma band (30-45 Hz). Volunteers of Experiment I that had already learned to deliberately modulate the gamma band participated in this experiment. A new feedback display was used that was designed to motivate volunteers to switch between the modulation of the two frequencies to move a ball along a track.

3.3.1   Volunteers and Procedure

Volunteers
Six of the twelve previously trained volunteers participated in the third experiment.

Data Collection

The resulting topography in Experiment I Figure (3.2b) showed that the increase of the gamma band was limited to the visual cortex. Thus for Experiment III, EEG was measured from 2 channels at locations PO7, PO8 (BrainVision amplifier and software) and not from the whole brain. The mastoid reference, EOG recordings and measurement of the neck muscle activity as well as all technical adjustments were kept identical to Experiment I.

BCI Task Procedure

The third experiment started with 4 sessions of warm-up training followed by 6 sessions of feedback training. Each warm-up session consisted of two passive periods (10s) followed by one feedback period. During the passive periods, the volunteers' screen displayed the game layout without any movement of the ball. Volunteers were advised to fixate the centre of the screen and to do nothing in particular. Within the passive period, the mean power for both alpha (8-12 Hz) and gamma frequency ranges (30-45 Hz) in the lateral occipital channels PO7 and PO8 was computed and used as a reference measure for the feedback period. During every second of the feedback period, the percentage change to the passive mean gamma or alpha power was computed. For change values below zero the ball did not move and a backwards movement of the ball was not possible. Thus, the ball was either moved to the right due to high gamma values or to the left due to high alpha values. A feedback session was completed with the ball moved into the target. After 4 sessions of warm-up training a mean gamma and alpha power baseline was determined from the measured passive periods. These baselines were set permanently for the following 6 sessions of feedback training.

Data Analysis

For the EEG offline analysis, data from both electrodes were segmented for both gamma (right movement) and alpha (left movement) periods. EEGs were corrected for blinks and eye movement artifacts by subtracting both EOG channels weighted by their transmission coefficient (Gratton et al., 1983). Both alpha and gamma segments were decomposed by a fast frequency analysis (Hanning Window).

3.3.2 Results

During offline analyses, the mean gamma power (30-45 Hz) and the mean alpha power (8-12 Hz) in both alpha and gamma segments for each volunteer per session
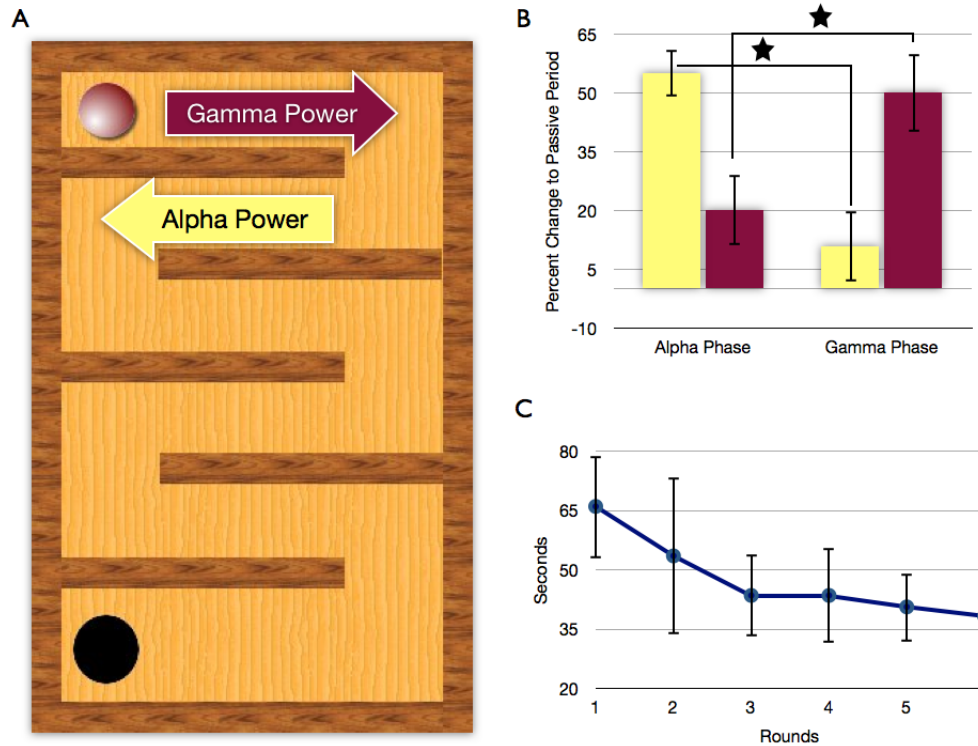
Figure 3.6: Experiment III: (a) Volunteers had to move the ball through a track of a game layout. A movement to the right was achieved by gamma frequencies above baseline and a movement to the left by high alpha frequencies. (b) Statistical tests revealed a higher increase of alpha power in the alpha phase than in the gamma phase (p<0.05) and a higher increase of gamma power in the gamma phase than in the alpha phase (p<0.05). (c) Volunteers played six rounds and showed a significant increase of speed after each round (p<0.001) and this improvement was related to a fast adaptation of the gamma band manipulation to the new layout indicating the transfer of the learned control over the gamma band by previous feedback training.

was computed. Statistical tests demonstrated higher gamma power in the gamma periods compared to the alpha periods averaged over all 6 sessions (t(5)=2.1, p< 0.05) with a percentage difference of 24%. Analogous computations showed significantly higher alpha power in alpha periods compared to gamma periods (t(5)=2.03, p< 0.05) with a percentage difference of 40% (see Figure 3.6b).

The goal of the volunteers was to move the ball as fast as possible. Therefore, a movement to the right was achieved by an increase of gamma band power and a movement to the left with an increase of alpha band power compared to the specific baseline (see Figure 3.6a). During just six rounds of training, the control over the speed of

the ball significantly increased. The amount of time for one 'game' decreased with training (repeated measures ANOVA, factor: 6 sessions: $F(5,25)=15.15$, $p<0.001$) (see Figure 3.6c). This effect was accompanied by a significant decrease in the number of ball steps needed to finish the track, especially during the movement of the ball to the right by higher gamma power (repeated measures ANOVA, factor: 6 sessions: $F(5,25)=4.72$, $p<0.005$). The number of steps for a movement to the left by higher alpha power showed no significant decrease (repeated measures ANOVA, factor: 6 sessions: $F(5,25)=1.16$, $p=0.36$).

3.3.3   Conclusion

Results of the third experiment demonstrated that volunteers were able to modulate both alpha and gamma band power. However, the results clearly showed faster adaption to modulating the gamma band than to alpha band due to previous feedback training of the gamma band, thus underlying the specificity of gamma band training. Furthermore, volunteers were clearly motivated by the new visual display design, as they were determined to move the ball as fast as possible into the goal.

In the next experiment, we examined the specificity of gamma band training using the custom-designed BCI with an additional control group. Since the new visual display design was motivating for the volunteers, we integrated the game layout into the new experiment.

3.4   Experiment IV: Control Group Experiment

In Experiment IV, we examined whether the gamma band activity increase was a specific result of BCI training. The experiment included a new feedback group and a control group that underwent identical training but without feedback. In addition, both groups conducted behavioral tests before and after training in order to examine visual performance effects even after BCI training.

3.4.1   Volunteers and Procedure

Volunteers
In Experiment IV, twenty eight new volunteers were recruited (mean age 29 years,

range 25-35, 10 females). 16 randomly selected volunteers participated in the feedback experiment and the other 12 were assigned to the control group.

Data Collection
For Experiment IV, EEG was measured from 2 channels at locations PO7, PO8 and used for the calculation of the feedback signal. EOG and neck muscle measurements as well as all technical details were kept identical to Experiment I.

BCI Task Procedure
In Experiment IV, the experimental sequence was slightly different from Experiments I, II and III. Each session started with two passive periods (10s each) followed by eight feedback periods. A mean passive baseline was calculated from the first two passive periods and used for the following eight feedback periods in a session. The gamma band was not divided into two sub-bands, as no differences were found between the two bands. Therefore, the 2 bars were removed from the experimental layout of the fourth experiment. As in Experiment I, a baseline gamma value was calculated and in the subsequent feedback period the volunteers tried to increase the presented gamma band value (mean over 30-45Hz at PO7/ PO8) above this baseline. The percentage change to the passive baseline was computed online every second during the feedback period and the gamma value was presented at the centre of the monitor (see Figure 3.7).

After the feedback period, the success (sum of percent change) was displayed as the distance the ball had moved on the track. Thus, the reward for a large amount of gamma band increase was a longer distance that the ball had moved towards the goal.

The first training day started with two behavioral tests, the spatial attention task (11 min) and the object detection task (5 min) in a pseudorandom order. After the tests, volunteers performed 12 sessions of feedback training resulting in a duration of about two hours for the whole experiment. On the second day, volunteers performed 12 sessions of feedback training without any behavioral tests. On the third day, volunteers started with 6 sessions of feedback training followed by the behavioral tests at the end.

Control Group
The control group had the exact same experimental procedure as the feedback group with 3 days of training, the same number of sessions, same behavioral tests, and most important of all, the same visual input as the feedback group. However, during the
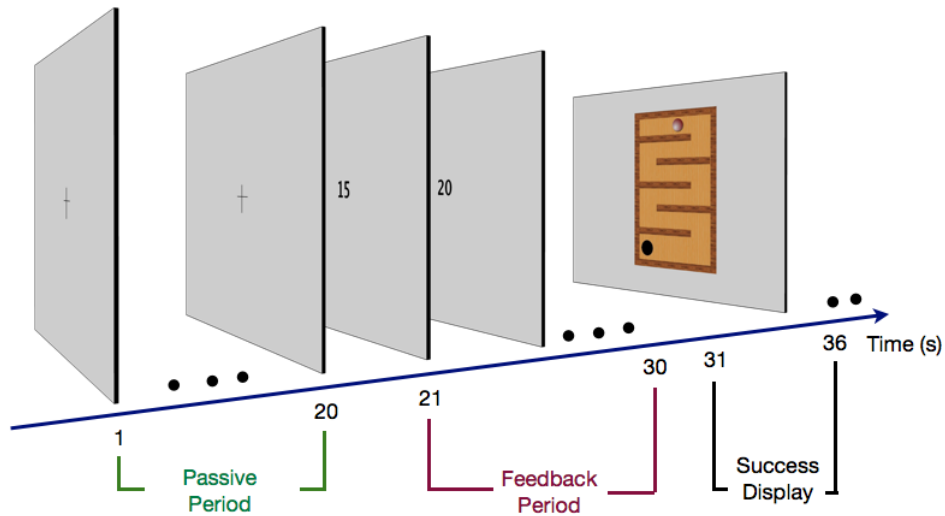
Figure 3.7: Experiment IV: Except for the actual task, the experimental design was identical for both groups. The task was to either increase the value at fixation (feedback group) or to detect a distinct number at fixation (control group). For the feedback group, the gamma band power change was visualized at fixation. The success of the intentionally increased gamma values was presented after the feedback period (game display). For the control group, random values within the range from the experimental group was displayed.

feedback periods the control group did not have a BCI control, since random values (value range adapted from feedback group) were presented at fixation instead of the actual gamma activity value as for the feedback group. In order to assure volunteer's attention to the presented values during the feedback period, they were advised to respond to a specific number. As in the feedback experiment, the success display was shown after each feedback period with comparable ball moves as in the feedback group.

Behavioral Experiments

Prior to and after the training, the performance of the two groups was assessed to test for specific improvements due to feedback training. This time, the tasks were performed offline, i.e. without any actual feedback.

Object Decision Task

During a simple image detection task, volunteers were instructed to detect objects in 50 images and to categorize them as 'living' or 'non-living'. Volunteers fixated a cross at the centre of the screen for 3000 ms followed by an image presented for a duration of 700 ms (size: 12 x 9 cm). 25 different images (size 336 x 252 pixels; 24 bit

color depth) were selected from a database of natural scenes with animals and plants and 25 out of a database with object images. Visibility of images was modulated by a scrambling method as described in Experiment II. All images were presented with 33% visibility and volunteers had 2000 ms to detect the images and to judge them as 'living' or 'non-living' by pressing a button. Volunteers were advised not to press the button if the image was not identified.

Spatial Attention Task

Volunteers fixated a $0.7°$ cross at the centre of the screen. Each trial began with an arrow (left ($<$), right ($>$), neutral ($<>$)) that occurred 100-2000 ms after the cross indicating where to attend. Depending on the given direction of the arrow, a $1°$ target square appeared peripheral $5°$ to the left or the right of the fixation arrow for 100 ms. The target was presented between 450 ms-2500 ms following the arrow. In 80% of the valid trials the (left or right) arrow correctly indicated the location of the target and in 20% of the invalid trials the arrow incorrectly indicated the location of the target. During the neutral cue the target appeared with a 50% probability on the left or right side. Volunteers were instructed to keep their eyes fixated to the centre and to respond to the target as quickly as possible by pressing the left or right button. 120 Trials with 30 right cues, 30 left cues and 60 neutral cues were presented with a short break between the sessions resulting in a duration of about 11 minutes.

Data Analysis

Data analysis was similar to Experiment I.

3.4.2   Results

In Experiment IV, the feedback group was trained to deliberately increase the gamma band activity as in Experiment I and the control group was exposed to an identical training setting with the exception that the feedback signal was not related to their actual gamma band activity. Overall, 12 of the 16 trained volunteers from the feedback group showed a clear increase in their ability to intentionally increase activity in the gamma band. As in the previous experiment, the gamma band activity of the feedback group increased across training days ($F(2,22)=3.79$, $p<0.05$) and was reliably higher compared to the passive period on the last training day ($t(11)=7.67$, $p<0.001$) (Figure 3.8a). The significant interaction between group and training session ($F(2,44)=3.34$, $p<0.05$) demonstrated that without the feedback

signal, no significant increase was achieved across training sessions (non-feedback training n.s.).
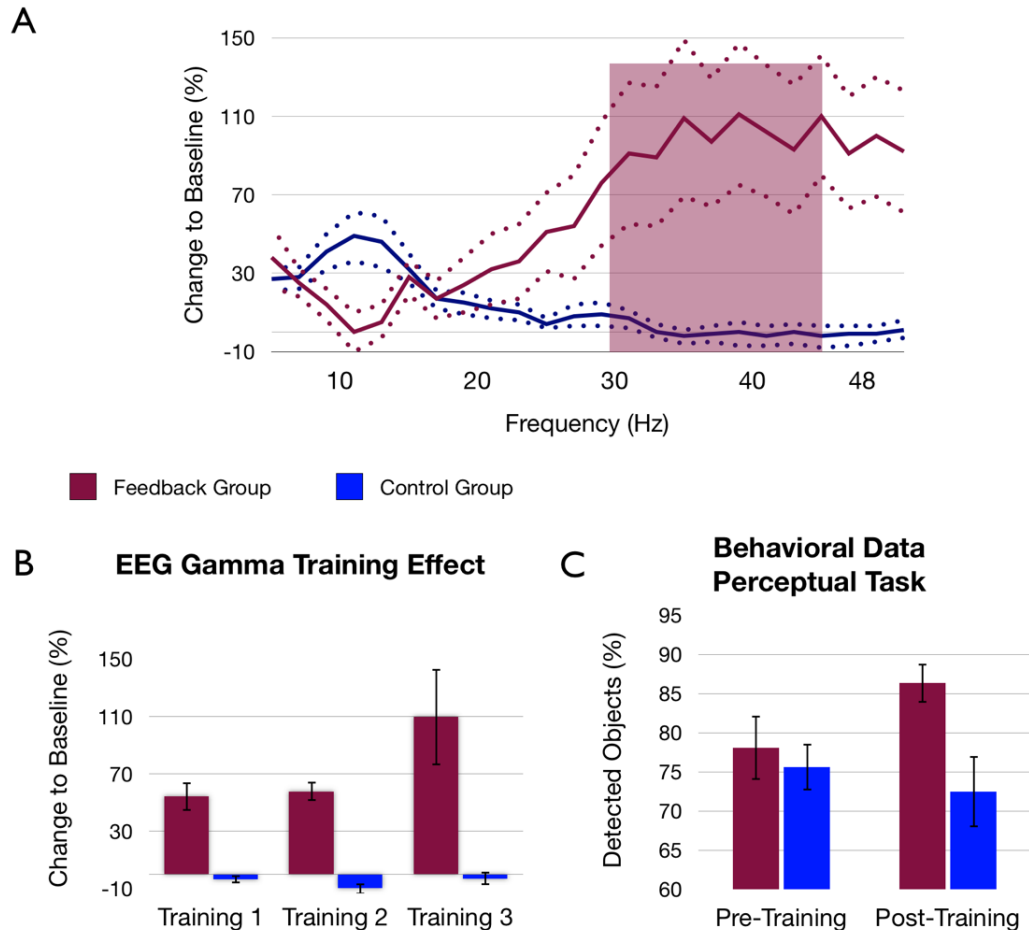

Figure 3.8: (a) Frequency spectra from the last training day for both groups (mean from channels PO7/PO8). Only for the feedback group (red) a reliable increase compared to the passive period was observed and this increase was limited to the trained gamma band (blue= control group). (b) The difference of the gamma band power to the passive period increased as a function of training for the feedback group (red) but not for the control group (blue). (c) Only the feedback group showed enhanced performance for the visual object identification task after training; more objects could be detected after successful gamma band training.

As Experiment II showed an effect on image processing during the ongoing feedback manipulation, the first task in this experiment investigated object detection within noisy images before and after feedback training (living vs. non-living object decision task). The second task was a simple spatial attention task (Posner et al., 1980) to test for more generalized effects on attentional functions (see section 3.4.1).

Interestingly, the behavioral tests revealed a very specific improvement related to the feedback training. After the training, only the feedback group detected more objects correctly ($t(11)=3.08$, $p=0.01$) and faster ($t(11)=2.82$, $p=0.02$) than prior to the training (Figure 3.8c), which was further expressed by a reliable training by group interaction effect ($F(1,22)=6.73$, $p<0.05$). In the spatial attention task statistical tests for both groups revealed faster response times for valid trials compared to neutral trials and slower response times for invalid trials ($F(2,44)=39.41$, $p<0.001$). Further statistical tests showed no differences between the two groups or training and therefore no specific effect of gamma training on the feedback group (n.s). Thus, no specific improvement was observed for the spatial attention task indicating that feedback training specifically supports visual object perception skills located in occipital areas used to generate the feedback signal.

3.4.3   Conclusion

In Experiment IV, it was important to demonstrate, that the increase in gamma band activity and visual performance was directly related to the feedback training and not to the repeated exposure to the experimental environment or an unspecific training of attention. We therefore conducted Experiment IV, which was designed to test for the specificity of the feedback effect using a control group that was exposed to an identical training setting but without feedback. In addition, this experiment was designed to investigate improvement in visual object performance skills that persisted and can be observed after the feedback training. Results in the feedback group replicated the results in Experiment I with an increased gamma band activity across training, while results in the control group revealed no changes in the gamma band. Thus, the control group design clearly showed that the increase in gamma band activity can be attributed to the feedback training and not to time-on-task or other non-specific effects.

In a next experiment, we extended our BCI method to a more effective and precise BCI training. To examine the functional difference of alpha and gamma band power and their influence on visual object processing, we aimed to present noisy images during ongoing alpha and gamma band modulation as in Experiment II.

3.5 Experiment V: Source-Based BCI Method with a Modulation of Two Frequencies

In Experiment V, we used a source-based BCI method to train volunteers to deliberately switch between modulating alpha (8-12Hz) and gamma band oscillations (around 40Hz) in a selective brain region in the visual cortex. In the process of developing a BCI method for gamma band oscillations, we assured that neural activity was not confounded by artifacts. Hence, various artifacts (including microsaccades) were detected online (see section 2.3.3.2 in Chapter 2). Furthermore, we examined the precision of training alpha and gamma band oscillations with a source-based BCI method in the visual cortex and examined the topographical distribution. As in Experiment II, we presented noisy images during modulation of alpha and gamma band oscillations for the purpose of disentangling the functional relations of the different frequencies and their influence on visual object processing.

3.5.1 Volunteers and Procedure

Volunteers

12 healthy, right-handed volunteers with normal or corrected to normal vision participated in the experiment (mean age 25). All volunteers had no prior BCI experience.

Data Collection

The volunteer sat in a separate room and watched a liquid crystal display monitor with a viewing distance of 1 m. EEG was measured from 58 active electrodes at standard locations (Fp1, Fp2, F3, F4, C3, C4, P3, P4, O1, O2, F7, F8, T7, T8, P7, P8, Fz, Cz, Pz, Oz, FC1, FC2, CP1, CP2, FC5, FC6, CP5, CP6, F1, F2, C1, C2, P1, P2, AF3, AF4, FC3, FC4, CP3, CP4, PO3, PO4, F5, F6, P5, P6, AF7, AF8, FT7, FT8, TP7, TP8, PO7, PO8, Fpz, AFz, CPz, POz) with a sampling rate of 250 Hz and all channels were referenced to Cz. In addition, for the detection of eye movements, we recorded vertical and horizontal EOG as described in section 2.1.1. Neck muscle activity was derived bipolar about 20 cm below the occipital electrodes over the trapezius muscle and electrode resistance was kept below 10 kOhm.

During the BCI experiment, EOG, EMG and microsaccadic artifacts were detected as described in section 2.3.3.2. An overview of detected artifact types is given in Table 2.2.
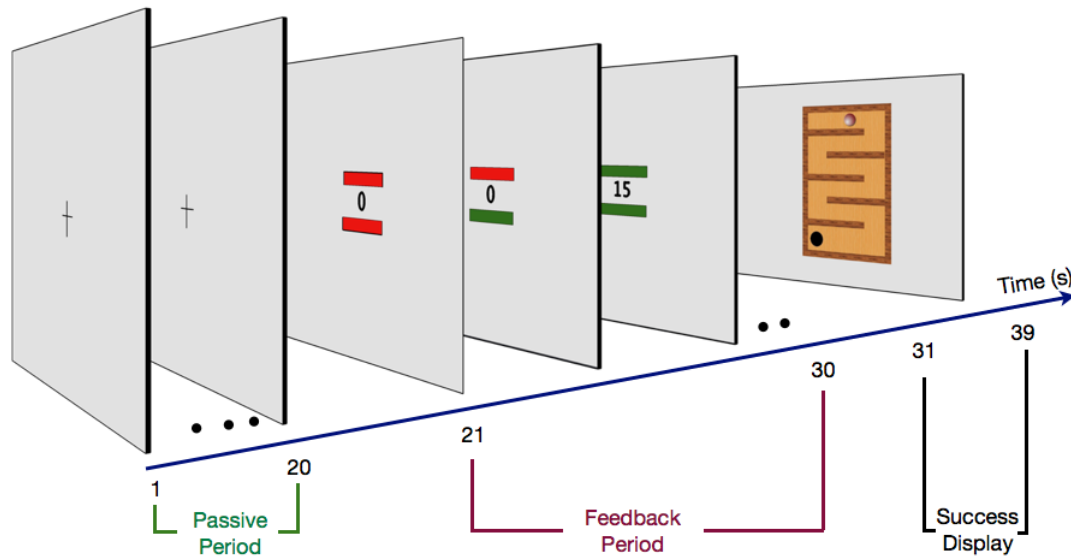
Figure 3.9: Experiment V: The BCI design. BCI training: During the passive period (total 20 seconds) volunteers fixated the central cross. This period was used to set an actual baseline value of alpha or gamma current density power in the ROIs. In the feedback period (second 21-30) volunteers were asked to increase the current density power in the ROIs (value at fixation) and at the same time avoid EOG (bar above value) and EMG (bar below value) artifacts by keeping the bars green. As an artifact occurred (at least one of the bars red) the presented value was set to zero. The success of the intentionally increased artifact free gamma or alpha values was presented after the feedback period (success display). (Salari et al., 2012)

BCI Task Procedure

Volunteers were trained for an hour once a week over a period of 3 weeks. Each training day consisted of 8 sessions of gamma band training and 8 sessions of alpha band training, which were presented in an alternating sequence. A session started with two passive periods (10s each) followed by eight feedback periods (10s each). The design of the experiment was arranged with a simple cross during the passive periods and a feedback value, representing Δ_{loreta} (see section 2.3.3.6) along with two bars (representing artifacts). The bars were placed central and close to the feedback value, in order to keep the volunteer focused to the feedback value and to avoid eye movement (see Figure 3.9).

Passive Period - During the passive period the volunteers fixated the central cross. During this period, the mean gamma (during gamma sessions) or alpha (during alpha sessions) current density power (see section 2.3.3.5) in the defined ROIs was computed and used as a reference measure for the following feedback periods. Anytime a blink or eye movement occurred during the passive period, the corresponding

segment (1 second) was removed to assure an artifact free baseline measurement. If more than 20 % of the passive period contained artifacts, then the session was stopped and a new session was started.

Feedback Period - Before each session, volunteers were verbally informed about an upcoming gamma or alpha session. During the feedback periods, volunteers were instructed to increase the presented value, which expressed the percentage change to the passive baseline. The feedback value on the screen was refreshed with a time resolution of one second. We avoided a faster refresh of the feedback value and color of the bars, in order to avoid rapid display changes that could effect neural activity. In addition two bars monitored EOG (upper bar) and EMG artifacts (lower bar) occurring within the past second of feedback training. Thus, volunteers were informed about a successful increase of activity in the defined frequency range without an influence of artifacts if the presented value increased and the two bars turned green. Respectively, the bars turned red if EOG or EMG artifacts occurred and the percent value was set to zero (see Figure 3.9 and data processing diagram 2.15).

Success Display - In order to keep the volunteers motivated, a "success display" was presented for 9 seconds after each feedback period. The success display informed the volunteers about their performance during the feedback period. The position of the ball in the game layout changed as a consequence of the intentionally increased values during the previous feedback period in the absence of artifacts. Thus, only values that were successfully increased during artifact free segments were used for ball movement. High values resulted in large distance movements of the ball, whereas low values resulted in shorter distance movements after a less successful feedback period. Hence, the success display was integrated into the design to keep the volunteers engaged and motivated, as larger ball movements were accomplished after a successful feedback period. The volunteers were asked to reach the goal as quickly as possible. Additionally, the success display served as a short break for the volunteers between each trial. Volunteers had eight feedback periods to reach the target. If the volunteer did not reach the goal within 8 feedback periods, a new session was started.

**Adaptive stimulation during different states of induced ongoing alpha
and gamma band activity**
After 3 days of training, the volunteers participated in an object detection task after BCI training. As in Experiment II, noisy images of 33% visibility were shown during

the feedback periods of both alpha and gamma band sessions. The selection of the images was identical to Experiment II. However, here we computed individual alpha and gamma band activity levels in each volunteer rather than high and low levels as in Experiment II. The individual alpha and gamma band levels were assessed by calculating the median positive feedback value for the alpha sessions and for the gamma sessions. If the determined value exceeded 20 then a maximum level value of 20 was set. 30 images were shown during the gamma band sessions and 30 images during the alpha band sessions. Thus, during a gamma band session, i.e., the artifact free (both bars green) feedback value was compared online against the determined gamma level. When the value was higher than the gamma level, a noisy image was shown for 2 seconds instead of the feedback display. Thus, images were only shown during artifact free segments. Volunteers pressed a button if they were able to detect an object within the noisy image and to correctly judge them as 'living' or 'non-living'.

Data Analysis

For the EEG offline analysis, data from all channels was first divided into passive and feedback periods. The first 1000 ms of both periods were removed in order to avoid effects evoked by the stimulus onset. Each passive and feedback period was then divided into equal size segments of one second. The data was preprocessed and controlled for artifacts as described for the online processing of data (see section 2.3.3.2, Chapter 2).

To evaluate the outcome of alpha and gamma band training with artifact control in the predefined ROIs, we applied a LORETA transformation on the alpha and gamma filtered channels. Artifact free segments (EOG and EMG bars green) were extracted and the median percent change of gamma/alpha activity in the ROIs compared to baseline was derived. Artifacts were also controlled for during the offline analysis in case they had not been detected. These segments were also controlled offline for artifacts that were possibly not detected. We conducted a repeated measures ANOVA with factors session and frequency band to compare the gamma and alpha band activity change during the alpha and gamma feedback periods.

To calculate the topographical distribution of BCI training, the electric potential differences (time domain EEG) in each electrode between the feedback and passive periods was calculated for both gamma and alpha periods for the last training day. To estimate the three-dimensional distribution of electrical activity (current density) of gamma and alpha BCI training, we applied sLORETA (The KEY In-
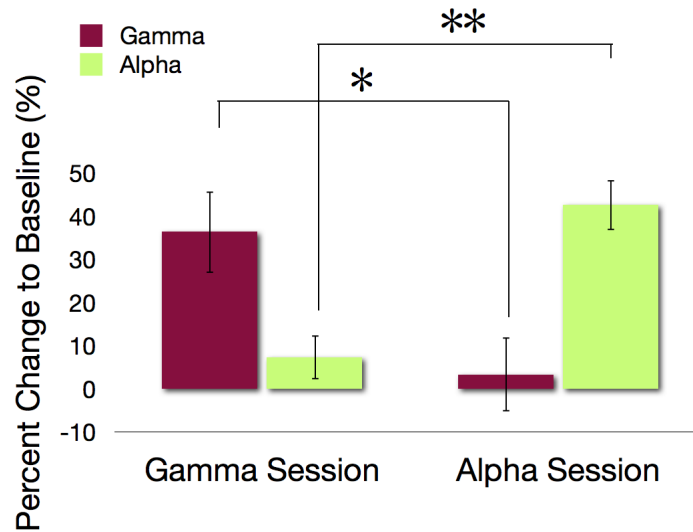
Figure 3.10: Percent change of gamma and alpha band activity in the gamma and alpha
sessions within the last training day. Statistical tests revealed a higher increase of alpha
power in the alpha sessions than in the gamma sessions (t(11)=7.14, p<0.001)(**p<0.01)
and a higher increase of gamma power in the gamma sessions than in the alpha sessions
(t(11)=2.75, p=0.018) (*p<0.05)). (Salari et al., 2012)

stitute for Brain-Mind Research, Zurich; Pascual-Marqui, 2002) to the subtracted
electric potential differences. The standardized LORETA method was applied for
the source estimation, since LORETA achieves low localization error (see section
2.3.3.4), whereas sLORETA is more exact and achieves less localization error. More
detailed information on sLORETA can be found in (Pascual-Marqui, 2002; Fuchs et
al., 2002; Jurcak et al., 2007).

The time-frequency analysis was calculated for the channels PO7/PO8, as 1.) they
are closest to the trained ROI and 2.) a time-frequency analysis cannot be applied
to the LORETA channels as they are filtered in the alpha or gamma band range.
The analysis was calculated based on a starting period of 1200 ms before and 1000
ms after image presentation for visual stimuli shown during alpha and gamma band
states.

3.5.2 Results

Analysis of Gamma and Alpha Activity in the ROIs

After three training sessions as in Experiment I, offline analyses of the last training
day showed that volunteers were able to selectively increase alpha and gamma band
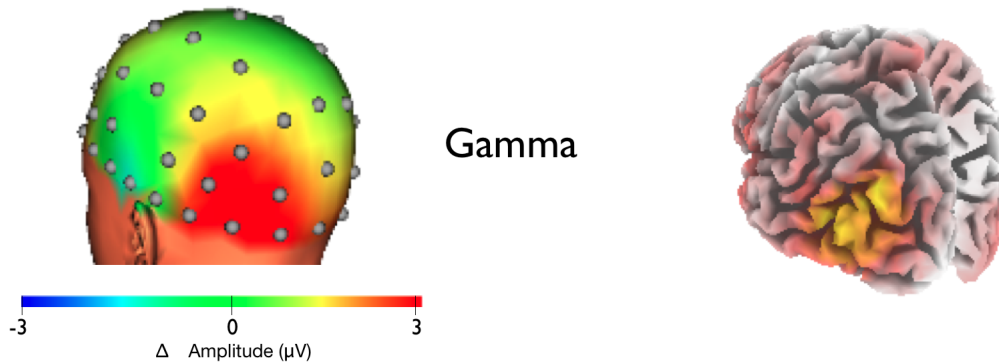
Figure 3.11: Topographic and spatial distribution of gamma band increase. (Left) On the sensor level: Topographic representation of the average change in gamma band activity (30-45 Hz) during the feedback period compared to the passive period within the last training session. The maximum change is localized at the occipital lobes close to the trained ROIs. (Right) Source estimation: sLORETA analysis of the subtracted electrode potential difference of the gamma feedback sessions compared to the passive baseline. The yellow area represents the maximum estimated change in gamma band activity compared to baseline. (Back view) (Salari et al., 2012)

power in the defined ROI in the LOC. Analyses of the power change of gamma band activity to the passive baseline revealed a significant increase of gamma activity within the gamma sessions, but not during the alpha sessions. Accordingly, alpha power change increased significantly during the alpha sessions, but not during the gamma band sessions (interaction of session (alpha/gamma) X frequency band (alpha/gamma), $F(1,11)= 33.75$, $p <0.001$) (Figure 3.10). Volunteers were able to selectively increase gamma band oscillations in the gamma sessions as compared to the alpha band activity ($t(11)=3.4$, $p<0.01$). No significant changes were found in the alpha band compared to baseline during gamma band sessions ($t(11) =1.41$, n.s.). This selective increase was also reliable in the alpha band sessions as the alpha band was increased while the gamma band remained unaffected ($t(11)=4.33$, $p<0.01$). The results show that volunteers learned to selectively influence each frequency band without affecting the other.

Topographical Analysis of BCI Training

Results of the topographical and spatial distribution of the feedback effect revealed that the increase in alpha activity during the alpha sessions and gamma activity during the gamma sessions was maximal at the occipital lobe (see Figure 3.11). While increased gamma band activity in the gamma sessions was limited to the occipital lobe, results of the alpha sessions revealed a more widespread activation, as the alpha band increased in both the occipital and parietal lobes (see Figure
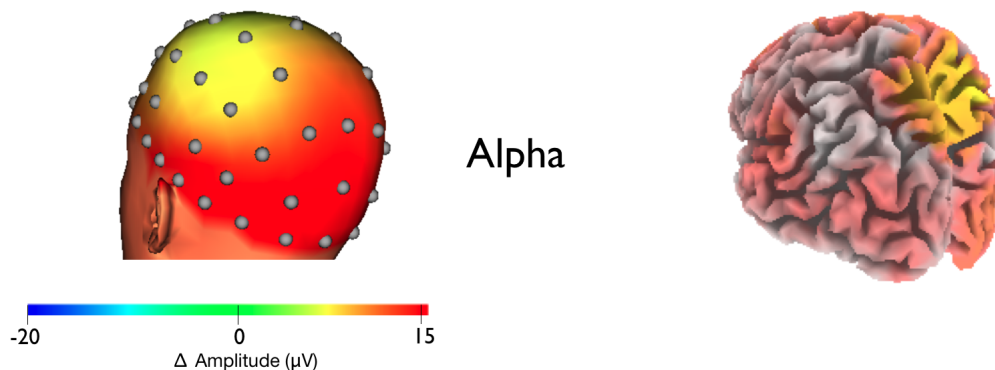
Figure 3.12: Topographic and spatial distribution of alpha band increase. (Left) On the
sensor level: Topographic representation of the average change of the alpha band activity
(8-12Hz) during the feedback period compared to the passive period within the last training
session. The maximum change is localized at the occipital and parietal lobes. (Right)
Source estimation: sLORETA analysis of the subtracted electric potential difference of the
alpha feedback sessions compared to the passive baseline. The yellow area represents the
maximum estimated change of the alpha band activity to baseline. (Back view) (Salari et
al., 2012)

3.12).

Analysis of Efficiency of Artifact Control

To assess the effect of artifact control during BCI training, we determined the amount
of artifact contaminated alpha/gamma segments (at least one of the artifact bars red)
within the first and last training days. At the individual level, four volunteers were
successful in avoiding artifacts on the first training day; success was defined as 35%
or less of the feedback segments affected by artifacts. All other volunteers showed
poor performance in artifact control on the first day. However, for these volunteers
in particular, our results revealed a significant decrease of artifact contaminated
segments across training (reduction of 17 % from first to last training day, $F(1,7) =$
6.02, $p<0.05$). Thus, our results demonstrate the efficiency of artifact control during
BCI training as volunteers learned to control artifacts across training.

**Analysis of the Influence of Increased Prestimulus Alpha or Gamma Band
Activity on Object Perception**

As in Experiment II, we tested for the consequences of selectively increased gamma
and alpha band activity on subsequent visual object processing. All volunteers from
the fifth experiment participated in the object detection task. Our results clearly
showed that volunteers were able to detect more objects during the gamma band

sessions than during the alpha band sessions. During prestimulus increased gamma band activity more objects were detected than during prestimulus increased alpha band activity (detected objects during gamma sessions: 81% ± 2.9 (s.e.m.) versus alpha band sessions: 74% ± 3.6(s.e.m); t(11) = 3.03, p=0.01) (Figure 3.13c). As in Experiment II, we applied the recognition task after BCI testing with 30 images shown during alpha session, 30 during gamma sessions and 60 additional new images. Analyses were identical to Experiment II. However, no significant differences were found between images detected during alpha and gamma band sessions.

The offline EEG analysis confirmed that the prestimulus gamma and alpha band activity differed for alpha and gamma band sessions. The percent change of alpha and gamma activity to baseline was analyzed in both alpha and gamma band sessions in the trained LOC. Statistical tests revealed increased alpha power during the alpha sessions but not during the gamma sessions and increased gamma power during the gamma sessions but not during the alpha band related sessions (interaction of session (alpha/gamma) X frequency band (alpha/gamma) F(1,11) = 45.53, p< 0.001). During gamma band sessions, gamma band was significantly increased as compared to baseline (t(11)= 3.1, p=0.01), while alpha band activity remained unchanged (t(11) = 1.01, n.s.). A reverse effect was found during the alpha sessions as alpha band activity was significantly increased (t(11)=4.26, p<0.01) and gamma band activity remained unaffected (t(11) = 0.46, n.s.) as compared to baseline. Thus, the modulation of both frequency bands remained highly selective as during the training part of the experiment.

To further evaluate the effects of induced oscillations within different frequency bands, a time-frequency analysis was performed at the sensor level (as in Experiment I for the electrodes PO7/ PO8). A comparison of the oscillatory states directly preceding task stimulus presentation demonstrates the selective induction of the different frequencies and the effects on the stimulus processing (Figure 3.13a,b). The induction of gamma band oscillations was clearly limited to the high frequency range and did not affect lower frequencies and the alpha band oscillations were also restricted to the trained frequency range. In order to test whether visual object processing was specific to an increase of gamma band activity in the LOC, we tested whether the results hold true for the parietal region as a maximal alpha effect was shown in that region (see Figure 3.12). Therefore, we calculated the change of alpha and gamma band activity during the prestimulus gamma band sessions in the parietal region [x,y,z] = [15, -63, 65]. This region is depicted from the results of
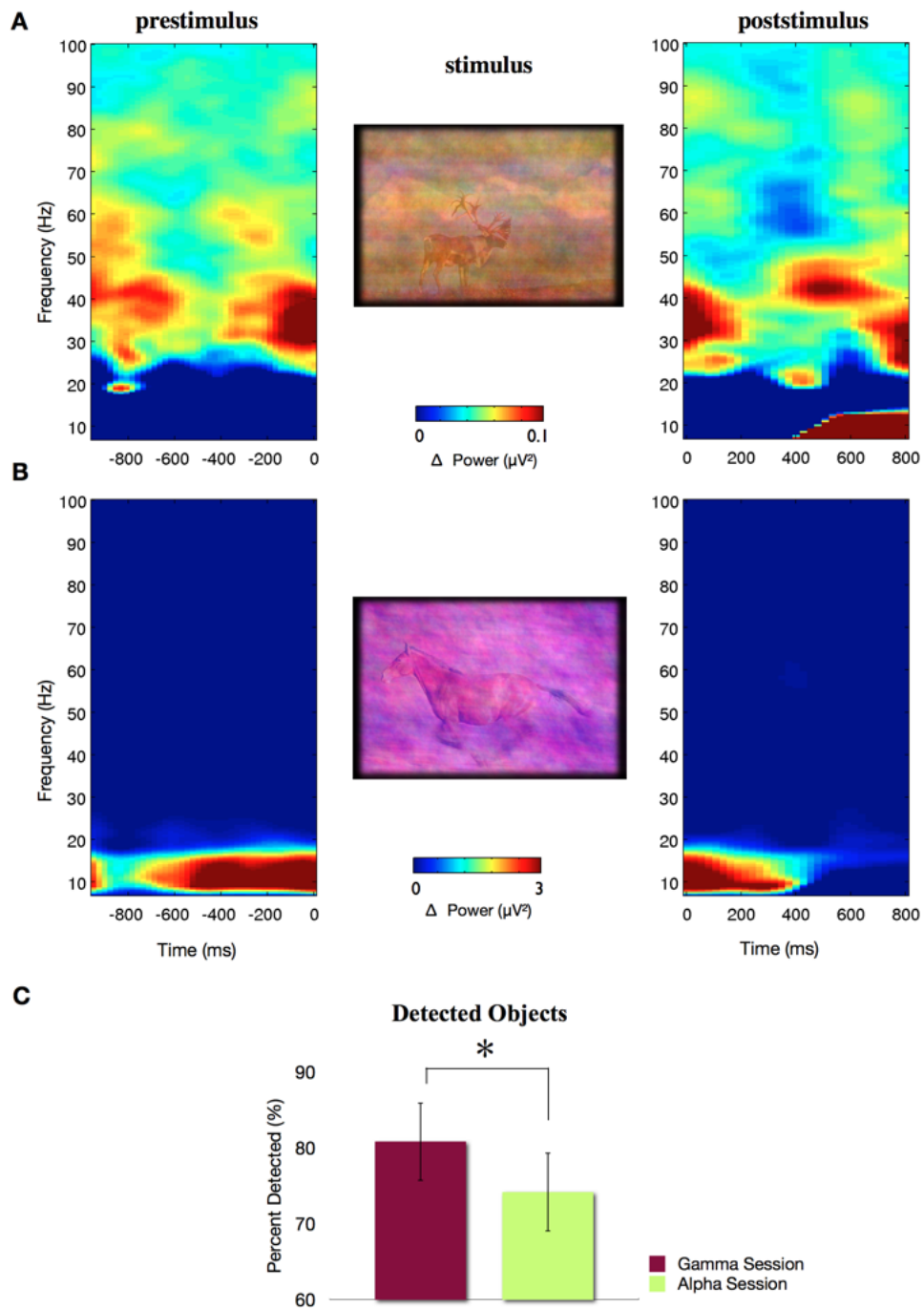
Figure 3.13: (a) Time-frequency analysis of the total power difference between the gamma
state compared to the alpha state for electrodes PO7/PO8 before and after stimulus onset
(grand mean over all participants). A clear difference is found in the trained frequency
range around 40 Hz. (b) Time-frequency analysis of the total power difference between the
alpha state and the gamma state for electrodes PO7/PO8 before and after stimulus onset
(grand mean over all participants). A clear difference is found in the trained frequency range
around 8-12 Hz. (c) Significantly more images were detected during gamma band sessions
than during alpha band sessions. (* p<0.05) (Salari et al., 2012)

source estimation, representing the maximum estimated change of the alpha band activity in the alpha sessions (see Figure 3.12). Results confirmed that during the prestimulus gamma band sessions no significant changes were found in the alpha or gamma band in the parietal region, which could explain the improvement in visual object processing.

3.5.3   Conclusion

Our results demonstrate that volunteers learned to selectively switch between modulating alpha or gamma band oscillations and benefited from online artifact information, as they learned to control artifacts across training. Topographical and spatial analyses show that gamma band increase was restricted to the visual cortex, while alpha band increase revealed a more widespread activation. Thus, a source-based BCI method may facilitate manipulation of a specified frequency range in a predefined brain region, yet with different topographical accuracy. Results of the object detection task during BCI revealed higher detection accuracy for images shown during gamma band sessions than during alpha band sessions. Thus, we were able to replicate results of Experiment II, as more images were detected during increased gamma band activity.

Chapter 4

General Discussion and Future Work

In the present dissertation, we examined the functional relevance of prestimulus gamma band oscillations in the LOC for subsequent visual object processing. To this effect, we designed and developed a non-invasive EEG-based BCI method. Our combined active and reactive BCI method allows for (i) a selective modulation of ongoing oscillatory activity by volunteers in an experimental setup and (ii) a direct examination of this modulation on visual object processing by adaptive stimulus presentation.

After the development of the BCI method, we conducted several experiments. In the first experiment, volunteers learned to increase gamma band oscillations in the visual cortex with a high degree of specificity regarding time, space and frequency. In a second experiment, as volunteers learned to deliberately modulate oscillations in the gamma band frequencies, we focused on the role of these oscillations for subsequent processing of visual stimuli. Results showed that increased gamma band activity improved visual object processing and also memory. In a third experiment, volunteers successfully learned to modulate two frequency ranges, the alpha and the gamma band in a new visual 'game' track display. In order to test for the specific modulation of gamma band oscillations due to BCI training, we conducted a fourth experiment. In this experiment, a feedback group was trained to modulate gamma band oscillations in the visual cortex, while a second control group was exposed to an identical training but without feedback. Both groups conducted visual performance tasks before and after training to test for specific gamma frequency training effects

after training. Only the feedback group but not the control group showed a specific gamma band increase and an improvement in visual object processing.

The unique role of gamma band oscillations for visual object processing is supported by the results from Experiment V. In a new group of volunteers we could replicate the relation of gamma band states to an improvement of visual object processing in a direct comparison to alpha band states. Our results demonstrate that an intentional modulation of distinct oscillatory brain states can improve subsequent visual object processing related to the underlying neural area and therefore suggests a direct link between prestimulus gamma band activity and visual object processing.

Throughout the experiments, we continued to improve the BCI method towards a source-based method for a precise cortical localization of training effects with an online detection of artifacts. In Experiments I to IV, volunteers were trained to increase gamma or alpha band oscillations in electrodes (PO7/PO8) which were approximately located over the LOC. With the source-based BCI method in Experiment V, we showed that volunteers learned to selectively increase gamma or alpha band oscillations directly in the LOC. To our knowledge, we are the first to modulate frequency oscillations in the LOC with a source-based BCI method. Moreover, we are the first to introduce an online estimation of specific brain states and the immediate presentation of stimuli during online BCI testing. Hence, the selective modulation and online estimation of ongoing oscillatory activity in the LOC underlines the value of the BCI method for the examination of a more direct association between oscillatory brain states and visual object processing.

Our main results are summarized here and discussed in detail in the next section:

Neuroscientific results:

- Prestimulus gamma band activity improves subsequent visual object processing and memory.

- Improvement of visual object processing is specific to gamma band oscillations.

BCI method results:

- Selective frequency modulation and adaptive stimuli presentation with the BCI method.

- Modulation of brain oscillations in a specified ROI is feasible with the source-based BCI method.

- Online detection of artifacts assists volunteers in learning to suppress artifacts.

4.1 Discussion of Neuroscientific Results

Prestimulus gamma band activity improves subsequent visual object processing and memory

Oscillations in the gamma band in the visual cortex have been linked to stimulus properties (Engel et al., 2001; Gray et al., 1989; Siegel & König, 2003) and visual awareness (Wyart & Tallon-Baudry, 2009; Rodriguez et al., 1999; Melloni et al., 2007). However, the influence of these spontaneous oscillations on visual object processing remains controversial. Therefore, in the second experiment after gamma band training, we examined the effect of different levels of gamma band activity on visual object processing. Within these different states of ongoing gamma band activity, noisy images were presented as visual stimuli. In accordance with our assumptions, results confirmed that the increase of the induced gamma band activity over the LOC enhanced visual object processing. Results of the frequency distribution in Experiment I (Figure 3.2c), as well as results of the prestimulus activity before object detection in Experiment II (Figure 3.4a), clearly demonstrated a selective enhanced effect in the trained gamma band and no other frequency showed a reliable effect of the BCI training. The relevance of the prestimulus gamma band activity is further supported by the comparison of detected against undetected images, regardless of the actual state. The only reliable difference before the onset of the stimulus is found in the gamma band (Figure 3.5a). Thus, all observed visual performance effects were only related to the gamma band activity. These observations were supported by the results from Experiment V, as more images were detected during increased gamma band activity than during increased alpha band activity.

Specific brain states denoted by rhythmic electrophysiological activity - oscillations - have been under debate for decades. Regarding gamma band oscillations, a recently proposed theory predicts that they are generated by fast-spiking interneurons which then rhythmically inhibit interneuron networks (Stanfords & Jefferys, 1996; Traub et al., 1997; Whittington et al., 1995, 2000; Deans et al., 2001). The theory describes networks of fast-spiking cells connected via gap-junctions (electrical synapses) that allow for synchronous inhibitory post-synaptic potentials (IPSPs) to local excitatory neurons. The excitatory neurons are thereby entrained to the rhythmic inhibitory activity. In accord with previous studies, the activation of the inhibitory interneu-

ron networks generate a short time window for effective (sensory induced) excitation (Cardin et al., 2009; Sohal et al., 2009; Lisman, 2005). This means that during specific phases of the oscillatory cycle, processing is enhanced rather than inhibited. We tested this hypothesis by training volunteers to generate gamma band oscillations in the LOC and then presented visual stimuli. Visual object processing was improved. The theory explains the important functional role of gamma band oscillations in the establishment of a neural state within a circumscribed network that facilitates the processing of new visual stimuli within that specific network.

Our results showed that the established gamma state did not only improve the processing of new visual stimuli but also improved memory recall of these visual stimuli. The interaction of gamma band oscillations with slow theta oscillations has been suggested to be involved in memory functions (Lisman, 2005). Lisman and colleagues (1995) have argued that these oscillations are a clocking system for a neural code that organize and allow multiple items to be stored in memory. Indeed, results of the recognition task in the second experiment showed a significant influence of gamma band oscillations on memory as results showed higher recognition rates for images that were previously detected during high gamma band states than during low gamma band states. A surprise recognition task was also performed in Experiment V, after volunteers had detected images during increased gamma or increased alpha band states. However, results of the recognition task after training did not show significant changes between recognition rates for images shown during gamma band states as compared to alpha band states. We assume that the comparable memory effect is related to different functional roles of alpha and gamma band activity.

Our results reveal convincing evidence that prestimulus gamma band oscillations improve perception. This is reflected in the amount of detected objects but also in a difference of memory performance between the two gamma band states. We suggest that the improvement in memory formation under the high gamma band state is also related to an enhanced perceptional processing that facilitates memory encoding. The results of the fifth experiment showed that alpha band activity did not improve perception and resulted in an equal memory formation for detected objects (the absolute amount of remembered objects is lower for alpha band states due to less detected objects during the object detection task). It could be assumed that the equal memory performance is related to the proposed functional role of alpha band oscillations and memory formation (Klimesch et al., 2003). This assumption

is supported by the results demonstrating that increased prestimulus alpha band oscillations remain increased in the poststimulus period and we suggest that memory encoding proceeds during the entire increased alpha state.

The equal memory performance in the fifth experiment thus could be related to an improved perceptual processing during elevated gamma band activity and to improved memorization of the objects during alpha band activity. Besides this more speculative interpretation, our experiments clearly demonstrate a functional relevance of prestimulus gamma band activity in the LOC for perceptual processing of visual objects.

Studies in animals and humans have shown a top-down attentional influence on gamma band activity resulting in visual performance differences (Steinmetz et al., 2000; Engel et al., 2001; Fries et al., 2001; Bichot et al., 2005). However, results of Experiment IV demonstrate, that mainly an attentional focus towards the visual display cannot account for the specific increase of gamma band activity in the feedback group, since in both feedback and non-feedback experimental groups, a common attentional focus towards the visual display was established. Hence, although both feedback and non-feedback groups attended equally to the visual display, a significant gamma band increase was only measured in the feedback group. In a study by Tallon-Baudry (2005), they examined the effect of attention on gamma band oscillations showing that attention modulates gamma band oscillations in a broad frequency range from 30 up to 140 Hz. However, the modulation of gamma band frequencies with our custom BCI method showed a narrow increase of prestimulus gamma band activity in the exact trained frequency range from 30 to 45 Hz. Results in Experiment V furthermore support the specific modulation of particular frequency ranges by our BCI method. Both alpha and gamma band frequencies were selectively modulated resulting in a narrowed prestimulus activity increase in the respective trained frequency range. Hence, our results reveal convincing evidence that the learned influence on gamma band activity cannot be related to an attentional mechanism.

Frequency specificity of gamma band oscillations for improved visual object processing

In contrast to the gamma band, prestimulus alpha activity is thought to have an inhibitory role on perception (Dijk et al., 2008; Hanslmayr et al., 2007; Ergenoglu et al., 2004). In a recent study, occipital and parietal transcranial magnetic stimulation

(TMS) at alpha frequency was found to impair target detection in the visual field contralateral to the stimulated hemisphere (Romei et al., 2010). Nevertheless, other studies also indicate a functional relevance of alpha band oscillations for visual object processing (Klimesch et al., 2003; Babiloni et al., 2006; Hanslmayr, Sauseng, et al., 2005). Therefore, in Experiment V, noisy images were presented during real-time classification of increased alpha or gamma band activity in an alternating fashion. Although the absolute change was larger for the alpha band (see Figure 3.10) the behavioral and neural indicators clearly showed an enhanced visual object processing during gamma band states (see Figure 3.13a,c). Thus, in agreement with our assumptions, volunteers detected more images during states of increased prestimulus gamma band activity as compared to states of increased prestimulus alpha band activity.

Recent studies combining EEG and fMRI measurements support a relevant functional role of ongoing gamma band oscillations for visual object processing. A positive correlation between gamma band oscillations and the fMRI response has been found in the visual cortex (Scheeringa et al., 2011). In contrast, alpha band oscillations have been shown to decrease the fMRI response in occipital areas (Scheeringa et al., 2011; Becker et al., 2011; Moosmann et al., 2003; De Munck et al., 2007). Thus, an increase in gamma band oscillations can lead to an increase of activity in the LOC and this increased fMRI response in the LOC has been shown to improve object detection (Rose et al., 2005). This assumption is supported by our results showing that an increase of ongoing gamma band oscillations in the LOC leads to improved visual object processing as compared to ongoing alpha band oscillations.

It could be argued that BCI training of the lower frequencies could also result in similar improvements in visual object processing. A recent study has shown a correlation between the phase of infraslow (0.01–1Hz) fluctuations during ongoing brain activity with the detection of sensory stimuli and amplitudes of $1 - 40$ Hz (Monto et al., 2008). Thus, the study suggests a possible correlation between the increased gamma band activity and the phase of infraslow fluctuations in the prestimulus period, which our technical settings did not allow us to measure.

The BCI method provided us with a way to disentangle the role of gamma and alpha bands in visual object processing and to demonstrate the dominant role of the gamma band state.

4.2 Discussion of the BCI Method

Selective frequency modulation and adaptive stimuli presentation with the BCI method

The results of the experiments show that gamma band oscillations can be induced by our BCI method. In all experiments, the effect of BCI training was limited to the trained frequency range, demonstrating the potential of the BCI method for a frequency specific modulation of ongoing oscillatory activity. Several methods including TMS (Romei et al., 2010; Marshall et al., 2006; Kanai et al., 2008) and attention (Gruber et al., 1999; Fries et al., 2001; Tallon-Baudry et al., 2005) have been implicated as methods to manipulate oscillations in different frequency bands. However, in most of these studies, the spectral effects do not only correspond to the predefined frequencies, but also affect other frequencies. To date, only a single simultaneously recorded TMS EEG study has ensured a frequency specific phase modulation in the alpha band range before stimulus onset (Dugué et al., 2011). Apart from these methods, several studies have applied a feedback approach to train participants to increase activity in different frequency ranges and tested visual performance effects (Klimesch et al., 2003; Hanslmayr, Klimesch, et al., 2005; Keizer et al., 2010). In all of these studies, performance tests were applied offline after neurofeedback training without an assessment of the actual oscillatory state preceding the actual visual performance test. Therefore, in our BCI method, visual performance tests were carried out online during the estimation of alpha or gamma band oscillations. We ensured the presentation of visual stimuli during modulation in the exact trained frequency range and topographic area.

Modulation of brain oscillations in a specified ROI is feasible with the source-based BCI method

Results of sourced-based BCI training with the LORETA method clearly demonstrated that volunteers learned to intentionally increase neural activity in the alpha and gamma band in the LOC. Analyses of the ROIs during the alpha and gamma periods revealed a clear increase of gamma activity during the gamma sessions and a clear increase of alpha activity during the alpha sessions. Thus, volunteers learned to selectively increase activity in both alpha and gamma frequency bands in the predefined ROIs, demonstrating that ongoing alpha and gamma band oscillations can be modulated by a source-based BCI method and, in particular, in a specific brain region.

Results of the distribution of the estimated three-dimensional electrical activity of the gamma band increase showed a selective enhanced effect in the LOC as indicated by the topography in Experiment I. Results of the topographical location and spatial distribution of the alpha band increase demonstrated a rather widespread enhanced effect in the trained lateral occipital and in the occipito-parietal region, with a maximum effect in the superior parietal lobe. Previous studies used source-based methods to generate a feedback signal to enhance low beta and to suppress low alpha in the anterior cingulate cortex (ACC) (Congedo et al., 2004). Based on this study, a further study explored the effect of training in the ACC on anterior regions (Cannon et al., 2007). The present results show that alpha band modulation within the LOC as selected region of interest does not ensure a maximal effect in the defined region. Therefore, post-hoc analyses are essential to evaluate other possible sources that may have affected the results. We show that alpha frequency band cannot be modulated with the same high spatial precision as the gamma band activity. Our results are in agreement with previous literature implicating the origin of posterior alpha oscillations from occipito-parietal areas, where it is modulated by visual input (Berger, 1929; Adrian & Matthews, 1934; Hari et al., 1997). In order to test whether visual object processing was specific to an increase of gamma band activity in the LOC, we tested whether the results hold true for parietal regions. Results demonstrated that no significant changes were found in the alpha band range in the parietal regions during prestimulus gamma sessions. Therefore, alpha activation in parietal regions cannot explain the improvement of visual object processing.

Online detection of artifacts assists volunteers in learning to suppress artifacts

Artifacts caused by EOG, microsaccades or EMG activity can lead to undesired changes in EEG brain signals. As we train volunteers to modulate oscillations in the gamma band, it is particularly important to account for with EMG artifacts, since EMG activity has a wide frequency range, being maximal at frequencies higher than 30 Hz (Anderer et al., 1999; McFarland et al., 1997) and thereby in a similar range as the gamma band activity. A recent discussion raised concerns regarding the neural origin of gamma band activity (Yuval-Greenberg et al., 2008), which provided evidence that increased gamma band activity can be an artifact induced by microsaccades. However, our results provide convincing evidence that the increased gamma band activity is neural rather than ocular in origin. Results of BCI training in Experiment I revealed no systematic changes between the amount and

amplitude of microsaccades in the feedback period compared to the passive period or across training. In addition, results of the object detection task in Experiment II also showed that saccadic activity did not affect high and low gamma states. Since there are no saccadic changes between the relevant periods, the increased gamma band activity in the feedback periods cannot be attributed to a microsaccade influence, but rather stems from neural activity. Importantly, the sensitivity of the applied SP detection method (see section 2.3.3.2) was confirmed as our results demonstrated saccadic changes during stimulus presentation, as reported previously (Yuval-Greenberg et al., 2008). In contrast to Experiments I to IV, in Experiment V, EOG, EMG and microsaccadic artifacts were detected online as volunteers trained to increase gamma or alpha band activity. Our results revealed a suppression of artifacts over the entire training period. Thus, our results clearly demonstrate that an additional visual feedback of artifacts (as in Experiment V) during BCI experiments is essential and in fact assists the volunteer in learning to gain better control of the actual physiological signals.

4.3 Future Work

The following section highlights interesting aspects for future work involving neuroscientific experiments with the BCI method and also further development of the BCI method.

4.3.1 Future Ideas for Neuroscientific Experiments with the BCI method

Up to this point, we have examined improvements in visual object processing due to increased prestimulus gamma band activity around 40 Hz. Interestingly, time-frequency analyses of the poststimulus period in both Experiments II (Figure 3.4a) and V (Figure 3.13a) reveal a clear gamma band increase in the range of 60 to 70 Hz right after stimulus presentation. These observations raise the question of whether feedback training of higher gamma band frequencies would have a greater impact on visual object processing as compared to gamma frequencies around 40Hz. Thus, in future work the advanced BCI method will be applied to train oscillations in the range of 60 to 70 Hz and to test for improved visual object processing.

The reported neuroscientific results in this dissertation could be specific for percep-

tual processing, as studies have shown that functions like memory processing may be supported by oscillatory states of frequencies within the theta band (Addante et al., 2011; Guderian et al., 2009b; Lisman, 2005). This assumption can be tested using the developed BCI method, as the resulting high specificity regarding frequency range and location of alpha and gamma training underpins the value of the BCI method for the examination of a more direct relationship between oscillatory brain states and behavior.

A further interesting experiment could consider a longer period of BCI training. In the conducted experiments, volunteers were trained for 3 days. Thus, with additional training days one could test for a reliable increase of gamma band activity across the training days and eventually find higher accuracy rates for image detection.

4.3.2   Future Ideas for Methodical Extensions of the BCI method

In the future it would be interesting to design and to develop a sLORETA (Pascual-Marqui, 2002) module, as it is more precise than LORETA (see section 2.3.3.4). In order to continue with a source-based BCI method, a custom-written module for sLORETA would allow us to use different interfaces apart from RecView. Furthermore, RecView is not open-source and working with existing modules and therefore black boxes hinders the incorporation of new modules and the extension of existing modules.

The visual display design of the BCI experiments plays a functional role in motivating volunteers to participate in the experiments. Thus, the exploration of different display designs and their effect on training would be highly interesting.

Furthermore, we would like to design and develop a new visual feedback display with a 3D overview of the volunteers head. Such a map would visualize the localization of the maximum increase of specific frequencies, which would possibly assist volunteers in learning how to modulate variable frequencies in different topographical areas.

Appendix

Parts of the dissertation have been published in PLoS ONE, 7(5) (Salari et al., 2012).

Digital Filter Design

The following outlines the calculation of the coefficients for a 2nd order IIR Butterworth high-pass filter with a cut-off frequency 0.5 Hz as introduced by (Milivojevic, 2009).

1. In a preliminary step, the filter specifications are set:

   - Type of filter: High-pass filter

   - Sampling frequency $f_s = 250$ Hz

   - Filter order $N = 2$.

   - Passband cutoff frequency $f_c = 0.5$ Hz.

   - Selected analog filter type: Butterworth filter

2. In a next step, transformation of analog filter system from the time domain into the frequency domain is achieved by using the transfer function $H_a(s)$ with $s = j\omega$ representing the complex frequency (from Laplace transform). Substituting $s = j\omega$ in equation 2.9 we get:

$$H_a(s)H_a(-s) = \frac{1}{1 + \left(\frac{s}{j}\right)^{2N}} \tag{4.1}$$

3. The Butterworth reference prototype filter transfer function has no zeros, only poles. As $N = 2$, with

$$s_k = \cos\frac{\pi}{2N}(2k + N - 1) + j\sin\frac{\pi}{2N}(2k + N - 1), \quad k = 1, 2, 3, \ldots, 2N \qquad (4.2)$$

the value of the poles are:

$$s_1 = \cos\frac{\pi}{4}(2 + 3) + j\sin\frac{\pi}{4}(2 + 3) = -0.7071 - j0.7071 \qquad (4.3)$$

$$s_2 = \cos\frac{\pi}{4}(4 + 3) + j\sin\frac{\pi}{4}(4 + 3) = 0.7071 - j0.7071 \qquad (4.4)$$

$$s_3 = \cos\frac{\pi}{4}(6 + 3) + j\sin\frac{\pi}{4}(6 + 3) = 0.7071 + j0.7071 \qquad (4.5)$$

$$s_4 = \cos\frac{\pi}{4}(8 + 3) + j\sin\frac{\pi}{4}(8 + 3) = -0.7071 + j0.7071 \qquad (4.6)$$

Since the poles must all be in the left half plane (negative real part) for a stable filter, the poles s_1 and s_4 are selected. In the following they are referred to as s_1 and s_2.

The reference analog prototype transfer function results in:

$$H_a(s) = \frac{1}{(s + 0.7071 + j0.7071)\,(s + 0.7071 - j0.7071)} \qquad (4.7)$$

4. As a next step, the Butterworth reference analog filter is transformed into a high-pass analog filter with the specified cut-off frequency ω_c. By performing the following transformation

$$H(s) = \frac{1}{\displaystyle\prod_{k=1}^{N}(-s_k)}\frac{s^N}{\displaystyle\prod_{k=1}^{N}\left(s - \frac{\omega_c}{s_k}\right)} \qquad (4.8)$$

with

$$\omega_c = \tan\left(\pi\frac{f_c}{f_s}\right) \qquad (4.9)$$

ω_c is calculated first:

$$\omega_c = \tan\left(\pi\frac{0.5}{250}\right) = 0.006 \qquad (4.10)$$

$$H(s) = \frac{1}{(-s_1)(-s_2)} \frac{s^2}{\left(s - \frac{0.006}{s_1}\right)\left(s - \frac{0.006}{s_2}\right)} \tag{4.11}$$

$$H(s) = \frac{1}{(0.7071 + j0.7071)(0.7071 - j0.7071)} \frac{s^2}{\left(s - \frac{0.006}{-0.7071 - j0.7071}\right)\left(s - \frac{0.006}{-0.7071 + j0.7071}\right)} \tag{4.12}$$

and the analog prototype filter cut-off frequency ω_c is determined with:

$$\omega_c = \tan\left(\pi\frac{f_c}{f_s}\right) \tag{4.13}$$

5. The analog filter is now transformed to a digital through bilinear transformation:

$$s = \frac{1 - z^{-1}}{1 + z^{-1}} \tag{4.14}$$

With the substitution of the complex variable s in 2.20 we obtain the following:

$$H(z) = H_0(-1)^{N-M} \frac{\prod\limits_{k=1}^{M}(1 - z_k)}{\prod\limits_{k=1}^{N}(1 - s_k)}(1 + z^{-1})^{N-M} \frac{\prod\limits_{k=1}^{M}\left(1 - \frac{1+z_k}{1-z_k}z^{-1}\right)}{\prod\limits_{k=1}^{N}\left(1 - \frac{1+p_k}{1-p_k}z^{-1}\right)} \tag{4.15}$$

With a more condensed form of the previous expression with the a_k and b_k coefficients we obtain:

$$H(z) = \frac{\sum\limits_{k=0}^{M} b_k z^{-k}}{1 + \sum\limits_{k=1}^{N} a_k z^{-k}} \tag{4.16}$$

$$H(z) = \frac{1 - 2z^{-1} + z^{-2}}{1 - 2z^{-1} + 0.98z^{-2}} \tag{4.17}$$

Setting the a_k and b_k coefficient in equation 2.11, we obtain the following second order high-pass IIR Butterworth filter with a cutoff frequency of $f_c = 0.5$ Hz and a sampling rate of 250 Hz:

$$y(n) = (x(n-0)\times 1) + (x(n-1)\times -2) + (x(n-2)\times 1) + (y(n-1)\times 2) + (y(n-2)\times -0.98) \tag{4.18}$$

Statistical Methods

Student's t-test

The Student's t-test assesses whether the means of two samples are statistically different from each other. Our data is mainly based on dependent samples, which means that a group of people have been tested twice (repeated measures). The paired t-test is defined as (Howell, 2009):

$$t = \frac{\bar{x}_1 - \bar{x}_2 - \mu_0}{\frac{s_1 - s_2}{\sqrt{n}}} \tag{4.19}$$

where $\bar{x}_1$ is the sample mean of testing. i.e., at day one and $\bar{x}_2$ is the sample mean of the same group at day two. s is the sample standard deviation for day one s_1 and day two s_2. n is the number of volunteers in a group. The degree of freedom used is $n-1$. The Null-hypothesis states that there is no effective difference between the two samples and that therefore the mean (μ_1) of samples from day 1 is equal to the mean (μ_2) of samples of day 2, $H_0 = \mu_1 - \mu_2 = 0 = \mu_0$. For a significant difference between the two samples the Null-hypothesis has to be rejected.

With the t value we get a p-value (can be looked up in the t-distribution table) that indicates how likely we could have gotten these results by chance. A statistically significant difference between the two samples is given, if the chance of obtaining the differences is under 5 % (p< 0.05). In this case the null hypothesis is rejected.

Analysis of Variance (ANOVA)

The student's t-test is mathematically identical to a one-way ANOVA with two samples of data. The ANOVA can be applied on one or more data samples, i.e. one group tested throughout 3 days. The test statistic for ANOVA has an F-distribution under the null hypothesis. The one-way ANOVA F-test statistic, with $K-1$, $N-K$

degrees of freedom under the null hypothesis, is defined as:

$$F = \frac{\sum_i n_i \frac{(\bar{x}_i - \bar{x})^2}{K-1}}{\sum_{ij} \frac{(x_{ij} - \bar{x}_i)^2}{N-K}} \tag{4.20}$$

where $\bar{x}_i$ denotes the sample mean in group i, n_i is the number of samples in a group. $\bar{x}$ is the overall mean of the data. x_{ij} is sample j in group i out of K groups and N is the overall sample size.

List of Figures

List of Tables

References

Addante, R., Watrous, A., Yonelinas, A., Ekstrom, A., & Ranganath, C. (2011). Prestimulus theta activity predicts correct source memory retrieval. *Proceedings of the National Academy of Sciences, 108*(26), 10702.

Adrian, E. D., & Matthews, B. H. (1934). The interpretation of potential waves in the cortex. *J Physiol, 81*(4), 440-71.

Anderer, P., Roberts, S., Schlogl, A., Gruber, G., Klosch, G., Herrmann, W., et al. (1999). Artifact processing in computerized analysis of sleep eeg - a review. *Neuropsychobiology, 40*(3), 150-7.

Ary, J., Klein, S., & Fender, D. (1981). Location of sources of evoked scalp potentials: corrections for skull and scalp thicknesses. *Biomedical Engineering, IEEE Transactions on*(6), 447–452.

Babiloni, C., Vecchio, F., Bultrini, A., Romani, G., & Rossini, P. (2006). Pre- and poststimulus alpha rhythms are related to conscious visual perception: a high-resolution eeg study. *Cerebral Cortex, 16*(12), 1690–1700.

Barkley, R. (2006). *Attention-deficit hyperactivity disorder: A handbook for diagnosis and treatment* (Vol. 1). The Guilford Press.

Barnett, S. (1990). *Matrices: methods and applications.* Clarendon Press.

Becker, R., Reinacher, M., Freyer, F., Villringer, A., & Ritter, P. (2011). How ongoing neuronal oscillations account for evoked fmri variability. *The Journal of Neuroscience, 31*(30), 11016.

Benali-Khoudja, M., Hafez, M., Alexandre, J., & Kheddar, A. (2004). Tactile interfaces: a state-of-the-art survey. In *Int. symposium on robotics.*

Berger, H. (1929). Uber das elekrenkephalogramm des menschen. *Arch Psycchiatr Nervenkr, 87*, 527-570.

Bichot, N. P., Rossi, A. F., & Desimone, R. (2005). Parallel and serial neural mechanisms for visual search in macaque area v4. *Science, 308*(5721), 529-34.

Birbaumer, N. (1997). *Slow cortical potentials: their origin, meaning, and clinical use.* Tilburg, The Netherlands: Tilburg Univ. Press.

Birbaumer, N., Elbert, T., Canavan, A., & Rockstroh, B. (1990). Slow potentials of the cerebral cortex and behavior. *Physiological Reviews, 70*(1), 1.

Birbaumer, N., Ghanayim, N., Hinterberger, T., Iversen, I., Kotchoubey, B., Kubler, A., et al. (1999). A spelling device for the paralysed. *Nature, 398*(6725), 297-8.

Birbaumer, N., Kubler, A., Ghanayim, N., Hinterberger, T., Perelmouter, J., Kaiser, J., et al. (2000). The thought translation device (ttd) for completely paralyzed

patients. *Rehabilitation Engineering, IEEE Transactions on*, *8*(2), 190–193.

Blankertz, B., Sannelli, C., Halder, S., Hammer, E., Kubler, A., Muller, K., et al. (2010). Neurophysiological predictor of smr-based bci performance. *NeuroImage*, *51*(4), 1303-1309.

Borasio, G., Sloan, R., & Pongratz, D. (1998). Breaking the news in amyotrophic lateral sclerosis. *Journal of the neurological sciences*, *160*, S127–S133.

Boylan, C., & Doig, H. R. (1989). Effect of saccade size on presaccadic spike potential amplitude. *Invest Ophthalmol Vis Sci*, *30*(12), 2521-7.

Brewster, S., Lumsden, J., Bell, M., Hall, M., & Tasker, S. (2003). Multimodal'eyes-free'interaction techniques for wearable devices. In *Proceedings of the sigchi conference on human factors in computing systems* (pp. 473–480).

Burger, H., & Van Milaan, J. (1948). Heart-vector and leads. *British heart journal*, *10*(4), 229.

Cannon, R., Lubar, J., Congedo, M., Thornton, K., Towler, K., & Hutchens, T. (2007). The effects of neurofeedback training in the cognitive division of the anterior cingulate gyrus. *Int J Neurosci*, *117*(3), 337-57.

Cardin, J. A., Carlen, M., Meletis, K., Knoblich, U., Zhang, F., Deisseroth, K., et al. (2009). Driving fast-spiking cells induces gamma rhythm and controls sensory responses. *Nature*, *459*(7247), 663-7.

Chibelushi, C., Deravi, F., & Mason, J. (2002). A review of speech-based bimodal recognition. *Multimedia, IEEE Transactions on*, *4*(1), 23–37.

Cincotti, F., Mattia, D., Aloise, F., Bufalari, S., Schalk, G., Oriolo, G., et al. (2008). Non-invasive brain-computer interface system: towards its application as assistive technology. *Brain research bulletin*, *75*(6), 796–803.

Congedo, M., Lubar, J. F., & Joffe, D. (2004). Low-resolution electromagnetic tomography neurofeedback. *IEEE Trans Neural Syst Rehabil Eng*, *12*(4), 387-97.

Cooley, J., & Tukey, J. (1965). An algorithm for the machine calculation of complex fourier series. *Math. Comput*, *19*(90), 297–301.

Deans, M., Gibson, J., Sellitto, C., Connors, B., & Paul, D. (2001). Synchronous activity of inhibitory networks in neocortex requires electrical synapses containing connexin36. *Neuron*, *31*(3), 477–485.

De Munck, J., Goncalves, S., Huijboom, L., Kuijer, J., Pouwels, P., Heethaar, R., et al. (2007). The hemodynamic response of the alpha rhythm: an eeg/fmri study. *Neuroimage*, *35*(3), 1142–1151.

Dijk, H. van, Schoffelen, J. M., Oostenveld, R., & Jensen, O. (2008). Prestimulus

oscillatory activity in the alpha band predicts visual discrimination ability. *J Neurosci*, *28*(8), 1816-23.

Donchin, E., Spencer, K. M., & Wijesinghe, R. (2000). The mental prosthesis: assessing the speed of a p300-based brain-computer interface. *IEEE Trans Rehabil Eng*, *8*(2), 174-9.

Drechsler, R. (2011). Ist neurofeedbacktraining eine wirksame therapiemethode zur behandlung von adhs? ein überblick über aktuelle befunde. *Zeitschrift für Neuropsychologie*, *22*(2), 131–146.

Duchowski, A. (2002). A breadth-first survey of eye-tracking applications. *Behavior Research Methods*, *34*(4), 455–470.

Dugué, L., Marque, P., & VanRullen, R. (2011). The phase of ongoing oscillations mediates the causal relation between brain excitation and visual perception. *The Journal of Neuroscience*, *31*(33), 11889.

Ebrahimi, T., Vesin, J., & Garcia, G. (2003). Brain-computer interface in multimedia communication. *IEEE Signal Processing Magazine*, *20*(1), 14-24.

Engel, A. K., Fries, P., & Singer, W. (2001). Dynamic predictions: oscillations and synchrony in top-down processing. *Nat Rev Neurosci*, *2*(10), 704-16.

Ergenoglu, T., Demiralp, T., Bayraktaroglu, Z., Ergen, M., Beydagi, H., & Uresin, Y. (2004). Alpha rhythm of the eeg modulates visual detection performance in humans. *Brain Res Cogn Brain Res*, *20*(3), 376-83.

Fasel, B., & Luettin, J. (2003). Automatic facial expression analysis: a survey. *Pattern Recognition*, *36*(1), 259–275.

Fatourechi, M., Bashashati, A., Ward, R. K., & Birch, G. E. (2007). Emg and eog artifacts in brain computer interface systems: A survey. *Clin Neurophysiol*, *118*(3), 480-94.

Fox, D. J., Tharp, D. F., & Fox, L. C. (2005). Neurofeedback: an alternative and efficacious treatment for attention deficit hyperactivity disorder. *Appl Psychophysiol Biofeedback*, *30*(4), 365-73.

Fries, P., Reynolds, J. H., Rorie, A. E., & Desimone, R. (2001). Modulation of oscillatory neuronal synchronization by selective visual attention. *Science*, *291*(5508), 1560-3.

Fuchs, M., Kastner, J., Wagner, M., Hawes, S., & Ebersole, J. S. (2002). A standardized boundary element method volume conductor model. *Clin Neurophysiol*, *113*(5), 702-12.

Fuchs, M., Wagner, M., Köhler, T., & Wischmann, H. (1999). Linear and nonlinear current density reconstructions. *Journal of clinical Neurophysiology*, *16*(3),

267.

Gastaut, H. (1952). Etude electrocorticographique de la reactivite des rythmes rolandiques. *Rev. neurol*, *87*, 176–182.

Gevensleben, H., Holl, B., Albrecht, B., Vogel, C., Schlamp, D., Kratz, O., et al. (2009). Is neurofeedback an efficacious treatment for adhd? a randomised controlled clinical trial. *Journal of Child Psychology and Psychiatry*, *50*(7), 780–789.

Gratton, G., Coles, M. G., & Donchin, E. (1983). A new method for off-line removal of ocular artifact. *Electroencephalogr Clin Neurophysiol*, *55*(4), 468-84.

Gray, C. M., Konig, P., Engel, A. K., & Singer, W. (1989). Oscillatory responses in cat visual cortex exhibit inter-columnar synchronization which reflects global stimulus properties. *Nature*, *338*(6213), 334-7-.

Grill-Spector, K., Kushnir, T., Edelman, S., Itzchak, Y., & Malach, R. (1998). Cue-invariant activation in object-related areas of the human occipital lobe. *Neuron*, *21*(1), 191–202.

Gruber, T., Muller, M. M., Keil, A., & Elbert, T. (1999). Selective visual-spatial attention alters induced gamma band responses in the human eeg. *Clin Neurophysiol*, *110*(12), 2074-85.

Gruzelier, J., Egner, T., & Vernon, D. (2006). Validating the efficacy of neurofeedback for optimising performance. *Prog Brain Res*, *159*, 421-31.

Guderian, S., Schott, B., Richardson-Klavehn, A., & Düzel, E. (2009a). Medial temporal theta state before an event predicts episodic encoding success in humans. *Proceedings of the National Academy of Sciences*, *106*(13), 5365.

Guderian, S., Schott, B., Richardson-Klavehn, A., & Düzel, E. (2009b). Medial temporal theta state before an event predicts episodic encoding success in humans. *Proceedings of the National Academy of Sciences*, *106*(13), 5365.

Habel, C., Kerzel, M., & Lohmann, K. (2010). Verbal assistance in tactile-map explorations: A case for visual representations and reasoning. In *Proceedings of aaai.*

Hämäläinen, M., Hari, R., Ilmoniemi, R., Knuutila, J., & Lounasmaa, O. (1993). *Reviews of modern Physics*, *65*(2), 413.

Hämäläinen, M., & Ilmoniemi, R. (1994). Interpreting magnetic fields of the brain: minimum norm estimates. *Medical and Biological Engineering and Computing*, *32*(1), 35–42.

Hammond, D. (2005). Neurofeedback with anxiety and affective disorders. *Child and Adolescent Psychiatric Clinics of North America*, *14*(1), 105-123.

Hanslmayr, S., Aslan, A., Staudigl, T., Klimesch, W., Herrmann, C. S., & Bauml, K. H. (2007). Prestimulus oscillations predict visual perception performance between and within subjects. *Neuroimage*, *37*(4), 1465-73.

Hanslmayr, S., Klimesch, W., Sauseng, P., Gruber, W., Doppelmayr, M., Freunberger, R., et al. (2005). Visual discrimination performance is related to decreased alpha amplitude but increased phase locking. *Neurosci Lett*, *375*(1), 64-8.

Hanslmayr, S., Sauseng, P., Doppelmayr, M., Schabus, M., & Klimesch, W. (2005). Increasing individual upper alpha power by neurofeedback improves cognitive performance in human subjects. *Appl Psychophysiol Biofeedback*, *30*(1), 1-10.

Hari, R., Salmelin, R., Makela, J. P., Salenius, S., & Helle, M. (1997). Magnetoencephalographic cortical rhythms. *Int J Psychophysiol*, *26*(1-3), 51-62.

Howell, D. (2009). *Statistical methods for psychology.* Wadsworth Pub Co.

Hu, W., Tan, T., Wang, L., & Maybank, S. (2004). A survey on visual surveillance of object motion and behaviors. *Systems, Man, and Cybernetics, Part C: Applications and Reviews, IEEE Transactions on*, *34*(3), 334–352.

Jaimes, A., & Sebe, N. (2007). Multimodal human-computer interaction: A survey. *Computer Vision and Image Understanding*, *108*(1-2), 116–134.

Jeffs, B., Leahy, R., & Singh, M. (1987). An evaluation of methods for neuromagnetic image reconstruction. *Biomedical Engineering, IEEE Transactions on*(9), 713–723.

Jensen, O., Gelfand, J., Kounios, J., & Lisman, J. (2002). Oscillations in the alpha band (9–12 hz) increase with memory load during retention in a short-term memory task. *Cerebral Cortex*, *12*(8), 877–882.

Jurcak, V., Tsuzuki, D., & Dan, I. (2007). 10/20, 10/10, and 10/5 systems revisited: their validity as relative head-surface-based positioning systems. *Neuroimage*, *34*(4), 1600-11.

Kamiya, J. (1968). Conscious control of brain waves. *Psychology Today*, *1*(11), 56–60.

Kanai, R., Chaieb, L., Antal, A., Walsh, V., & Paulus, W. (2008). Frequency-dependent electrical stimulation of the visual cortex. *Current Biology*, *18*(23), 1839–1843.

Kandel, E., Schwartz, J., Jessell, T., Mack, S., & Dodd, J. (1991). *Principles of neural science* (Vol. 3). Elsevier New York.

Katevas, N., Sgouros, N., Tzafestas, S., Papakonstantinou, G., Beattie, P., Bishop, J., et al. (1997). The autonomous mobile robot senario: a sensor aided in-

telligent navigation system for powered wheelchairs. *Robotics & Automation Magazine, IEEE, 4*(4), 60–70.

Keizer, A. W., Verment, R. S., & Hommel, B. (2010). Enhancing cognitive control through neurofeedback: a role of gamma-band activity in managing episodic retrieval. *Neuroimage, 49*(4), 3404-13.

Kelly, S. P., Lalor, E. C., Finucane, C., McDarby, G., & Reilly, R. B. (2005). Visual spatial attention control in an independent brain-computer interface. *IEEE Trans Biomed Eng, 52*(9), 1588-96.

Keren, A. S., Yuval-Greenberg, S., & Deouell, L. Y. (2009). Saccadic spike potentials in gamma-band eeg: characterization, detection and suppression. *Neuroimage, 49*(3), 2248-63.

Klimesch, W., Sauseng, P., & Gerloff, C. (2003). Enhancing cognitive performance with repetitive transcranial magnetic stimulation at human individual alpha frequency. *Eur J Neurosci, 17*(5), 1129-33.

Knuth, D. (1998). The art of computer programming. *Seminumerical Algorithms, 2*, 232.

Koles, Z. (1998). Trends in eeg source localization. *Electroencephalography and clinical Neurophysiology, 106*(2), 127–137.

Koles, Z., Flor-Henry, P., & Lind, J. (2001). Low-resolution electrical tomography of the brain during psychometrically matched verbal and spatial cognitive tasks. *Human brain mapping, 12*(3), 144–156.

Konen, C., & Kastner, S. (2008). Two hierarchically organized neural systems for object information in human visual cortex. *Nature Neuroscience, 11*(2), 224–231.

Kourtzi, Z., & Kanwisher, N. (2001). Representation of perceived object shape by the human lateral occipital complex. *Science, 293*(5534), 1506.

Kozelka, J., & Pedley, T. (1990). Beta and mu rhythms. *Journal of Clinical Neurophysiology, 7*(2), 191.

Kreiman, G., Koch, C., & Fried, I. (2000). Cateogry-sepcfic visual responses of single neurons in the human medial temporal lobe. *Nature Neuroscience, 3*, 946-953.

Krishnaveni, V., Jayaraman, S., Anitha, L., & Ramadoss, K. (2006). Removal of ocular artifacts from eeg using adaptive thresholding of wavelet coefficients. *J Neural Eng, 3*(4), 338-46.

Kubler, A., Kotchoubey, B., Hinterberger, T., Ghanayim, N., Perelmouter, J., Schauer, M., et al. (1999). The thought translation device: a neurophysi-

ological approach to communication in total motor paralysis. *Experimental Brain Research*, *124* (2), 223–232.

Linkenkaer-Hansen, K., Nikulin, V. V., Palva, S., Ilmoniemi, R. J., & Palva, J. M. (2004). Prestimulus oscillations enhance psychophysical performance in humans. *J Neurosci*, *24* (45), 10186-90.

Lisman, J. (2005). The theta/gamma discrete phase code occuring during the hippocampal phase precession may be a more general brain coding scheme. *Hippocampus*, *15* (7), 913–922.

Lubar, J. F., & Shouse, M. N. (1976). Eeg and behavioral changes in a hyperkinetic child concurrent with training of the sensorimotor rhythm (smr): a preliminary report. *Biofeedback Self Regul*, *1* (3), 293-306.

Malach, R., Reppas, J. B., Benson, R. R., Kwong, K. K., Jiang, H., Kennedy, W. A., et al. (1995). Object-related activity revealed by functional magnetic resonance imaging in human occipital cortex. *Proc Natl Acad Sci U S A*, *92* (18), 8135-9.

Marshall, L., Helgadottir, H., Molle, M., & Born, J. (2006). Boosting slow oscillations during sleep potentiates memory. *Nature*, *444* (7119), 610-3.

McFarland, D., McCane, L. M., David, S. V., & Wolpaw, J. R. (1997). Spatial filter selection for eeg-based communication. *Electroencephalogr Clin Neurophysiol*, *103* (3), 386-94.

McFarland, D., Sarnacki, W., & Wolpaw, J. (2010). Electroencephalographic (eeg) control of three-dimensional movement. *Journal of Neural Engineering*, *7*, 036007.

Melloni, L., Molina, C., Pena, M., Torres, D., Singer, W., & Rodriguez, E. (2007). Synchronization of neural activity across cortical areas correlates with conscious perception. *The Journal of Neuroscience*, *27* (11), 2858.

Middendorf, M., McMillan, G., Calhoun, G., & Jones, K. S. (2000). Brain-computer interfaces based on the steady-state visual-evoked response. *IEEE Trans Rehabil Eng*, *8* (2), 211-4.

Milivojevic, Z. (2009). *Digital filter design.*

Miltner, W. H., Braun, C., Arnold, M., Witte, H., & Taub, E. (1999). Coherence of gamma-band eeg activity as a basis for associative learning. *Nature*, *397* (6718), 434-6.

Mirta, S., & Kaiser, J. (1993). *Handbook for digital signal processing.* John Wiley & Sons, Inc.

Mishkin, M., Ungerleider, L., & Macko, K. (1983). Object vision and spatial vision: Two cortical pathways. *Trends in neurosciences*, *6*, 414–417.

Monastra, V., Lynn, S., Linden, M., Lubar, J., Gruzelier, J., & LaVaque, T. (2005). Electroencephalographic biofeedback in the treatment of attention-deficit/hyperactivity disorder. *Applied Psychophysiology and Biofeedback*, *30*(2), 95–114.

Monastra, V., Lynn, S., Linden, M., Lubar, J., Gruzelier, J., & LaVaque, T. (2005). Electroencephalographic biofeedback in the treatment of attention-deficit/hyperactivity disorder. *Applied Psychophysiology and Biofeedback*, *30*(2), 95–114.

Monto, S., Palva, S., Voipio, J., & Palva, J. M. (2008). Very slow eeg fluctuations predict the dynamics of stimulus detection and oscillation amplitudes in humans. *J Neurosci*, *28*(33), 8268-72.

Moosmann, M., Ritter, P., Krastel, I., Brink, A., Thees, S., Blankenburg, F., et al. (2003). Correlates of alpha rhythm in functional magnetic resonance imaging and near infrared spectroscopy. *Neuroimage*, *20*(1), 145–158.

Mulert, C., Juckel, G., Augustin, H., & Hegerl, U. (2002). Comparison between the analysis of the loudness dependency of the auditory n1/p2 component with loreta and dipole source analysis in the prediction of treatment response to the selective serotonin reuptake inhibitor citalopram in major depression. *Clinical neurophysiology*, *113*(10), 1566–1572.

Neuper, C., Scherer, R., Reiner, M., & Pfurtscheller, G. (2005). Imagery of motor actions: differential effects of kinesthetic and visual-motor mode of imagery in single-trial eeg. *Cognitive Brain Research*, *25*(3), 668–677.

Nijboer, F., Furdea, A., Gunst, I., Mellinger, J., McFarland, D., Birbaumer, N., et al. (2008). An auditory brain-computer interface (bci). *Journal of neuroscience methods*, *167*(1), 43–50.

Park, T. (2010). *Introduction to digital signal processing: Computer musically speaking.* World scientific publishing company.

Parks, T., & Burrus, C. (1987). *Digital filter design.* Wiley-Interscience.

Pascual-Marqui, R. D. (2002). Standardized low-resolution brain electromagnetic tomography (sloreta): technical details. *Methods Find Exp Clin Pharmacol*, *24 Suppl D*, 5-12.

Pascual-Marqui, R. D., Lehmann, D., Koenig, T., Kochi, K., Merlo, M. C., Hell, D., et al. (1999). Low resolution brain electromagnetic tomography (loreta) functional imaging in acute, neuroleptic-naive, first-episode, productive schizophrenia. *Psychiatry Res*, *90*(3), 169-79.

Pascual-Marqui, R. D., Michel, C. M., & Lehmann, D. (1994). Low resolution

electromagnetic tomography: a new method for localizing electrical activity in the brain. *Int J Psychophysiol*, *18*(1), 49-65.

Penfield, W., & Perot, P. (1963). The brains record of auditory and visual experience. *Brain*, *86*(4), 595-696.

Peniston, E., Marrinan, D., Deming, W., & Kulkosky, P. (1993). Eeg alpha-theta brainwave synchronization in vietnam theater veterans with combat-related post-traumatic stress disorder and alcohol abuse. *Advances in Medical Psychotherapy*, *6*, 37–50.

Penrose, R. (1955). A generalized inverse for matrices. In *Proc. cambridge philos. soc* (Vol. 51, p. C655).

Pfurtscheller, G., Allison, B., Brunner, C., Bauernfeind, G., Solis-Escalante, T., Scherer, R., et al. (2010). The hybrid bci. *Frontiers in neuroscience*, *4*.

Pfurtscheller, G., Brunner, C., Schlogl, A., & Silva, F. H. Lopes da. (2006). Mu rhythm (de)synchronization and eeg single-trial classification of different motor imagery tasks. *Neuroimage*, *31*(1), 153-9.

Pfurtscheller, G., & Silva, F. Lopes da. (1999). Event-related eeg/meg synchronization and desynchronization: basic principles. *Clinical Neurophysiology*, *110*(11), 1842–1857.

Pham, M., Hinterberger, T., Neumann, N., Kubler, A., Hofmayer, N., Grether, A., et al. (2005). An auditory brain-computer interface based on the self-regulation of slow cortical potentials. *Neurorehabilitation and Neural Repair*, *19*(3), 206.

Phillips, C., Rugg, M., & Friston, K. (2002a). Anatomically informed basis functions for eeg source localization: combining functional and anatomical constraints. *NeuroImage*, *16*(3), 678–695.

Phillips, C., Rugg, M., & Friston, K. (2002b). Systematic regularization of linear inverse solutions of the eeg source localization problem. *NeuroImage*, *17*(1), 287–301.

Piccione, F., Giorgi, F., Tonin, P., Priftis, K., Giove, S., Silvoni, S., et al. (2006). P300-based brain computer interface: reliability and performance in healthy and paralysed participants. *Clinical neurophysiology*, *117*(3), 531–537.

Pizzagalli, D., Nitschke, J., Oakes, T., Hendrick, A., Horras, K., Larson, C., et al. (2002). Brain electrical tomography in depression: the importance of symptom severity, anxiety, and melancholic features. *Biological Psychiatry*, *52*(2), 73–85.

Posner, M. I., Snyder, C. R., & Davidson, B. J. (1980). Attention and the detection of signals. *J Exp Psychol*, *109*(2), 160-74.

Potamianos, G., Neti, C., Gravier, G., Garg, A., & Senior, A. (2003). Recent advances in the automatic recognition of audiovisual speech. *Proceedings of the IEEE, 91*(9), 1306–1326.

Potamianos, G., Neti, C., Luettin, J., & Matthews, I. (2004). *Audio-visual automatic speech recognition: An overview.* MIT Press.

Rabiner, L., & Gold, B. (1975). Theory and application of digital signal processing. *Englewood Cliffs, NJ, Prentice-Hall, Inc., 1975. 777 p., 1.*

Rockstroh, B. (1989). *Slow cortical potentials and behaviour.* Urban & Schwarzenberg.

Rodriguez, E., George, N., Lachaux, J., Martinerie, J., Renault, B., & Varela, F. (1999). Perception's shadow: long-distance synchronization of human brain activity. *Nature, 397*(6718), 430–433.

Romei, V., Gross, J., & Thut, G. (2010). On the role of prestimulus alpha rhythms over occipito-parietal areas in visual input regulation: correlation or causation? *J Neurosci, 30*(25), 8692-7.

Rose, M., & Buchel, C. (2005). Neural coupling binds visual tokens to moving stimuli. *J Neurosci, 25*(44), 10101-4.

Rose, M., Schmid, C., Winzen, A., Sommer, T., & Buchel, C. (2005). The functional and temporal characteristics of top-down modulation in visual selection. *Cereb Cortex, 15*(9), 1290-8.

Roth, P., & Pun, T. (2003). Design and evaluation of a multimodal system for the non-visual exploration of digital pictures. In *Interact 2003.*

Salari, N., Büchel, C., & Rose, M. (2012). Functional dissociation of ongoing oscillatory brain states. *PLoS ONE, 7*(5).

Scheeringa, R., Fries, P., Petersson, K., Oostenveld, R., Grothe, I., Norris, D., et al. (2011). Neuronal dynamics underlying high-and low-frequency eeg oscillations contribute independently to the human bold signal. *Neuron, 69*(3), 572–583.

Sellers, E., & Donchin, E. (2006). A p300-based brain-computer interface: initial tests by als patients. *Clinical Neurophysiology, 117*(3), 538–548.

Sibert, L., & Jacob, R. (2000). Evaluation of eye gaze interaction. In *Proceedings of the sigchi conference on human factors in computing systems* (pp. 281–288).

Siegel, M., & König, P. (2003). A functional gamma-band defined by stimulus-dependent synchronization in area 18 of awake behaving cats. *The Journal of neuroscience, 23*(10), 4251.

Simpson, R., & Levine, S. (1997). Adaptive shared control of a smart wheelchair operated by voice control. In *Intelligent robots and systems, 1997. iros'97.,*

proceedings of the 1997 ieee/rsj international conference on (Vol. 2, pp. 622–626).

Sirota, A., Montgomery, S., Fujisawa, S., Isomura, Y., Zugaro, M., & Buzsaki, G. (2008). Entrainment of neocortical neurons and gamma oscillations by the hippocampal theta rhythm. *Neuron, 60*(4), 683-97.

Smith, S., et al. (1997). The scientist and engineer's guide to digital signal processing.

Sohal, V. S., Zhang, F., Yizhar, O., & Deisseroth, K. (2009). Parvalbumin neurons and gamma rhythms enhance cortical circuit performance. *Nature, 459*(7247), 698-702.

Squire, L. (2003). *Fundamental neuroscience* (Vol. 1). Academic Pr.

Squire, L., & Zola-Morgan, S. (1991). The medial temporal lobe memory system. *Science, 253*(5026), 1380-1386.

Stanfords, I., & Jefferys, J. (1996). A mechanism for generation of long-range synchronous fast oscillations in the cortex. *Nature, 383*, 17.

Steinmetz, P. N., Roy, A., Fitzgerald, P. J., Hsiao, S. S., Johnson, K. O., & Niebur, E. (2000). Attention modulates synchronized neuronal firing in primate somatosensory cortex. *Nature, 404*(6774), 187-90.

Sterman, M. (1977). Effects of sensorimotor eeg feedback training on sleep and clinical manifestations of epilepsy. *Biofeedback and behavior, 2*, 167.

Sterman, M. B., & Egner, T. (2006). Foundation and practice of neurofeedback for the treatment of epilepsy. *Appl Psychophysiol Biofeedback, 31*(1), 21-35.

Supèr, H., Togt, C. van der, Spekreijse, H., & Lamme, V. (2003). Internal state of monkey primary visual cortex (v1) predicts figure–ground perception. *The Journal of neuroscience, 23*(8), 3407.

Sutter, E. (1992). The brain response interface: communication through visually-induced electrical brain responses. *Journal of Microcomputer Applications, 15*(1), 31–45.

Tallon-Baudry, C., & Bertrand, O. (1999). Oscillatory gamma activity in humans and its role in object representation. *Trends Cogn Sci, 3*(4), 151-162.

Tallon-Baudry, C., Bertrand, O., Henaff, M. A., Isnard, J., & Fischer, C. (2005). Attention modulates gamma-band oscillations differently in the human lateral occipital cortex and fusiform gyrus. *Cereb Cortex, 15*(5), 654-62.

Tiitinen, H., Sinkkonen, J., Reinikainen, K., Alho, K., Lavikainen, J., & Naatanen, R. (1993). Selective attention enhances the auditory 40-hz transient response in humans. *Nature, 364*(6432), 59-60.

Traub, R., Jefferys, J., & Whittington, M. (1997). Simulation of gamma rhythms in networks of interneurons and pyramidal cells. *Journal of computational neuroscience*, *4*(2), 141–150.

Vernon, D. (2005). Can neurofeedback training enhance performance? an evaluation of the evidence with implications for future research. *Applied psychophysiology and biofeedback*, *30*(4), 347–364.

Vernon, D., Egner, T., Cooper, N., Compton, T., Neilands, C., Sheri, A., et al. (2003). The effect of training distinct neurofeedback protocols on aspects of cognitive performance. *Int J Psychophysiol*, *47*(1), 75-85.

Vidal, J. (1973). Toward direct brain-computer communication. *Annual review of Biophysics and Bioengineering*, *2*(1), 157–180.

Weinstein, D., Zhukov, L., & Johnson, C. (2000). Lead-field bases for electroencephalography source imaging. *Annals of biomedical engineering*, *28*(9), 1059–1065.

Welford, B. (1962). Note on a method for calculating corrected sums of squares and products. *Technometrics*, *4*(3), 419-420.

Whittington, M., Faulkner, H., Doheny, H., & Traub, R. (2000). Neuronal fast oscillations as a target site for psychoactive drugs. *Pharmacology & therapeutics*, *86*(2), 171–190.

Whittington, M., Traub, R., Jefferys, J., et al. (1995). Synchronized oscillations in interneuron networks driven by metabotropic glutamate receptor activation. *Nature*, *373*(6515), 612–615.

Wilson, J., Mellinger, J., Schalk, G., & Williams, J. (2010). A procedure for measuring latencies in brain–computer interfaces. *Biomedical Engineering, IEEE Transactions on*, *57*(7), 1785–1797.

Wolpaw, J., Birbaumer, N., McFarland, D., Pfurtscheller, G., & Vaughan, T. (2002). Brain-computer interfaces for communication and control. *Clinical neurophysiology*, *113*(6), 767–791.

Wolpaw, J., & McFarland, D. (2004). Control of a two-dimensional movement signal by a noninvasive brain-computer interface in humans. *Proc Natl Acad Sci U S A*, *101*(51), 17849-54.

Wyart, V., & Tallon-Baudry, C. (2009). How ongoing fluctuations in human visual cortex predict perceptual awareness: baseline shift versus decision bias. *J Neurosci*, *29*(27), 8715-25.

Yang, M., Kriegman, D., & Ahuja, N. (2002). Detecting faces in images: A survey. *Pattern Analysis and Machine Intelligence, IEEE Transactions on*, *24*(1), 34–

58.

Yao, D., & He, B. (2001). A self-coherence enhancement algorithm and its application to enhancing three-dimensional source estimation from eegs. *Annals of biomedical engineering*, *29*(11), 1019–1027.

Yu, C., & Ballard, D. (2004). A multimodal learning interface for grounding spoken language in sensory perceptions. *ACM Transactions on Applied Perception (TAP)*, *1*(1), 57–80.

Yuval-Greenberg, S., Tomer, O., Keren, A. S., Nelken, I., & Deouell, L. Y. (2008). Transient induced gamma-band response in eeg as a manifestation of miniature saccades. *Neuron*, *58*(3), 429-41.

Zander, T., & Kothe, C. (2011). Towards passive brain–computer interfaces: applying brain–computer interface technology to human–machine systems in general. *Journal of Neural Engineering*, *8*, 025005.

Zhang, X., Broun, C., Mersereau, R., & Clements, M. (2002). Automatic speechreading with applications to human-computer interfaces. *EURASIP Journal on Applied Signal Processing*, *2002*(1), 1228–1247.

Zoefel, B., Huster, R., & Herrmann, C. (2010). Neurofeedback training of the upper alpha frequency band in eeg improves cognitive performance. *Neuroimage*.

Wissenschaftliche Veröffentlichungen

Salari, N., Büchel, C. and Rose, M.. *Functional dissociation of ongoing oscillatory brain states*, PLoS ONE, 2012.

Rose, M., Haider, H., **Salari, N.** and Büchel, C. *Functional dissociation of hippocampal mechanism during implicit learning based on the domain of associations* , J Neurosc, 2011.

Salari, N., Büchel, C. and Rose, M.. *Neurofeedback training of gamma band oscillations improves perceptual processing* (submitted)

Erklärung

Ich versichere an Eides statt, dass ich die vorstehende Arbeit selbständig und ohne fremde Hilfe angefertigt und mich anderer als der im beigefügten Verzeichnis angegebenen Hilfsmittel nicht bedient habe. Alle Stellen, die wörtlich oder sinngemäß aus Veröffentlichungen entnommen wurden, sind als solche kenntlich gemacht.

Ich bin mit einer Einstellung in den Bestand der Bibliothek des Fachbereichs Informatik einverstanden.

Neda Salari